STUDIA
UNIVERSITATIS BABEŞ-BOLYAI

PHYSICA

2

1978

CLUJ-NAPOCA

ANUL XXIII 1978

STUDIA
UNIVERSITATIS BABEŞ-BOLYAI

PHYSICA

2

Redacţia 3400 CLUJ-NAPOCA, str M Kogălniceanu, 1 ● Telefon 1 34 50

SUMAR — CONTENTS — SOMMAIRE — СОДЕРЖАНИЕ

STUDIA UNIV. BABEŞ–BOLYAI, PHYSICA 2, 1978

IONIC TRANSPORT COEFFICIENTS IN RARE-EARTH AND ACTINIDE LIQUID METALS

SPERANŢA COLDEA

1. **Introduction.** Up to the present day the measurement of the viscosity and the diffusion of liquid metals has interested metalurgists. In recent years the liquid metals have been used as heat transfer fluids in several systems. So there are „the heat pipes" and the nuclear power reactors, where the viscosity is an important engineering property. For many other reasons the knowledge of the viscosity coefficients of a rare-earth or actinide liquid metal is essentially needed.

Empirically derived viscosity values for liquid metals have been somewhat successful, but because of inadequate understanding of the liquid state, these values are questionable. These data must be compared with several proposed models for the ionic transport coefficients in liquid metals.

On the other hand the relationship between viscosity and selfdiffusion of these fluids is of a great theoretical interest.

In this respect we shall propose a useful approach which permits to estimate the viscosity and self-diffusion coefficients of the rare-earth actinide liquid metals. For this purpose we shall take into account the previously analysed empirical relationships with some other physical properties of the liquid metals, as Debye's temperature, the activation energy, the temperature -dependent diameter and entropy [1]. The so calculated values were shown to be in good agreement with the available experimental data for the viscosity of most liquid metals, but far less so for diffusion results [1]

2. **Viscosity of rare-earth and actinide metals.** The viscosities of all fluids are strongly dependent upon the temperature. The data for most liquid metals — over a temperature range of several hundred degrees — are adequately represented by the Arrhenius equation [2]:

$$\mu = \text{A. exp } (\text{E/RT}) \tag{1}$$

where A is a constant, E is the activation energy for viscous flow, R is the gas constant and T— the temperature

But this empirical equation does not account for any variation in the density of the liquid which is also dependent upon temperature. In order to account for these density variations this equation was modified by A n d r a d e in the following manner [3]:

$$\mu_m \cong 5{,}7.10^{-4} \ (A.T_m)^{1/2}/\text{V}^{2/3} \tag{2}$$

which relates the viscosity at the melting point μ_m to the atomic weight A, the melting temperature T_m and to the molar volume V.

On the other hand one obtains, in the case of self-diffusion, from a simple kinetic approach for ionic transport coefficients of liquid metals [1]:

$$D = D_0 \exp \gamma \cdot \exp (-E/RT) \tag{3}$$

where

$$D_0 = 4{,}8686 \cdot 10^{-7}\, \vartheta_D \cdot (V_{at}^m)^{2/3} \tag{4}$$

V_{at}^m is the atomic volume at the melting point, ϑ_D being the Debye's temperature which can be expressed by the Lindemann's relation as [4]:

$$\vartheta_D \cong C \cdot \sqrt{T/A\ (V_{at}^m)^{2/3}} \tag{5}$$

The activation energy at the temperature T can be written as.

$$E_{act}^T = E - \gamma RT \tag{6}$$

where E is the contribution to activation energy which does not depend on temperature, whereas the latter term depends upon the temperature and entropy [1].

Using the Stokes-Einstein relation [5]—[6] .

$$\mu = kT/6D \cdot \sigma \tag{7}$$

one obtains the shear viscosity of a liquid metal as [1].

$$\mu \cong B.T. \exp (-\gamma). \exp (E/RT) \tag{8}$$

where

$$B = 3{,}9915 \cdot 10^{-3}/(V_{at}^m)^{2/3} \cdot \theta_D \tag{9}$$

and

$$\exp (-\gamma) = B_{exp}/B_{teor.}. \tag{10}$$

Inserting now the experimental values of B, V_{at}^m, E and the calculated values of B and γ, we can easily estimate the theoretical data of the viscosities by means of the realations (8)—(10) These data are presented in table 1 and are compared with the values of the viscosity of lanthanum, cerium and prasheodymium, which are calculated by the Vadovic-Colver modified hard-sphere theory [7] and with the ones obtained by the Pasternak's corresponding states theory [2] of the ionic transport coefficients The expressions for the shear viscosity of liquid metals in these theories are [7].

$$\mu \cong 0{,}23 \frac{\eta}{\eta_m} \cdot \frac{1}{rN_A} (RTM/\pi)^{1/2} \left[[9{,}385 \left(\frac{T_m \cdot \rho}{T \cdot \rho_m} \right) - 1 \right] \tag{11}$$

where η and η_m are the packing fractions at the temperature T and at the melting point T_m, r is the hard-sphere radius , ρ being the density and N_A — the Avogadro's number, and respectively [2]

$$\mu = [(V^*)^{2/3} \mu^*]/(MR \quad \in/k)^{1/2} \cdot (NV^2)^{-1/3} \tag{12}$$

with μ^* — the reduced viscosity, V^* — the reduced atomic volume and M — the atomic mass.

The above-obtained results for viscosity of La, Ce and Pr are given in table 1, together with the ones of the computation of η on the base of Andrade's formula (2) and with the experimental data. The hard-sphere calculations are in good agreement ($\pm$ 7%) with the experimental viscosity-values (at T_m) for La, Pr and Yb (table 1). However, the calculated values are too small for Ce, U and Pu (by 17,22 and 31% respectively; table 2).

The viscosities which have been calculated by means of the relation (12) were too large for La, Pr and Yb (by 16, 13 and 18% respectively) and too small for Ce, U and Pu (by 4%,7% and 20% respectively, table 1 and 2).

Table 1

Viscosity values of the rare-earth metals calculated by several theoretical methods and the experimental data

Liquid metal	T_m(°K)	[11] μ_{exp} (cP)	$\mu_{calc.\ exp}$(cP)	[3] μAndrade(cP)	[7], [12] μ_{HS}(cP)	[2] μ_{CS}(cP)	[8]—[9] μ_{KT}(cP)
La	1203	2,65 2,45	2,452	2,86	2,61	3,01	2,7
Ce	1077	3,20 2,89	2,882	2,91	2,66	3,07	2,707
Pr	1208	2,85 2,80	2,796	3,04	2,79	3,22	—

Table 2

Viscosity values of actinide liquid metals calculated by several theoretical methods and the experimental data

Liquid metal	T_m(°K)	[11] μ_{exp} (cP)	[7], [12] μ_{HT}(cP)	[2] μ_{CS}(cP)	[8]—[9] μ_{KT}(cP)	[3] μAndrade(cP)
U	1406	6,53	5,12	6,05	5,88	5,8744
Pu	913	5,93 6,0	4,11	4,75	5,04	5,89

Using the relations (8)—(9) one obtains the viscosity of liquid uranium as:

$$\mu_U \cong 1{,}91.10^{-6}\ T \cdot \exp\ (-\gamma)\ \exp\ (10\,245/RT) \tag{13}$$

or, with $\exp\ (-\gamma) = 0{,}56$, $T_m = 1406°\text{K}$, $\vartheta_D = 157°\text{K}$ then also obtaining the final expression:

$$\mu_U \cong 1{,}07 \cdot 10^{-6} \cdot T \cdot \exp\ (10 \cdot 245/RT) \tag{13'}$$

and similarly, for the viscosity of plutonium one obtains

$$\mu_{Pu} \cong 6{,}12 \cdot 10^{-3} \exp\ (4120/RT) \tag{13''}$$

Consequently there is $\mu_U^{T_m} = 5{,}8$ cP ($T_m = 1406°$ K) and $\mu_U^T = 2{,}8$ cP (at $T = 2000°\text{K}$), whereas for liquid plutonium we obtain: $\mu_{Pu}^{T_m} = 5{,}04$ cP ($T_m = 913°\text{K}$).

The above viscosities are in agreement with the results which have been obtained by using the hard-sphere theory [7], the Andrade's formula [3] and the corresponding states theory [2] (table 2). However, our values are too small when compared to the experimental data: $\mu_U^{T_m} = 6{,}53$ cP and $\mu_{Pu}^{T_m} = 5{,}93$ cP or 6,0 cP.

Taking the melting point of Thorium as $T_m = 2020°\text{K}$, the formula (8) shows that $\mu_{Th}^{T_m} = 5{,}04$ cP, as well as $\mu_{Pu}^{T_m}$.

We have to mention that the shear viscosity of this actinide metal was not measured yet.

In spite of his relatively not too large activation energy ($E = 3100$ cal/atg) there is the experimental value of the viscosity of uranium which takes the largest value among the viscosity coefficients which are given in the present day literature. In this respect it seems that the only liquid metal whose viscosity approaches that of plutonium and uranium, are iron, cobalt and nickel $\mu_{Fe} = 5{,}8$ cP, $\mu_{Co} = 5{,}2$ cP and $\mu_{Ni} = 5{,}6$ cP

3. **Self-diffusion of rare-earth and actinide metals.** Using the well-known Stokes-Einstein relation (7) and the result for shear viscosity (8) we can write the self-diffusion of liquid metals as [6]:

$$D = kT/\mu\ \sigma \tag{14}$$

where $k = 2{,}8 \cdot 10^{-17}$ erg/grd and σ is the Pauling's ionic diameter

Similarly, using the Sutherland modification of the above equation [5], there is:

$$D = 0{,}84 \cdot kT/\mu \cdot \sigma \tag{15}$$

where σ is a function of temperature T, which has the form [1]

$$\mu \cong 0{,}644\ (M/\rho_m)^{1/3}[1 - 0{,}112\ (T/T_m)^{1/2}] \cdot (10^{-8}\ \text{cm}) \tag{16}$$

We have to notice that whereas the viscosity has been measured in 32 liquid metals, self-diffusion has been measured for only 9 of these metals. In this respect the use of the above relations (14)—(16) permits the estimation of self-diffusion for the metals for which this coefficient has not been measured.

Taking into account the relations (3)—(4) for self-diffusion of liquid metals it is possible to calculate this coefficient, if the values of θ_{Debye}, V_{at}^{m}, E and γ are known for the considered metals. The so obtained results are given in tables 3 and 4, for rare-earth and actinide liquid metals respectively.

Analysing the tables 3 and 4 we can remark that the values of self-diffusion of molten lanthanum and cerium are in good agreement with both the experimental data and the values of this quantity, obtained from the relation (14) and from another theoretical method [10]. But the value of D for uranium (at the melting point) is too small in comparison with the value estimated from the relation (14). Unfortunately, the relations (3)—(4) cannot be used to estimate the self diffusion of molten plutonium, because the data for ϑ_D, V_{at}^{m} and γ are not yet available.

As a conclusion, it is quite evident that the relation (15) for the self-diffusion is unuseful because it gives too small values in the case of lanthanum, cerium and praseodymium.

But, in any case, the self-diffusion coefficient of rare-earth and actinide liquid metals changes with temperature according to the well-known relation [5]:

$$D_1 = D_0 \cdot \exp(-Q/RT) \tag{17}$$

where D_0 is a constant and Q is the corresponding activation energy.

4. **Conclusions.** Making a comparison between several approaches to estimate the viscosity values of the lanthani de liquid metals (cerium, lanthanum and praseodymium), it can be observed a good agreement of the values calculated from hard-sphere theory [7], from the Andrade's relation [3] and from the simple kinetic theory [1], with the experimental data. The corresponding states theory values [7] for the lanthanide liquid metals viscosities are greater than the other results of table 3.

Table 3

Self-diffusion values of the lanthanide metals, calculated by several theoretical methods and the experimental data

Liquid metal	$D^T m$ calc · rel · (14) (10^5 cm²/s)	$D'^T m$ calc · rel · (15)—(16) (10^5 cm²/s)	$D^T m$ calc. rel · (3)—(4) (10^5 cm²/s)	$D^T m$ [10] teor · (10^5 cm²/s)	$D^T m$ [12] exp · (10^5 · cm²/
La	3,45 3,53	0,2965	3,53	3,614	3,45
Ce	2,89 2,842	0,243	2,97	2,627	2,942
Pr	2,80 3,79	0,235	3,66	3,06	2,936

Guetering the value of $\mu^T m$ (at the melting point) predicted by Andrade [3] with the value of activation energy E anticipated by Grosse [8], there results the possibility to define suitable equations expressing the change of viscosity with temperature. So, the comparison of the sets of theoretical equations [8]:

$$\mu_{La} = 5{,}714 \cdot 10^{-3} \exp\,(3850/RT) \tag{18}$$

$$\mu_{Ce} = 5{,}56 \cdot 10^{-3} \exp\,(3550/RT) \tag{19}$$

$$\mu_{Pr} = 6{,}243 \cdot 10^{-3} \cdot \exp\,(3800/RT) \tag{20}$$

and of experimental equations [9]

$$\mu_{La} = 1{,}464 \cdot 10^{-2} \cdot \exp\,(1231/RT) \tag{21}$$

$$\mu_{Ce} = 1{,}310 \cdot 10^{-2} \exp\,(1679/RT) \tag{22}$$

$$\mu_{Pr} = 1{,}758 \cdot 10^{-3} \cdot \exp\,(1118/RT) \tag{23}$$

indicates that the predicted values for the activation energy E is about two to three times larger than the corresponding experimental values for E of lanthanum, cerium and praseodymium.

Similarly, we can write some theoretical [9] and experimental expressions (from viscosities data) [5] for the lanthanide liquid metals diffusion. As theoretical predictions:

$$D_{La} = 5{,}94 \cdot 10^{-4} \exp\,(-7171/RT) \tag{24}$$

$$D_{Ce} = 5{,}91 \cdot 10^{-4} \exp\,(-6420/RT) \tag{25}$$

$$D_{Pr} = 5{,}91 \cdot 10^{-4} \exp\,(-7201/RT) \tag{26}$$

and experimental equations

$$D_{La} = 1{,}789 \cdot 10^{-4} \exp\,(-3880/RT) \tag{27}$$

$$D_{Ce} = 1{,}945 \cdot 10^{-4} \exp\,(-4044/RT) \tag{28}$$

$$D_{Pr} = 1{,}673 \cdot 10^{-4} \exp\,(-3648/RT) \tag{29}$$

The theories of Grosse [8] and of Sutherland for the self-diffusion [5] predict much higher activation energies (E and Q) for lanthanum, cerium and praseodymium, than experimentally observed

Table 4

Self-diffusion values of the actinide metals, calculated by the relations (3) – (4) and by the relations (15) – (16)

Liquid metal	T(°K)	$\tau_{T(10^8\ cm)}$	D_{calc} rel (15) (10^5 cm²/s)	D_{calc} rel (3) – (4) (10^5 cm²/s)
Pu	T_m = 913	1,355	2,28	—
	= 921	1,3898	2,2857	
	= 972	1,387	2,5285	
	1190	1,3765	4,2857	
U	T_m = 1406	1,354	3,178	1,95
	2000	1,3375	10,68	

However, the temperature ranges of the present experimental investigations are too small Since the viscosities of these molten metals (at the melting point) are low ($\sim$ 3 cP) and all three have long liquid ranges and moderate densities, these liquid metals must be studied at very high temperatures.

(Received December 10, 1977)

REFERENCES

1. S Coldea, *Calculation of ionic transport coefficients by a simple kinetic theory of liquids*, to be published in „Studii şi cercetări de fizică".
2. A. D. Pasternak, Phys. Chem. Liquids, **3**, 41, (1972)
3. E. N. C Andrade, Phil. Magas., **17**, 497, 698 (1934)
4. J. Lindemann, Handbuch der Physik, **13**, 1 (1928)
5 W. Sutherland, Phil Mag, **9**, 781 (1905)
6. W. Jost, *Diffusion in Solid, Liquids, Gases*, Acad Press, New York, 1952
7 C. J. Vadovic and C. P. Colver, Phil Mag, **21**, 971, (1971), **24**, 509 (1971)
8 A V. Grosse, J Inorg Nucl Chem, **23**, 23, 333 (1961)
9 L J Wittenberg and D Ofte, *Physicochemical Measurements in Metals Research*, part 2, p. 193, (1970), Interscience Publ., New York
10 P. J McGonigal, J Phys. Chem, **66**, 1686, (1962)
11 B J Alder, D M Gass and T. E Wainwright, J. Chem Phys., **53**, 3813 (1970).
12 D. Ofte and L J Wittenberg, Trans. Met Soc AIME, **227**, 1706, (1963).

COEFICIENŢI DE TRANSPORT IONIC ÎN METALE LICHIDE LANTANIDE ŞI ACTINIDE

(Rezumat)

Pentru a calcula coeficienţii de transport ionic ca viscozitatea laminară şi autodifuzia în metale lichide, în prezenta lucrare se aplică o teorie cinetică simplă a lichidelor.

În prima parte a lucrării este prezentată metoda de calcul a coeficientului de viscozitate în metale lantanide şi actinide în stare lichidă În partea a doua a lucrării se calculează autodifuzia în aceste metale lichide simple, pe baza aceleiaşi teorii cinetice a fenomenelor de transport în lichide. Se face o comparaţie a valorilor obţinute pentru viscozitatea şi autodifuzia lantanidelor şi actinidelor lichide cu valorile experimentale cunoscute şi cu valori ale acestor coeficienţi de transport, obţinute prin alte metode Se găseşte o bună concordanţă a diferitelor valori ale viscozităţii în cazul actinidelor lichide (uraniu şi plutoniu) şi valori mai mari decît cele experimentale în cazul lantanidelor considerate

Valorile autodifuziei, calculate pentru lanthanum şi cerium, sînt în bună concordanţă atît cu datele experimentale, cît şi cu cele obţinute prin alte metode Coeficientul de autodifuzie a uraniului este mic în comparaţie cu valoarea sa calculată din relaţia Stokes-Einstein, mărimea sa experimentală nefiind cunoscută.

STUDIA UNIV. BABEŞ–BOLYAI, PHYSICA, 2, 1978

AN IMPROVED SCALE–INVARIANCE IN QUANTUM FIELD THEORY

AL. ANGHEL, M. CRIŞAN

The aim of the present paper is to propose and demonstrate an improved form of scale invariance in Quantum Field Theory (QFT).

As it is well-known the scale invariance arguments have been proved to be of great interest in QFT in conjunction with the renormalization group (RG) problem and the asymptotic behaviour at large momenta. The standard form of scale invariance in QFT is.

$$\Phi(\lambda x) = \lambda^{-\Delta_\Phi} \Phi(x) \tag{1}$$

where $\Phi(x)$ is the field operator, Δ_Φ the canonic dimension of the field operator and λ is a real, arbitrary parameter. For a free-field theory in d — space-time dimension:

$$\Delta_\Phi = (d-2)/2 \tag{2}$$

Consider now a self-interacting theory described by the following Lagrangian density:

$$L(x) = \frac{1}{2}(\partial_\mu \Phi)^2 + \frac{1}{2} m_0^2 \Phi^2 + \frac{U_0}{4!} \Phi^4 \tag{3}$$

As it is now a well-established fact [1–3] the dimension of the field Φ and of other composite field operators like $\overset{(n)}{\Phi}(x)$ (n — arbitrary integer number) is changed when the interaction term is switched on from its canonicaly free-field value (2). Using the RG method this deviation from canonical scaling can be determined as a power series expansion in the parameter $\varepsilon = 4 - d$ and a specified value of the fixed-point of RG — equations

We propose now an improved scaling relation which leads directly to the idea of RG and fixed point behaviour. We postulate that in the presence of the interaction term in the lagrangian density, the field operator $\Phi(x)$ and the composite field operators $\overset{(n)}{\Phi}(x)$ become functions of the renormalized coupling constant U_R. The improved scaling relation which we propose is:

$$\Phi^{(n)}(\lambda x, u_K) = \lambda^{-n\Delta_\Phi} \Phi^{(n)}(x; \bar{U}_K(\lambda) F_n(\lambda, U_R) \tag{4}$$

The boundary conditions $\lambda = 1$ and $U_R = 0$ impose:

$$\bar{U}_R(1; U_R) = U_R \tag{5 a}$$

$$F_n(1\ U_R) = 1 \tag{5 b}$$

$$\bar{U}_R(\lambda; U_R = 0) = 0 \tag{6 a}$$

$$F_n(\lambda; U_R = 0) = 1 \tag{6 b}$$

Taking the derivate with respect to λ and then put $\lambda = 1$, the result is:

$$x\frac{\partial}{\partial x}\Phi^{(n)}(x, U_R) = -n\Delta\,\Phi^{(n)}(x,\ U_R) + \\ + \frac{\partial\Phi^n(x;\ U_R)}{\partial u_R}\cdot\frac{\partial\bar{U}(\lambda, U_R)}{\partial\lambda}\bigg|_{\lambda=1} + \\ + \frac{\partial F_n(\lambda,\ U_R)}{\partial\lambda}\bigg|_{\lambda=1}\Phi^{(n)}(x,\ U_R)$$

or: (7)

$$\left[x\frac{\partial}{\partial x} + n\,\Delta_\Phi - \frac{\partial F_n(\lambda; U_R)}{\partial\lambda}\bigg|_{\lambda=1}\right]\Phi^{(n)}(x; U_R) = \\ \frac{\partial\Phi^{(n)}(x,\ U_R)}{\partial U_R}\,\frac{\partial\bar{U}_R(\lambda;\ U_R)}{\partial\lambda}\bigg|_{\lambda=1} \tag{8}$$

Eq (8) is a first-order, inhomogeneous differential equations.
Suppose now that there is a particular value of U_R: $U_R = U_R^*$ such that

$$\frac{\partial\Phi^{(n)}(x;\ u_R^*)}{\partial u_R}\bigg|_{U_R = U_R^*} = 0 \tag{9 a}$$

or:

$$\frac{\partial\bar{u}_R(\lambda;\ u_R^*)}{\partial\lambda}\bigg|_{\lambda=1} = 0 \tag{9 b}$$

Then from eq.(8) we get:

$$\left[x\frac{\partial}{\partial x} + n\,\Delta_\Phi - \frac{\partial F_n(\lambda,\ u_R^*)}{\partial\lambda}\bigg|_{\lambda=1}\right]\Phi^{(n)}(x;\ u_R^*) = 0 \tag{10}$$

which is an homogeneous first-order differential equation. Upon integrating it we arrive at:

$$\Phi^{(n)}(\lambda x,\ u_R^*) = \lambda^{-(\Delta n_\Phi + \delta_\Phi)}\,\Phi^{(n)}(x, u_R^*) \tag{11}$$

where:

$$\delta_\Phi = -\frac{1}{n}\frac{\partial F(\lambda;\ u_R^*}{\partial\lambda}\bigg|_{\lambda=1} \tag{12}$$

It is clear now that starting from the assumption of improved scaled invariance (4) we get anomalous dimension $\Delta_\Phi + \delta_\Phi$ of field operators for a specific value of the coupling constant $U_R = U_R^*$. This is indeed a fixed-point-like behaviour.

Our aim is now to determine the functions $\bar{U}_R(\lambda,\ U_R)$ and $F_n(\lambda;\ U_R)$, perturbatively. To this end we consider the renormalized N — point vertex functions $\Gamma_N(\{pi\};\ U_R)$ with all external momenta $\{pi;\}$ of the same order of magnitude p. It is obvious that these functions will also satisfy the improved scaling relation in momentum space.

$$\Gamma_N(\lambda p;\ U_R) = \lambda^{d - N\Delta_\Phi}\,\Gamma_N(p;\ \bar{U}_R(\lambda))\,F_n(\lambda, U_R) \tag{13}$$

Calculating perturbatively the N-point vertex function Γ, we get the following general result:

$$\Gamma_N(p, U_R) = \Gamma_N^0(p) + \sum_{i=1}^{\infty} U_R^i \gamma_i(p) \tag{14}$$

Developing $\Gamma_N(p; \bar{U}_R(\lambda))$ în power series in U_R

$$\Gamma_N(\lambda; \bar{U}_R(\lambda)) = \Gamma_N^0(p) + \sum_{i=1}^{\infty} U_R^i \gamma (p) \left.\frac{\partial^i \bar{U}_R(\lambda, U_R)}{\partial U_R^i}\right|_{u_R=0} \tag{15}$$

and similarly

$$F_N(\lambda, U_R) = 1 + \sum_{i=1}^{\infty} U_R^i f_i(\lambda) \tag{16}$$

and matching eqs (13), (14), (15) and (16) we get

$$\Gamma_N^0(\lambda p) + \sum_{i=1}^{\infty} u_R^i \gamma_i(\lambda p) = \lambda^{d - N\Delta_\Phi} \left[\Gamma_N^0(p) + \sum_{i=1}^{\infty} U_R^i \gamma_i(p) \Psi_i(\lambda)\right] \cdot \left[1 + \sum_{i=1}^{\infty} U_R^i f_i(\lambda)\right] \tag{17}$$

which is the most general result one can obtain in the perturbation theory. From eq (17) the coefficients $f_m(x)$ and

$$\Psi_i(\lambda) = \left.\frac{\partial^i \bar{U}_R(\lambda, U_R)}{\partial U_R}\right|_{U_R=0} \tag{18}$$

can be determined, and thus the functions $\bar{u}_R = u_R(\lambda, u_R)$ and $F_N = F_N(\lambda; u_R)$ are obtained for different models of interacting fields. Finally, we can summarise the result as follows, the scale invariance in QFT can be improved in order to include implicitly the fixed point behaviour. This generalised scale invariance relation, which was hypothetical assumed can be proved in RNG — framework. This result will be used in order to determine the anomalous dimension for different models in QFT

(Received January 14, 1978)

REFERENCES

1 K. G Wilson, Phys Rev **179,** 1499 (1969)
2. K. G. Wilson, Phys Rev **D2,** 1473 (1970)
3. C. DiCastro, G. Joan-Lasinio, *The RNG Approach to Critical Phenomena,* în *Phase Transitions and Critical Phenomena,* Vol 6, Edited by C Domb and M. S Green (1976) Academic Press.

ÎMBUNĂTĂŢIREA INVARIANTEI DE SCALĂ ÎN TEORIA CUANTICĂ A CÎMPULUI

(Rezumat)

În lucrare se propune o variantă îmbunătăţită a invarianţei de scală în teoria cuantică a cîmpurilor, care stabileşte o legătură directă cu comportarea de punct fix.

STUDIA UNIC. BABEŞ–BOLYAI, PHYSICA, 2, 1978

ELECTRICAL SWITCHING PHENOMENA IN $xFe_2O_3 \cdot (1-x)[3B_2O_3 \cdot PbO]$ GLASS SYSTEM

I. ARDELEAN and V. SEVIANU

1. **Introduction.** The electrical switching phenomenon in some chalcogenide glasses was first reported by Ovshinsky [1]. This effect comprises a sudden increase of magnitude of conductivity when a sufficiently high electric field is applied to the material This low-resistance state (on state) is stable even after the external potential was removed.

Drake et al [2] have observed memory phenomena in oxide glasses ($CuO : P_2O_5$) containing a large proportion of oxide of certain variable valence transition metal ions (Cu^+ and Cu^{2+}) The switching phenomenon in silicate glasses in the presence of Fe_2O_3 clusters was evidenced by Ersov et al [3] Chakravorty [4, 5] has observed such memory switching effects induced in some phase-separated oxide glasses by ion-exchange treatments.

The study of switching phenomenon is important both for his eventual applications and for clearing, and understanding the conduction mechanism in glasses

In this paper we present some results regarding the switching phenomenon evidenced in $xFe_2O_3 \cdot (1-x)[3B_2O_3 \cdot PbO]$ glass system

2 **Experimental.** 2.1 *Glass preparation.* The $xFe_2O_3 \cdot (1-x)[3B_2O_3 \cdot PbO]$ glasses preparation was described previously [6]. The structure has been studied by X–rays [7], I R absorption spectra [6], the Mossbauer effect and electron microscope [8] and by magnetic measurements [9]. These measurements evidenced that the iron ions in $3B_2O_3 \cdot PbO$ glass do not form clusters. The iron cations seem to be randomly distributed in the matrix The measurements based on the Mossbauer effect demonstrated the presence of both the Fe^{3+} and Fe^{2+} ions.

Electrical conductibility measurements indicated a semiconductor behaviour of $xFe_2O_3 \cdot (1-x)[3B_2O_3 \cdot PbO]$ glasses [10].

In order to study the switching phenomenon, samples of thickness of about 20 μm and of dimensions of about 5×5 mm were prepared The measurements were carried out at room temperature.

2 2 *Switching circuit* The block-circuit that we used in order to evidenciate the switching phenomenon is given in Fig. 1. In this circuit we used a dc power supply BM 20S, pulse generator PGP–2 and electronic multimeter E 0403. The impulses are rectangular with an amplitude up to 10 V and a width up to maximum 10 ms

The sample-holder consists of an insulator plated with copper. The contact between the sample and the copper plate was obtained by using silver paste. The other electrode was a silver wire contacting the sample through silver paste. The sample-holder construction is so that the attachment of an upper electrode

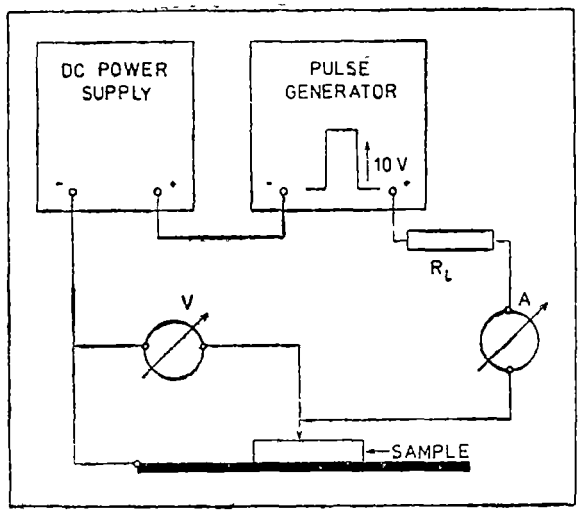

Fig. 1.

allows the application of an electrical field. An electric field of 10^3V/cm was used

3. **Results and discussions.** Measurements on samples in $xFe_2O_3 \cdot (1-x)[3B_2O_3 \cdot PbO]$ glass system lead to voltage-current characteristic specific to the behaviour of glasses which contain transition metal ions in different valency states [2]. Figure 2 shows a typical voltage-current characteristic of samples with 50 mol% Fe_2O_3 upon application a dc field and voltage pulses. The initial resistance of samples was of $1,5 \times 10^9\Omega$ (off state) and at 23 V it switched in a state having resistance of $1,1 \times 10^3\Omega$ (on state). In the main for various samples this jump varied between 10^3 and $10^8\Omega$ (3—8order of magnitude). We noticed that after the transition into the high conductibility state (on state) the sample keeps up this state until the return at zero voltage when it passes again into the low conductibility state (off state).

Both the application of voltage pulses with amplitudes up to 10 V and a width up to 10 ms and of an electrical field of 10^3V/cm determined the switching phenomenon previously described, but the switching voltage was changed depending on these parameters.

We specify that by repeating the jump from on state into off state, the switching voltage does not reproduce exactly, fact evidentiated also by other

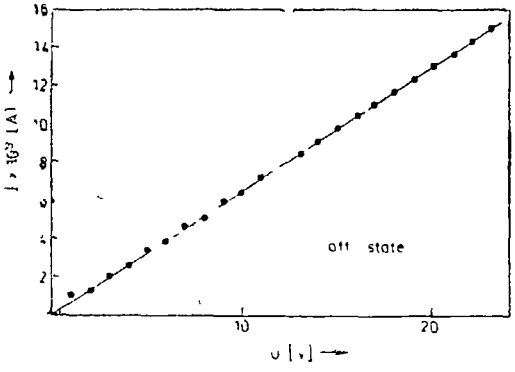

Fig. 2a.

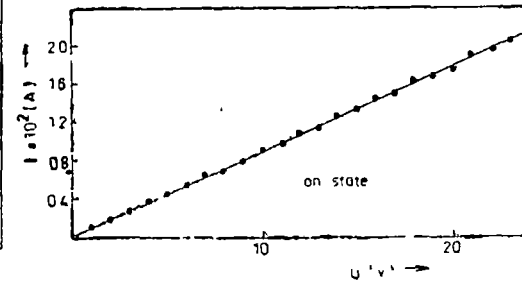

Fig. 2b.

authors [2, 4, 5]. In our samples switching voltage changed between 15 V and 30 V.

4. **Conclusions.** We may conclude that the $xFe_2O_3 \cdot (1-x)[3B_2O_3\ PbO]$ semiconducting glasses show marked deviations from normal semiconductor behaviour. These glasses can be reversibly switched electrically, between two states which differ in resistance by 3—8 orders of magnitude Switching phenomenon can appear with or without applied electrical fields or voltage pulses.

(Received January 20, 1978)

REFERENCES

1. S. R. Ovshinsky, Phys. Rev. Lett **21**, 1450 (1968)
2. C. F. Drake, I. F. Scanlon and A Engel, Phys. sat Solidi **32**, 193 (1969).
3. O. S. Ersov et al., Izv. A. N. SSSR Neorgan. materială, **11**, 939 (1975)
4. D. Chakravorty, Appl. Phys. Lett, **24**, 62 (1974).
5. D Chakravorty and C. S. Murthy, J Phys. D: Appl Phys **8**, L 162 (1975).
6. I. Ardelean et al., Studia Univ Babeş—Bolyai, Phys. **1**, 53 (1977).
7. I. Ardelean and E Indrea, to be published.
8. E. Burzo and I. Ardelean, to be published.
9. I Ardelean, E. Burzo and I. Pop, Solid State comm **23**, 211 (1977).
10. I. Ardelean and V Sevianu, Studia Univ Babeş—Bolyai, Phys, 1, 59 (1978).

FENOMENE DE COMUTARE ELECTRICĂ ÎN SISTEMUL DE STICLE $xFe_2O_3 \cdot (1-x)[3B_2O_3 \cdot PbO]$

(Rezumat)

Sticlele din sistemul $xFe_2O_3 \cdot (1-x)[3B_2O_3 \cdot PbO]$ prezintă fenomenul de comutare reversibil între două stări de conductibilitate a căror rezistență electrică diferă prin 3—8 ordine de mărime. Fenomenul de comutare apare atît în lipsa cît și în prezența cîmpului electric. Prezența cîmpului electric și aplicarea unor pulsuri de tensiune nu schimbă forma caracteristicu volt-amperice dar modifică tensiunea de comutare.

STUDIA UNIV. BABEŞ–BOLYAI, PHYSICA, 2, 1978

SPIN WAVES IN INTERMETALLIC COMPOUNDS $Ho_2Fe_xAl_{17-x}$

V. CRIŞAN

1. Introduction. The intermetallic compounds $Ho_2Fe_xAl_{17-x}$ showing an ferrimagnetic behaviour [1] have an Ni_2Th_{17} type of structure. In each unit cell there are 2 formulae eq. 4 atoms of Ho, $2x$ atoms of Fe, and $2(17-x)$ atoms of Al. In the present calculations $x = 2$ The model used, for spin waves calculation, is shown in fig. 1. The Ho atoms are in $2(b)$ and $2(d)$ positions [2], the atoms of Fe in $2(a)$ and $2(c)$ positions and the positions of Al atoms, which are not shown in the picture, in $12(k)$ $12(j)$ and $6(g)$ [3].

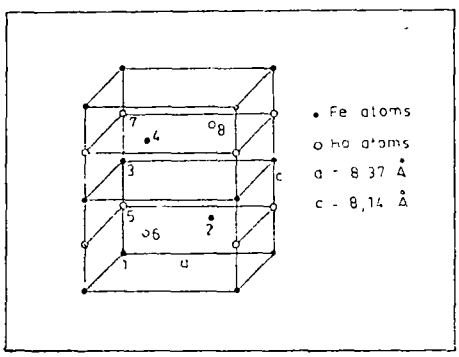

Fig 1

It is convenient to introduce „local coordinate frames" associated with the various spin states. The structure in question contains 4 spins per primitive magnetic unit cell pointing along and 4 spins pointing against the z directions. These spins form 2 sublattices and we use the indices λ and $\lambda'(=1, 2)$ as labels for them. The components of the spin operator for the k th spin in the lth cell and λ th sublattice are denoted by:

$$(S^{\lambda}_{lk,x},\ S^{\lambda}_{lk,y},\ S^{\lambda}_{lk,z})$$

k runs over 1, 2, ...4 for $\lambda = 1$ or 2,

2. The equations of motion. We used a Heisenberg Hamiltonian with isotropic exchange and an effective anisotropic field [4]

$$\mathcal{H} = \frac{1}{2}\left[\sum_{ll'}\sum_{\substack{kk'\\ lk\neq ll'}} \mathcal{J}^{l'k'1}_{lk1}\,\vec{S}^{1}_{lk}\,\vec{S}^{1}_{l'k'} + \sum_{ll'}\sum_{k=1}^{\mu}\sum_{\mathcal{X}=1}^{\nu}\mathcal{J}^{l'\mathcal{X}z}_{lk1}\,(S^{1}_{lk,x}S^{2}_{l'\mathcal{X},x} - S^{1}_{lk,y}S^{2}_{l'\mathcal{X},y} -\right.$$

$$- S^{1}_{lk,z}S^{2}_{l'\mathcal{X},z}) + \sum_{ll'}\sum_{\mathcal{X}=1}^{\nu}\sum_{k=1}^{\mu}\mathcal{J}^{l'k1}_{l\mathcal{X}2}\,(S^{2}_{l'\mathcal{X},x}S^{1}_{l'k,x} - S^{2}_{l\mathcal{X},y}S^{1}_{l'k,y} - S^{2}_{l\mathcal{X},z}S^{1}_{l'k,z}) +$$

$$\left. + \sum_{ll'}\sum_{\substack{\mathcal{X},\mathcal{X}'=1\\ lk\neq l'k'}} \mathcal{J}^{l'\mathcal{X}'2}_{l\mathcal{X}2}\,\vec{S}^{2}_{l\mathcal{X}}\,\vec{S}^{2}_{l'\mathcal{X}'}\right] + \sum_{l}\left[\sum_{k=1}^{\mu}\mu_B g^{1}_{k}H^{1}_{Ak}S^{1}_{lk,z} + \sum_{\mathcal{X}=1}^{\mu}\mu_B g^{2}_{\mathcal{X}}\,H^{2}_{\mathcal{X}k}S^{2}_{l\mathcal{X},z}\right].$$

The quantity H^{λ}_{Ak} denotes the effective anisotropic field associated with the sublattice λ and with the kth atom of the cell, and is directed along the z axis. μ_B is the Bohr magneton and g^{μ}_{k} the g — factor $J^{l'k'\lambda'}_{lk\lambda}$ are the exchange

integral associated with the pair of sites $(lk\lambda,\ l'k'\lambda')$ μ and ν are the number of atoms in the unit cells of the two sublattices. The exchange integrals have translational periodicity and also have permutation symmetry. The negative signs before the y and z — component terms in the second and the third summations arise from the relative orientations of the local frames for the two sublattices 1 and 2. The spin operators will be regarded as expressed in the Heisenberg representation. We suppose that the structure in question contains μ spins per primitive magnetic unit cell pointing along and ν spins pointing against the z direction.

Using the raising and lowering operators $S_+ = S_x \pm iS_y$ the Hamiltonian becomes

$$\mathcal{H} = \frac{1}{2}\Bigg[\sum_{\substack{ll' \\ lk \neq l'k'}}\sum_{kk'} \mathcal{J}^{l'k'1}_{lk1}\left\{S^1_{lk,z}S^1_{l'k',z} + \frac{1}{2}\left(S^1_{lk,+}S^1_{l'k'-} + S^1_{l'k',+}S_{lk,-}\right)\right\} +$$

$$+\sum_{ll'}\sum_{k}\sum_{\mathcal{X}} \mathcal{J}^{l'\mathcal{X}2}_{lk1}\left\{-S^1_{lk,z}S^2_{l'\mathcal{X},z} + \frac{1}{2}\left(S^1_{lk,+}S^2_{l'\mathcal{X},+} + S^1_{lk,-}S^2_{l\mathcal{X},-}\right)\right\} +$$

$$\sum_{ll'}\sum_{\mathcal{X}}\sum_{k} \mathcal{J}^{l'k1}_{l\mathcal{X}2}\left\{-S^2_{l\mathcal{X},z}S^1_{l'k,z} + \frac{1}{2}\left(S^2_{l\mathcal{X},+}S^1_{l'k,+} + S^2_{l\mathcal{X},-}S^1_{l'k,-}\right)\right\} +$$

$$+\sum_{\substack{ll' \\ (l\mathcal{X}\neq l'\mathcal{X}'}}\sum_{\mathcal{X}\mathcal{X}'} \mathcal{J}^{l'\mathcal{X}'2}_{l\mathcal{X}2}\left\{S^2_{l\mathcal{X},z}S^2_{l'\mathcal{X},z} + \frac{1}{2}\left(S^2_{l\mathcal{X},+}S^2_{l'\mathcal{X}',-} + S^2_{l\mathcal{X}k,-}S^2_{l'\mathcal{X}',+}\right)\right\}\Bigg] +$$

$$+\sum_{l}\left[\sum_{k}\mu_B g^1_k H^1_{Ak}S^1_{lk,z} + \sum_{\mathcal{X}}\tilde{\mu}_B g^2_{\mathcal{X}}H^1_{A\mathcal{X}}S^2_{l\mathcal{X},z}\right]$$

Using the following commutation rules:

$$[S^\lambda_{lk,\alpha},\ S^{\lambda'}_{l'k',\beta}] = i\hbar\, S^\lambda_{lk,\gamma}\,\delta_{ll'}\,\delta_{kk'}\,\delta_{\lambda\lambda'} \qquad ((\alpha,\beta,\gamma)\to\text{cyclic }(x,y,z))$$

$$[S^\lambda_{lk,+},\ S^{\lambda'}_{l'k',-}] = 0$$

$$[S^\lambda_{lk,-},\ S^{\lambda'}_{l'k',+}] = 0$$

$$[S^\lambda_{lk,+},\ S^{\lambda'}_{l'k',-}] = 2\hbar\, S^\lambda_{lk,z}\,\delta_{ll'}\,\delta_{kk'}\,\delta_{\lambda\lambda'}$$

$$[S^\lambda_{lk,z},\ S^{\lambda'}_{l'k',\pm}] = \pm\hbar\, S^\lambda_{lk,\pm}\,\delta_{ll'}\,\delta_{kk'}\,\delta_{\lambda\lambda'}$$

the Heisenberg equations are:

$$\pm i\dot{S}^1_{lk,\pm} = -\sum_{\substack{l' \\ l'k'\neq lk}}\sum_{k'=1} \mathcal{J}^{l'k'1}_{lk1}\left\{S^1_{lk,\pm}S^1_{l'k',z} - S^1_{l'k',\pm}S^1_{lk,z}\right\} + \sum_{l'}\sum_{\mathcal{X}=1}^{\nu} \mathcal{J}^{l'\mathcal{X}2}_{lk1}\left\{S^1_{lk,\pm}S^2_{l'\mathcal{X},z} +\right.$$

$$\left. + S^2_{l'\mathcal{X},\mp}S^1_{lk,z}\right\} - \mu_B \underset{k=1,2,\ldots,\mu}{g^1_k H^1_{Ak}S^1_{lk,\pm}};\quad \pm i\dot{S}^2_{l\mathcal{X},\pm} = -\sum_{l'}\sum_{\substack{\mathcal{X}'=1 \\ (l'\mathcal{X}'\neq l\mathcal{X})}} \mathcal{J}^{l'\mathcal{X}'2}_{l\mathcal{X}2}\left\{S^2_{l\mathcal{X},\pm}S^2_{l'\mathcal{X}',z} -\right.$$

$$\left. - S^2_{l'\mathcal{X}',\pm}S^2_{l\mathcal{X},z}\right\} + \sum_{l'}\sum_{k'} \mathcal{J}^{l'k'1}_{l\mathcal{X}2}\left\{S^2_{l\mathcal{X},\pm}S^1_{l'k',z} + S^1_{l'k',\mp}S^2_{l\mathcal{X},z}\right\} - \mu_B \underset{k=1,2,\ldots,\nu}{g^2_k H^2_{Ak}S^2_{l\mathcal{X},\pm}}$$

We now make the linearisation of the above equations That is whenever a product involving $S^{\lambda}_{lk,z}$ and a raising or lowering operator occurs in the above equations, then we replace, $S^{\lambda}_{lk,z}$ by the c — number $S^{\lambda}_{k,0}$ where the latter denotes the equilibrium, spin value for the sublattice $(k\lambda)$. The resulting linearized equations are

$$\pm i S^{\lambda}_{lk,\pm} = -\sum_{\substack{l' \\ (l'k' \neq lk)}} \sum_{k' \in \lambda} \mathcal{J}^{l'k'\lambda}_{lk\lambda} \{S^{\lambda}_{lk,\pm} S^{\lambda}_{k',0} - S^{\lambda}_{l'k',\pm} S^{\lambda}_{k,0}\} + \sum_{l'} \sum_{\substack{k' \in \lambda' \\ \lambda \neq \lambda'}} \mathcal{J}^{l'k'\lambda'}_{lk\lambda} \{S^{\lambda}_{lk,\pm} S^{\lambda'}_{k',0} +$$

$$+ S^{\lambda'}_{l'k',\mp} S^{\lambda}_{k,0}\} - \mu_B \underset{\substack{k=1,2,\\ k=1,2,}}{g^{\lambda}_{k} H^{\lambda}_{Ak} S^{\lambda}_{lk}} \quad \begin{matrix} , \mu \text{ if } \lambda = 1 \\ , \nu \text{ if } \lambda = 2 \end{matrix}$$

The notation $k' \in \lambda$ implies that k' runs over 1, 2, ... μ if $\lambda = 1$ and over 1, 2, ..., ν if $\lambda = 2$.

We now introduce the spectral representations of $S_{\lambda k}(t)$ as follows.

$$S^{\lambda}_{lk,+} = \left[\frac{S^{\lambda}_{k,0}}{N}\right]^{1/2} \sum_{q} S^{\lambda}_{k,+}(q) \exp\left[i\vec{q}\vec{R}(l)\right] = \left[\frac{S^{\lambda}_{k,0}}{N}\right]^{1/2} \int_{-\infty}^{+\infty} d\omega \sum_{q} S^{\lambda}_{k,+}(q, \omega)$$

$$\exp\left(i\left[\vec{q}\vec{R}(l) - \omega t\right]\right)$$

$$S^{\lambda}_{lk,-} = \left[\frac{S^{\lambda}_{k,0}}{N}\right]^{1/2} \sum_{q} S^{\lambda}_{k,-}(-q) \exp\left[i\vec{q}\vec{R}(l)\right] =$$

$$= \left[\frac{S^{\lambda}_{k,0}}{N}\right]^{1/2} \int_{-\infty}^{+\infty} d\omega \sum_{q} S^{\lambda}_{k,-}(-q, -\omega) \exp\left(i\left[\vec{q}\vec{R}(l) - \omega t\right]\right)$$

Here $\vec{R}(l)$ denotes a vector of the primitive magnetic lattice and N is the number of magnetic unit cells in the crystal which, as usually, is presumed to be subject to cyclic boundary conditions. The wavevector $\vec{q}$ ranges over the first Brillouin zone of the magnetic lattice. The factor $\left[\frac{S^{\lambda}_{k,0}}{N}\right]^{1/2}$ has been introduced for normalization convenience.

The equation of motion will be:

$$\omega S^{\lambda}_{k,\pm}(\pm q, \pm\omega) = \pm\left[\sum_{k' \in \lambda} D(q, kk'\lambda\lambda') S^{\lambda}_{k',\pm}(\pm q, \pm\omega) + \sum_{\substack{k' \in \lambda' \\ (\lambda \neq \lambda')}} D(q, kk'\lambda\lambda')\right.$$

$$\left. S^{\lambda'}_{k',\mp}(\mp q, \mp\omega)\right]$$

where

$$D(\vec{q}, kk'\lambda\lambda') = [S^{\lambda}_{k,0} S^{\lambda'}_{k,0}]^{1/2} \mathcal{J}^{k'\lambda'}_{k\lambda}(q) - \delta_{\lambda\lambda'} \delta_{kk'} \times \{g^{\lambda}_{k} \mu_B H^{\lambda}_{Ak} + \sum_{k'' \in \lambda} \mathcal{J}^{k''\lambda}_{k\lambda}(0) S^{\lambda}_{k'',0} -$$

$$- \sum_{\substack{k'' \in \lambda'' \\ (\lambda'' \neq \lambda)}} \mathcal{J}^{k''\lambda''}_{k\lambda}(0) S^{\lambda''}_{k'',0}\}, \quad \mathcal{J}^{k''\lambda}_{k\lambda}(q) = \sum_{l} \mathcal{J}^{l'k'\lambda'}_{lk\lambda} \exp(i\vec{q}[\vec{R}(l') - \vec{R}(l)])$$

$D(q, kk'\lambda\lambda')$ is a $2(\mu + \nu)$ dimensional matrix for which we have to solve the eigenvalue problem

3. **Numerical results.** The numerical calculation was performed in the vicinity of Γ using the following approximations: $\mathcal{J}_{ik\lambda}^{i'k'\lambda'} = J_{HH}$ = exchange integrals between Ho atoms are constant for any $kk'll'$ ($\lambda = \lambda' = 2$). For $\lambda = \lambda' = 1$ the exchange integrals between Fe atoms J_{FF} are constants for any $kk'll'$. The same approximation is valid for the intersublattice interactions J_{FH}.

In fig. 2 is shown the spin vaves spectrum for different values of exchange parameters.

fig 2*a*: $J_{HH}/J_{FF} = 0.18$, $J_{FH}/J_{FF} = -0.25$

fig. 2*b* $J_{HH}/J_{FF} = 0.18$, $J_{FH}/J_{FF} = -0.50$

fig. 2*c*. $J_{HH}/J_{FF} = 0.18$, $J_{FH}/J_{FF} = -0.75$

fig. 2*d*: $J_{HH}/J_{FF} = 0.20$, $J_{FH}/J_{FF} = -0.75$

and

$$\frac{g_k^\lambda \mu_B H_{Ak}^\beta}{\mathcal{J}_{FF}} = 7.45 \text{ for all } k \text{ an } \lambda.$$

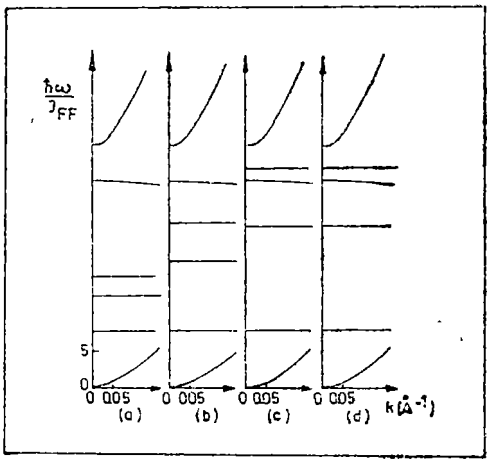

Fig 2

The branches from 14 in fig 2*a*, 2*l* in fig. 2*b*, 28 in fig 2*c* and fig. 2*d* are degenerates. The branch number 8 has the values between 10^8 and 10^{10} and was not drawn in the pictures.

The author wants to thank prof Iuliu Pop for helpful discussion on the subject

(Received January 24, 1978)

REFERENCES

1 Z. Gulacs, M. Popescu, I. Rus, Studia Univ. Babeş–Bolyai, Phys., **1**, 63 (1978)
2 Perrson, *A hand of Latt spacings and Structure of met and alloys*, vol 2 Oxford, 1967
3 *International tables for X-ray crystallography*, vol I, Ed. The Kynach Press Birmingham, England, 1952
4 V C Sahni, G Venkatarman, Adv Phys, **23**, 547 (1974)

UNDE DE SPIN ÎN COMPUŞII INTERMETALICI $Ho_2Fe_xAl_{17-x}$

(Rezumat)

Folosind metoda ecuaţiilor de mişcare, se calculează spectrul undelor de spin în compusul intermetalic $Ho_2Fe_2Al_{15}$. S-au obţinut opt ramuri una acustică şi şapte optice Calculele numerice au fost făcute pentru lungimi de undă mari ($k \to 0$)

STUDIA UNIV. BABEŞ–BOLYAI, PHYSICA, 2, 1978

INSTABILITY OF CIRCULARLY POLARIZED ELECTROMAGNETIC WAVES IN THE RELATIVISTIC ELECTRON BEAM-PLASMA SYSTEM

J. KARÁCSONY

The study of the wave instability in the electron beam-plasma system is the subject of many investigations. However, most of these works are restricted only to the treatment of the electrostatic instability Our aim is to examine the stability of the electromagnetic waves propagating parallel to the beam direction into a relativistic electron beam-plasma system immersed in a magnetic field

In most experimental situations, the relativistic electron beam propagates parallel to the external magnetic field, therefore it is important to consider this case for a theoretical study. Unlike the other papers concerned with the study of electron beam-plasma interaction and which neglect the self-magnetic field of the beam, in our paper, to avoid any contradiction with Maxwell's equations, arising from the omission of this self-magnetic field, we will assume that in the plasma there is a homogeneous return current. It is well-known that an intense relativistic electron beam can propagate in the presence of a dense plasma by inducing a plasma return current which is approximately equal and opposite to the beam current [1—4]. In this way the self-magnetic field of the system is nearly zero, but on the other hand in the unperturbed state the plasma electrons are no more at rest, so the plasma contains a current flow.

In our model, we will consider a relativistic electron beam having the number density of electrons n_{bo} and the average velocity of electrons $\vec{v}_0$ oriented parallel to the external magnetic field $\vec{B}_0$. This magnetic field is assumed to be oriented along the positive Oz axis, $\vec{B}_0 = B_0\vec{e}_z$ ($\vec{e}_z$ is the basic vector of Oz-axis.) The unperturbed plasma electron mean velocity $\vec{v}_1$, producing the return current, is oriented in opposite direction to the beam electron velocity and it is equal with $-(n_{bo}/n_0)\vec{v}_0$. (n_0 is the plasma electron density and it satisfies the condition $n_0 \gg n_{bo}$) The last expression for plasma electron mean velocity results from the current neutralization condition

$$\vec{j}_{bo} + \vec{j}_{po} = 0 \tag{1}$$

where $\vec{j}_{bo}$ and $\vec{j}_{po}$ denote the unperturbed beam current density and plasma current density, respectively. Since we are concerned with high frequency oscillations we will assume the positive ion at rest, they only forming a stationary background of charge which neutralizes the unperturbed electron gas at each point.

The stability of the oscillations can be investigated by solving the dispersion relation that we will obtain in the following way.

The linearized equation of motion is

$$\left(\frac{\partial}{\partial t}+\vec{v}_0\cdot\nabla\right)\left[\frac{\vec{v}'}{\sqrt{1-v_0^2/c^2}}+\frac{\vec{v}_0(\vec{v}_0\cdot\vec{v}')}{c^2(1-v_0^2/c^2)^{3/2}}\right]=-\frac{e}{m}\left[\vec{E}+\frac{1}{c}[\vec{v}<\vec{B}_0\right)+\frac{1}{c}(\vec{v}_0\times\vec{B}')] \quad (2)$$

for the beam electrons, and

$$\left(\frac{\partial}{\partial t}+\vec{v}_1\cdot\nabla\right)\vec{v}_1'=-\frac{e}{m}\left[\vec{E}'+\frac{1}{c}(\vec{v}_1'\times\vec{B}_0)+\frac{1}{c}(\vec{v}_1\times\vec{B}')\right] \quad (3)$$

for the plasma electrons. In these equations the perturbed electric field, magnetic field and velocities are denoted by $\vec{E}'$, $\vec{B}'$, $\vec{v}'$ and $\vec{v}_1'$, respectively For plane waves of the form $\exp[i(\omega t-kz)]$ the perturbed velocities for the beam and plasma are:

$$v_x'=\frac{ie\gamma_0(\omega-kv_0)}{m\omega[(\omega-kv_0)^2-\omega_c^2\gamma_0^2]}[(\omega-kv_0)E_x'+i\omega_c\gamma_0E_y'] \quad (4)$$

$$v_y'=\frac{ie\gamma_0(\omega-kv_0)}{m\omega[(\omega-kv_0)^2-\omega_c^2\gamma_0^2]}[-i\omega_c\gamma_0E_x'+(\omega-kv_0)E_y'] \quad (5)$$

$$v_z'=\frac{ie\gamma_0^3}{m(\omega-kv_0)}E_z' \quad (6)$$

$$v_{1x}'=\frac{ie(\omega+kv_1)}{m\omega[(\omega+kv_1)^2-\omega_c^2]}[(\omega+kv_1)E_x'+i\omega_cE_y'] \quad (7)$$

$$v_{1y}'=\frac{ie(\omega+kv_1)}{m\omega[(\omega+kv_1)^2-\omega_c^2]}[-i\omega_cE_x'+(\omega+kv_1)E_y'] \quad (8)$$

$$v_{1z}'=\frac{ie}{m(\omega+kv_1)}E_z' \quad (9)$$

In the above expressions $\omega_c=eB_0/mc$ is the cyclotron frequency and

$$\gamma_0=\sqrt{1-v_0^2/c^2}$$

From Maxwell's equations we obtain the wave equation

$$\frac{\partial^2\vec{E}'}{\partial^2t}+c^2\nabla\times(\nabla\times\vec{E}')=-4\pi\frac{\partial(\vec{j}_b'+\vec{j}_p')}{\partial t} \quad (10)$$

which becomes

$$(k^2c^2-\omega^2)\vec{E}'-\vec{k}c^2(\vec{k}\cdot\vec{E}')=-4\pi i\omega(\vec{j}_b'+\vec{j}_p') \quad (11)$$

for plane waves. The perturbed currents $\vec{j}_b'$ and $\vec{j}_p'$ are of the form

$$\vec{j}_b'=-e(n_{b0}\vec{v}'+n_b'\vec{v}_0) \quad (12)$$

$$\vec{j}_p'=-e(n_0\vec{v}_1'+n'\vec{v}_1) \quad (13)$$

From the continuity equations, the perturbed beam density n_b' and the perturbed plasma density n' are:

$$n_b' = \frac{n_{b0}\, kv_x'}{\omega - kv_0} \tag{14}$$

and

$$n' = \frac{n_0 kv_{1x}'}{\omega + kv_1} \tag{15}$$

respectively.

Combining equations (4)—(15), we then obtain

$$\begin{pmatrix} D_{11} & D_{12} & 0 \\ D_{12}^* & D_{22} & 0 \\ 0 & 0 & D_{33} \end{pmatrix} \cdot \begin{pmatrix} E_x \\ E_y \\ E_z \end{pmatrix} = 0 \tag{16}$$

where

$$D_{11} = D_{22} = c^2k^2 - \omega^2 + \frac{\omega_{b\perp}^2 (\omega - kv_0)^2}{(\omega - kv_0)^2 - \omega_c^2\gamma_0^2} + \frac{\omega_p^2(\omega + kv_1)^2}{(\omega + kv_1)^2 - \omega_c^2} \tag{17}$$

$$D_{12} = i\, \frac{\omega_c \gamma_0 \omega_{b\perp}^2 (\omega - kv_0)}{(\omega - kv_0)^2 - \omega_c^2\gamma_0^2} + i\, \frac{\omega_c \omega_p^2 (\omega + kv_1)}{(\omega + kv_1)^2 - \omega_c^2} \tag{18}$$

$$D_{33} = -\omega^2 + \frac{\omega_{b\|}^2 \omega^2}{(\omega - kv_0)^2} + \frac{\omega_p^2 \omega^2}{(\omega + kv_1)^2} \tag{19}$$

The D_{12}^* term in expression (16) is the complex conjugates of D_{12} The electron plasma frequency, transverse beam frequency, and longitudinal beam frequency are $\omega_p^2 = 4\pi n_0 e^2/m$, $\omega_{b\perp}^2 = 4\pi n_{b0} e^2 \gamma_0/m$ and $\omega_{b\|}^2 = 4\pi n_{b0} e^2 \gamma_0^3/m$, respectively

Since $D_{13} = D_{23} = 0$ the expression (16) yields

$$\omega^2 - \frac{\omega_{b\|}^2 \omega^2}{(\omega - kv_0)^2} - \frac{\omega_p^2 \omega^2}{(\omega + kv_1)^2} = 0 \tag{20}$$

from $D_{33} = 0$ and

$$c^2k^2 - \omega^2 + \frac{\omega_{b\perp}^2 (\omega - kv_0)^2}{(\omega - kv_0)^2 - \omega_c^2\gamma_0^2} + \frac{\omega_p^2(\omega + kv_1)^2}{(\omega + kv_1)^2 - \omega_c^2} = \mp$$

$$\mp \left[\frac{\omega_c \gamma_0 \omega_{b\perp}^2 (\omega - kv_0)}{(\omega - kv_0)^2 - \omega_c^2\gamma_0^2} + \frac{\omega_c \omega_p^2 (\omega + kv_1)}{(\omega + kv_1)^2 - \omega_c^2} \right] \tag{21}$$

from $(D_{11}D_{22} - D_{12}D_{12}^*) = 0$.

The equation (20) is the electrostatic dispersion relation and from (21) we obtain the dispersion relations for right-handed and respectively left-handed polarized waves, under the following forms

$$\omega^2 - k^2c^2 - \frac{\omega_p^2(\omega + kv_1)}{\omega + kv_1 - \omega_c} - \frac{\omega_{b\perp}^2(\omega - kv_0)}{\omega - kv_0 - \omega_c\gamma_0} = 0 \tag{22}$$

$$\omega^2 - k^2c^2 - \frac{\omega_p^2(\omega + kv_1)}{\omega + kv_1 + \omega_c} - \frac{\omega_{b\perp}^2(\omega - kv_0)}{\omega - kv_0 + \omega_c\gamma_0} = 0 \tag{23}$$

Both the equations (22) and (23) can be represented as

$$F_p + \varepsilon F_b = 0 \tag{24}$$

where

$$F_p = \omega^2 - k^2c^2 - \frac{\omega_p^2(\omega + kv_1)}{\omega - kv_1 \mp \omega_c} \tag{25}$$

$$F_b = -\frac{\gamma_0\omega_p^2(\omega - kv_0)}{\omega - kv_0 \mp \omega_c\gamma_0} \tag{26}$$

and the upper or lower sign corresponds to the right or left-handed circularly polarized waves, respectively.

The expression F_p does not depend on the parameters of the beam and hence the equality

$$F_p = 0 \tag{27}$$

represents the dispersion equation for the plasma waves which can be transmitted through the plasma in the absence of the beam. The expression εF_b represents the perturbation produced by the beam. Since it has been assumed that $n_{b0} \ll n_0$ which is equivalent to $\varepsilon \ll 1$, and if the expression F_b is bounded, then for sufficiently small values of ε, the contribution of the εF_b term to the dispersion equation (24) is negligible. Thus the effect of the beam is singificant only in the neighbourhood of singularities of the expression F_b. Motivated by this consideration, those waves will be analyzed according to the fact whether they satisfy the condition.

$$\omega = kv_0 \pm \omega_c\gamma_0 + \eta \tag{28}$$

where

$$|\eta| \ll |kv_0 \pm \omega_c\gamma_0| \tag{29}$$

An instability occurs when $\mathrm{Im}\eta < 0$ and $|\mathrm{Im}\eta|$ denotes the rate of growth of the excited wave.

Approximating F_p in the neighbourhood of $\omega = kv_0 \pm \omega_c\gamma_0$ by Taylor series and retaining the first two terms in the series, we obtain:

$$(F_p)_{\omega = kv_0 \pm \omega_c\gamma_0 + \eta} = (F_p)_{\omega = kv_0 \pm \omega_c\gamma_0} + \eta(\partial F_p/\partial\omega)_{\omega = kv_0 \pm \omega_c\gamma_0} \tag{30}$$

Inserting this expression toghether with (28) into the dispersion equation (24), it results:

$$\eta^2(\partial F_p/\partial\omega)_{\omega = kv_0 \pm \omega_c\gamma_0} + \eta(F_p)_{\omega = kv_0 \pm \omega_c\gamma_0} \mp \varepsilon\gamma_0^2\omega_p^2\omega_c = 0 \tag{31}$$

The discriminant of (31) is

$$\Delta = [(F_p)_{\omega = kv_0 \pm \omega_c\gamma_0}]^2 \pm 4\varepsilon\gamma_0^2\omega_p^2\omega_c(\partial F_p/\partial\omega)_{\omega = kv_0 \pm \omega_c\gamma_0} \tag{32}$$

In order to exist an instability this discriminant must be negative. The expression (32) is negative if we have the following inequalities:

$$(\partial F_p/\partial\omega)_{\omega = kv_0 + \omega_c\gamma_0} < 0 \tag{33}$$

and

$$\frac{[(F_p)_{\omega = kv_0 + \omega_c\gamma_0}]^2}{|(\partial F_p/\partial\omega)_{\omega = kv_0 + \omega_c\gamma_0}|} < 4\varepsilon\gamma_0^2\omega_p^2\omega_c \tag{34}$$

for right-handed polarized waves, and

$$(\partial F_p/\partial\omega)_{\omega = kv_0 - \omega_c\gamma_0} > 0 \tag{35}$$

and

$$\frac{[(F_p)_{\omega = kv_0 - \omega_c\gamma_0}]^2}{(\partial F_p/\partial\omega)_{\omega = kv_0 - \omega_c\gamma_0}} < 4\varepsilon\gamma_0^2\omega_p^2\omega_c \tag{36}$$

for left-handed polarized waves

Since ε is very small the inequalities (34) and (35) are satisfied only when

$$(F_p)_{\omega = kv_0 \pm \omega_c\gamma_0} \approx 0 \tag{37}$$

The expression (37) shows that the beam electron cyclotron frequency as seen by a stationary observer, $kv_0 + \omega_c\gamma_0$, must be in the immediate neighbourhood of the roots of the equation $F_p(\omega, \vec{k}) = 0$. This condition signifies a resonance between the cyclotron frequency of the electrons in the beam and the frequency of plasma waves.

Inserting (37) in the equation (31), we obtain for the rate of growth the following expression

$$Im\eta = \left| \frac{\varepsilon\gamma_0^2\omega_p^2\omega_c}{(\partial F_p/\partial\omega)_{\omega = kv_0 \pm \omega_c\gamma_0}} \right|^{1/2} \tag{38}$$

the plus and minus sign corresponding to the right or left-handed circularly polarized waves, respectively.

We will now discuss the implications of the relation (33). Taking into account the expression (25), we obtain:

$$\left[2\omega + \frac{\omega_p^2\omega_c}{(\omega + kv_1 - \omega_c)^2}\right]_{\omega = kv_0 + \omega_c\gamma_0} < 0 \tag{39}$$

The above inequality can be satisfied only if ω takes negative values, therefore $kv_0 + \omega_c\gamma_0$ must be negative This expression becomes negative if $v_0 < -c\omega_c/\sqrt{k^2c^2 + \omega_c^2}$, that is for the beam propagating in the direction opposite to that of $\vec{B}_0$. Because the phase velocity ω/k of correspondent waves has a negative sign, it follows that these waves will propagate in the same direction as the beam.

Consequently, an electron beam may excite a right-handed circularly polarized electromagnetic wave in the relativistic electron beam-plasma system if the beam moves in the same direction as the wave and both propagate in the opposite direction to that of the external magnetic field Since the phase velocity of the excited waves is lower than that of the beam, the physical mechanism responsible for their excitation is the anomalous Doppler effect.

A similar discussion applied to the relation (35) shows that a relativistic electron beam can excite a left-handed circularly polarized wave in the plasma if the beam moves in the same direction as the wave, and both propagate in the direction of the external magnetic field. The physical mechanism responsible for the instability is also the anomalous Doppler effect.

(Received January 26, 1978

REFERENCES

1. J. L. Cox and W. H. Bennett, Phys Fluids, **13**, 182 (1970).
2. D A. Hammer and N Rostoker, Phys Fluids, **13**, 1831 (1970)
3. R. Lee and R N Sudan, Phys. Fluids, **14**, 1213 (1971)
4 K R. Chu and N Rostoker, Phys. Fluids, **16**, 1472 (1973)

INSTABILITATEA UNDELOR ELECTROMAGNETICE CIRCULAR POLARIZATE ÎN SISTEMUL FASCICUL RELATIVIST DE ELECTRONI-PLASMĂ

(Rezumat)

Se studiază undele electromagnetice circular polarizate în sistemul fascicul relativist de electroni-plasmă, aflat într-un cîmp magnetic omogen Ţinînd cont de existenţa curentului invers indus în plasmă, se determină condiţiile în care pot fi excitate undele polarizate la dreapta şi cele polarizate la stînga.

STUDIA UNIV BABEŞ–BOLYAI, PHYSICA, 2, 1978

PROPRIETĂŢILE STRUCTURALE ŞI CATALITICE ALE OXIZILOR DE ALUMINIU PROMOTAŢI CU CeO_2(II)

IULIU POP, VASILE CRIŞAN, NICOLAE DULĂMIŢĂ, RENATE GOSS, LIVIA DĂRĂBAN

1. **Introducere.** Modificările sturcturale şi proprietăţile catalitice ale oxidului de aluminiu promotat cu CeO_2 obţinut prin descompunerea termică a hidroxidului de aluminiu, depind esenţial de condiţiile în care s-a obţinut şi s-a tratat termic hidroxidul de aluminiu

Folosind tehnica difracţiei de raza X, în oxizii de aluminiu promotaţi cu CeO_2 s-au identificat o serie de modificări structurale. Alături de rezultatele structurale, în lucrare se mai prezintă date referitoare la suprafaţa specifică şi distribuţia de pori în catalizatorul solid.

2. **Prepararea probelor.** Probele studiate de oxizi de aluminiu promotaţi cu CeO_2, au fost obţinute prin calcinarea hidroxizilor de aluminiu la temperatura de 823 K Hidroxizii de aluminiu au fost obţinuţi în prezenţa a 200 cm^3 de glicol la temperatura de 295 K (denumite probe cu glicol la rece) o serie, şi altă serie la temperatura de 328 K (denumite probe cu glicol la cald), substanţele de pornire fiind azotatul de aluminiu şi azotatul de ceriu [1]. În funcţie de cantitatea de azotat de ceriu utilizată, în oxizii de aluminiu rezultaţi apar diferite cantităţi de CeO_2 Astfel, în cele două serii de probe, cu glicol la rece şi la cald, pentru simplitate s-au introdus notaţiile la, 1b şi 1c, corespunzător conţinutului de CeO_2 de 10, 20, 30% şi analog 2a, 2b, 2c, 2d pentru concentraţia de 0; 10, 20, 30% CeO_2

3. **Tehnica experimentală.** Spectrele de raze X au fost obţinute cu un spectrometru tip TUR–M62, folosind radiaţia $K\alpha$ a unui anod de Cu cu lungimea de undă $\lambda = 1{,}5418$ Å prin filtru de Ni în camera Debye-Scheerer. Indexarea liniilor de pe rontgenogramă s-a făcut prin metoda analitică Suprafaţa specifică şi microporozitatea (5–300 Å) s-au determinat cu ajutorul instalaţiei BET. Porii cu dimensiunile cuprinse între 150 şi 75 000 Å au fost măsuraţi cu ajutorul unui porozimetru cu mercur de tip Carlo-Erba (1–1 000 at) [2]

4. **Rezultate şi concluzii.** Proba la cuprinde un amestec de două faze cu simetrie cubică caracterizate prin parametrii de reţea $a = 5{,}41$ Å, respectiv 7,69 Å Faza cu $a = 5{,}41$ Å corespunde modificării αCeO_2, iar faza cu $a = 7{,}69$ Å modificării η-aluminei Liniile intense cu indicii Miller 400 şi 440, caracteristice η-aluminei [2] apar la 1,92 Å şi 1,24 Å (vezi tabelul 1)

Proba 1b constă tot din amestecul a două faze cu simetrie cubică, caracterizate prin parametrii de reţea $a = 4{,}67$ Å, corespunzător modificaţiei αCeO_2 şi $a = 8{,}16$ Å corespunzător modificaţiei ηAl_2O_3 (vezi tabelul 2).

Tabel 1

10% CeO_2

Nr.	Int	d[A°]	hkl CeO_2	hkl Al_2O_3
1	s	2.8770	1 0 0	
2	s	2 5359		3 0 0
3	ffi	2.1913	2 1 1	
4	fi	2 1320		3 2 0
5	fi	1.9258	2 2 0	4 0 0
6	s	1 8175	3 0 0	4 1 1
7	m	1.5466		4 3 0
8	i	1.3612	4 0 0	4 4 0
9	m	1 2636		6 1 0
10	i	1.1590	3 3 4	
11	s	1.1263		6 3 1
12	m	1.1001		7 0 0
	a[Å]		5 41	7 69

Tabel 2

20%CeO_2

Nr	Int	d[A°]	hkl CeO_2	hkl Al_2O_3
1	s	3 0793	1 1 0	
2	fi	2 0798	2 1 0	
3	i	2 0405		4 0 0
4	s	1.8736	2 1 1	3 3 1
5	s	1 6210	2 2 0	
6	i	1 4271	3 1 1	4 3 3
7	s	1 3117	3 2 0	
8	i	1 2070		6 3 1
9	s	1 1391	4 1 0	7 1 1
	a[Å]		4.67	8.16

În mod analog, proba 1c cuprinde amestecul a două faze cu simetrie cubică cu parametrii a = 5,38 Å, corespunzător modificației αCeO_2 și a = 7,68 Å, corespunzător modificației ηAl_2O_3 (tabelul 3).

Tabloul structural al probelor din seria cu glicol la cald apare modificat și mai complex față de cele cu glicol la rece. Proba fără bioxid de ceriu, 2a, constă dintr-un amestec de două faze, una cubică cu parametrul de rețea a = 7,894 Å, corespunzătoare modificației ηAl_2O_3 și alta tetragonală cu parametrii a = 3,2 Å și c = 2,9 Å, corespunzătoare modificației $\gamma' Al_2O_3$ (vezi tabelul 4).

Tabel 3

30%CeO_2

Nr	Int	d[A°]	CeO_2 hkl	Al_2O_3 hkl
1	s	3 1759		2 1 1
2	m	2 7227		2 2 0
3	fi	2 4362		3 0 1
4	i	2 3742	2 1 1	
5	i	2.1130	2 2 0	3 0 2
6	fs	2 0021	2 2 1	3 2 1
7	fs	1 9297		4 0 0
8	fs	1 8416	3 0 1	
9	fs	1 6184	3 0 2	
10	fs	1 5350		5 0 0
11	i	1 4570	4 0 0	
12	s	1 4062		5 2 1
13	s	1 3326		5 0 3
14	m	1 2198		6 2 0
15	s	1 1601		6 2 2
		a[Å]	5.38	7.68

Tabel 4

0% CeO_2

Nr	Int.	d[A°]	ηAl_2O_3 hkl	γAl_2O_3
1	ffs	3 4800	2 1 0	
2	ffs	3 2094	2 1 1	
3	ffs	2 8839		1 0 0
4	fi	2 4170		1 1 0
5	i	2 1280	3 2 1	
6	fi	1 8200	3 3 1	1 1 1
7	s	1 6750	3 3 2	
8	s	1 5850	4 3 0	2 0 0
9	i	1 4590		2 1 0
10	fs	1 4010	4 4 0	2 1 0
11	s	1 3380	5 3 1	
12	i	1 2251		2 1 1
13	i	1 1656		2 2 0
		a[Å]	7 894	3.2

Proba 2b cuprinde un amestec de trei faze: două faze cu structura de simetrie cubică, avînd parametrii a = 8,132 Å şi a = 4,20 Å, corespunzător modificaţiei ηAl_2O_3, şi respectiv αCeO_2, iar faza a treia cu structura tetragonală, caracterizată prin valorile parametrilor a = 3,03 Å şi c = 3,62 Å, corespunzător modificaţiei $\gamma' Al_2O_3$ (vezi tabelul 5).

Tabel 5

10%CeO_2

Nr	Int.	d[A°]	ηAl_2O_3 hkl	CeO_2 hkl	$\gamma' Al_2O_3$ hkl
1	fs	4 008	2 0 0		
2	fs	3 0354		2 0 0	1 0 0
3	fs	2 6961	3 0 0	2 1 0	
4	s	2 4727	3 1 1	2 1 1	
5	s	2 1110			1 1 0
6	m	2.0429	4 0 0	3 0 0	
7	i	1.8468			1 1 1
8	m	1 8294	4 2 0	3 1 1	
9	i	1 6300	4 3 0	3 2 1	
10	ffs	1.5267		4 0 0	2 0 0
11	ffs	1 4999	4 3 2		
12	ffs	1.4375	4 4 0	4 1 1	
13	m	1 3104			2 1 0
14	m	1.1694	7 0 0	5 1 1	2 2 0
15	fs	0 1084	7 2 1	5 2 1	2 2 0
	a[Å]		8 132	4 20	3.03
	c[Å]				3 62

Pentru probele 2c şi 2d compoziţia structurală este analogă probei 2b, însă din cauza conţinutului mărit de CeO_2 valorile parametrilor reticulari pentru fazele cubice şi tetragonală sînt diferite. Astfel, proba 2c are parametrii a = = 7,887 Å corespunzător modificaţiei ηAl_2O_3 şi a = 5,495 Å corespunzător modificaţiei αCeO_2, iar a = 4,14 Å şi c = 3,266 Å corespunzător modificaţiei $\gamma' Al_2O_3$ (vezi tabelul 6).

Tabel 6

20%CeO_2

Nr	Int	d[A°]	ηAl_2O_3 hkl	CeO_2 hkl	$\gamma' Al_2O_3$
1	m	3.1399		1 1 1	1 0 0
2	fs	2.7281		2 0 0	
3	fi	1.8974	4 1 0		
4	s	1.8364			1 1 1
5	fi	1 6380			2 0 0
6	ffs	1.3974	4 4 0	4 0 0	2 1 0
7	s	1.3042	6 1 0		2 1 1
8	m	1.1717	6 3 0		
	a[Å]		7.887	5.495	3 14
	c[Å]				3 266

În cazul probei 2d valorile parametrilor pentru modificațiile similare sînt a = 8,058 Å pentru ηAl_2O_3; a = 5,36 Å pentru αCeO_2 și a = 2,721 Å; c = = 3,329 Å pentru modificația $\gamma' Al_2O_3$ (vezi tabelul 7).

Tabel 7

(30 % CeO_2)

Nr	Int	d[A°]	ηAl_2O_3 hkl	CeO_2 hkl	$\gamma' Al_2O_3$ hkl
1	ss	3.1322		1 1 1	
2	s	2.7146	3 0 0	2 0 0	1 0 0
3	fs	2 3562		2 1 0	
4	fs	2.1031			1 1 0
5	fs	2 0147	4 0 0		
6	fs	1.8956	4 1 1	2 2 0	
7	fi	1.8451			
8	i	1.7975	4 2 0	3 0 0	
9	fs	1 6106	4 3 0	3 1 1	
10	fs	1.5191			
11	fs	1 4756	5 2 1	3 2 0	
12	fs	1 4428		3 2 1	1 0 2
13	fs	1.3896	5 3 0		2 0 0
14	s	1 3054	5 3 2	4 1 0	
15	fs	1 2811			7 1 2
16	fs	1 2198	6 2 2		2 1 0
17	i	1 1682		4 2 1	
18	s	1 0923		4 2 2	
a[Å]			8.058	5 36	2 721
c[Å]					3 392

Dependența sistematică a parametrilor reticulari pentru modificațiile structurale observate în funcție de concentrația adaosului de CeO_2 în oxizii de aluminiu, este reprezentată în figura 1, pentru setul de probe cu glicol la rece, și în figura 2, pentru setul de probe cu glicol la cald.

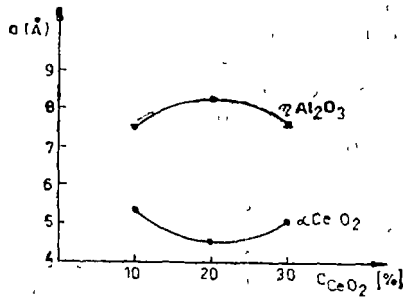

Fig. 1.

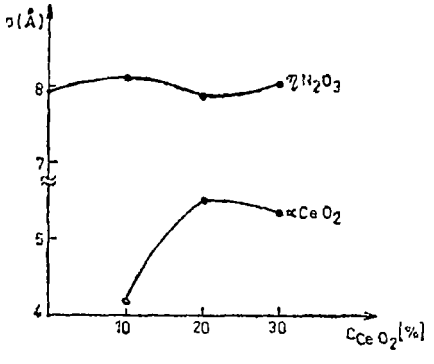

Fig. 2.

În figura 3 este redată dependența volumului celulei tetragonale de concentrație în CeO_2 pentru setul de probe cu glicol la cald

Dependența suprafeței specifice de concentrația de CeO_2 pentru ambele seturi de probe este ilustrată în figura 4, pentru probele cu glicol la rece, iar în figura 5 pentru cele cu glicol la cald

Variația volumului total al porilor în funcție de concentrația în CeO_2 pentru ambele seturi de probe este prezentată în figurile 6 și 7

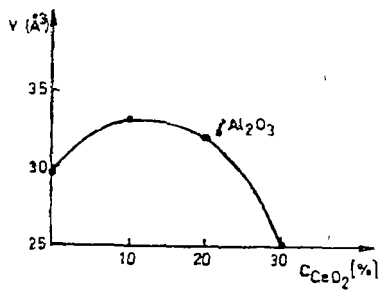

Fig. 3

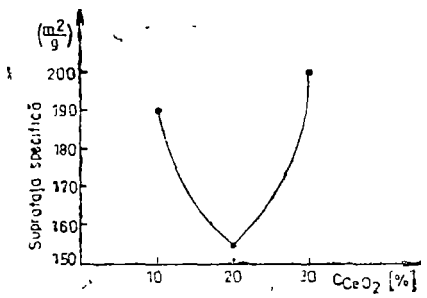

Fig 4

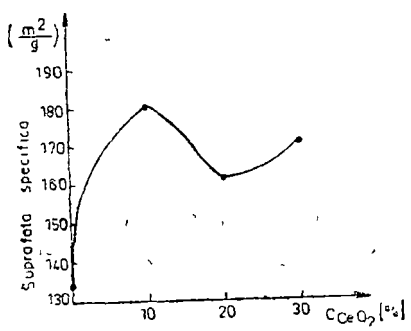

Fig 5

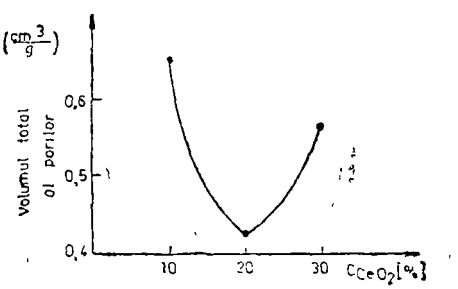

Fig. 6

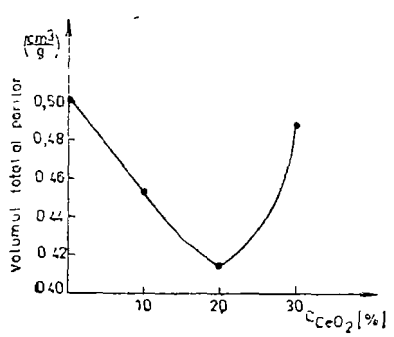

Fig 7

Corelînd datele structurale cu cele catalitice rezultă un model de interpretare al rezultatelor prezentate mai sus Dilatația celulei cristaline sau creșterea parametrilor de rețea duce la micșorarea corespunzătoare a volumului porilor catalizatorilor și implicit a parametrilor caracteristici, adică a suprafeței specifice. Această concluzie este valabilă în condițiile în care prevalează microporii (5—300 Å) pe lîngă numărul total constant al porilor din probă (cazul cînd nu apar pori suplimentari).

În cazul macroporilor (300—75 000 Å) o dilatație a celulei cristaline poate duce la o transformare a macroporilor în micropori și deci la scăderea volumului total al porilor și concomitent la o creștere a suprafeței specifice

Suprafața specifică a modificațiilor ηAl_2O_3 și $\gamma' Al_2O_3$ este mult mai mare decît pentru αCeO_2.

În felul acesta, rezultatele obținute de noi pun în evidență o transformare a macroporilor în micropori pentru setul de probe cu glicol la cald în intervalul de concentrație de CeO_2 cuprins între 0 și 10% αCeO_2

Pentru setul de probe cu glicol la rece, cu concentrațule între 10 și 20% αCeO_2, apare o creștere a parametrului de rețea pentru modificația ηAl_2O_3 de la 7,69 Å la 8,16 Å și o scădere a parametrului pentru αCeO_2 de la 5,41 Å la 4,67 Å. Luînd în considerare valorile suprafeței specifice de aproximativ 170 m^2/g pentru ηAl_2O_3 și 50 m^2/g pentru CeO_2, în ansamblu rezultă o creștere a parametrului de rețea însoțită de o micșorare a volumului porilor și a suprafeței specifice. Între concentrațiile de 20% și 30% se obține o scădere a parametrului reticular pentru modificația ηAl_2O_3 de la 8,16 Å la 7,68 Å și o creștere de parametru pentru αCeO_2 de la 4,67 Å la 5,38 Å. Rămîne însă preponderentă variația rețelei pentru Al_2O_3. Astfel, prin contracția rețelei se obține o creștere a volumului porilor și implicit a suprafeței specifice

Pentru setul de probe cu glicol la cald, cu concentrațiile dintre 10 și 20% CeO_2, se obține o scădere a parametrului reticular pentru modificația ηAl_2O_3 de la 8,132 Å la 7,887 Å și a volumului celulei tetragonale a modificației γAl_2O_3 de la 33,2 $Å^3$ la 32,2 $Å^3$, urmată de o creștere accentuată a parametrului pentru αCeO_2 de la 4,20 Å la 5,495 Å Cu toate că valoarea suprafeței specifice pentru αCeO_2 este mai mică decît pentru modificațiile η și γ' ale aluminei, în variația rezultantă a suprafeței specifice contribuția cea mai mare o aduce αCeO_2 Prin urmare, se obține o scădere a suprafeței specifice și a volumului porilor

La concentrațiile cuprinse între 20 și 30% de CeO_2, parametrul reticular pentru ηAl_2O_3 crește de la valoarea 7,887 Å la 8,058 Å iar pentru αCeO_2 scade de la valoarea 5,49 la 5,36 Å, iar volumul celulei modificației $\gamma' Al_2O_3$ de la 32,2 $Å^3$ la 24,6 $Å^3$ Scăderea valorilor pentru αCeO_2 și $\gamma' Al_2O_3$ compensează creșterea parametrului pentru Al_2O_3 și, deci, suprafața specifică și volumul porilor cresc. Astfel se poate afirma că probele studiate constau dintr-un amestec mecanic de faze din modificări cristaline de ηAl_2O_3; $\gamma' Al_2O_3$ și αCeO_2. În plus, parametrii reticulari ai modificărilor η și γ' alumină se schimbă foarte mult în funcție de concentrația de αCeO_2, obținîndu-se anomalii în dependență de concentrație. De asemenea tratamentul termic cu glicol are o mare influență, după cum se poate constata din compararea datelor pentru cele două serii de probe studiate

Corelarea datelor structurale cu cele catalitice a permis interpretarea în mod unitar a datelor de suprafață specifică și a distribuției porilor în catalizatorii studiați

(Intrat în redacție la 2 februarie 1978)

BIBLIOGRAFIE

1. I Pop, N Dulămiță, V Crișan, R Goss, Studia Univ Babeș-Bolyai, Phys., 2, 62, (1977).
2. H. C. Stumph, A S Russell, Ind Eug Chem **42**, 1398 (1950)

ON THE STRUCTURAL AND CATALYTIC PROPERTIES OF ALUMINIUM OXIDES PROMOTED WITH CeO_2(II)

(Summary)

The relationship between structural and catalytic properties of aluminium oxides promoted with CeO_2 are discussed. The model which we have done, permitted us to explain in a unitary way the textural measurements.

STUDIA UNIV. BABEŞ—BOLYAI, PHYSICA, 2, 1978

STUDIUL STRUCTURAL AL UNOR CATALIZATORI DE CeO_2 PE SUPORT DE ALUMINĂ

IULIU POP, VASILE CRIŞAN, NICOLAE DULĂMIŢĂ, LIA OLARU şi CORNELIA PETRUŢIU

1. **Introducere.** Aluminele promotate cu bioxid de ceriu, sau cu oxizi ai altor elemente de tranziţie, prezintă o serie de proprietăţi catalitice, ceea ce le conferă posibilitatea de aplicare în diverse procese tehnologice din industria chimică şi petrochimică.

Unele schimbări în structura şi însuşirile catalitice ale aluminelor obţinute prin calcinarea hidroxidului de aluminiu şi promotate cu bioxid de ceriu depind esenţial de condiţiile în care s-a obţinut şi tratat termic hidroxidul de aluminiu. Astfel aluminele sînt parţial sau total deshidratate, aşa cum s-a mai arătat anterior [1, 2]

Prin difracţie de raze X s-au identificat toate modificările structurale survenite în oxizii de aluminiu promotaţi cu CeO_2

Datele structurale obţinute au fost corelate cu parametrul catalitic determinat, respectiv cu valorile suprafeţei specifice

2. **Prepararea probelor.** Aluminele s-au obţinut prin calcinarea hidroxizilor de aluminiu la diverse temperaturi Pentru obţinerea probelor, supuse studiului, s-a dizolvat azotat de aluminiu şi azotat de ceriu în apă încălzită la 328—333 K. Hidroxidul de aluminiu şi hidroxidul de ceriu s-au precipitat în prezenţa carbonatului de amoniu S-au preparat două seturi de probe, notate cu A şi respectiv cu B.

Setul A de probe s-a obţinut prin uscare la 373 K şi calcinare în curent de aer cald. Setul B de probe a fost îmbătrînit lăsîndu-se timp de 20 ore în soluţia în care s-au precipitat hidroxizii de aluminiu şi de ceriu. După îmbătrînire, probele au fost supuse unui tratament similar ca şi setul de probe A, rezultînd în felul acesta probe cu concentraţii diferite de CeO_2, în funcţie de cantitatea de azotat de ceriu utilizată Din ambele seturi s-au preparat cîte patru probe avînd concentraţiile 2, 4, 6, 8% CeO_2.

3. **Tehnica experimentală.** Studiul structural al probelor catalitice investigate s-a făcut prin metoda Debye-Scherrer, folosind o instalaţie tip TUR—M62 cu radiaţia $K\alpha$ a unui anod de cupru, avînd lungimea de undă $\lambda = 1{,}5418$ Å, trecută prin filtru de nichel. Indexarea roentgenogramelor s-a făcut prin metoda analitică, reuşindu-se identificarea tuturor liniilor detectate.

Suprafaţa specifică a catalizatorului s-a determinat cu ajutorul unei instalaţii BET.

4 **Rezultate experimentale şi discuţii.** Din tabloul de difracţie al razelor X se desprinde un fapt esenţial şi anume, că modul de preparare al probelor influenţează asupra spectrului de raze X şi implicit asupra structurii probelor. Astfel, spectrul de difracţie pentru setul A de probe prezintă un număr mai redus de linii faţă de setul B de probe. Prin urmare, tratamentul de îmbătrînire la

care a fost supus setul B de probe a determinat o scădere a vitezei de cristalizare și prin aceasta un grad mai ridicat de cristalizare. Așa se poate explica prezența numărului mai mare de linii apărute pe roentgenogramele setului B de probe. Pentru comparație, la proba cu concentrația de 2% CeO_2 în setul A de probe au putut fi citite pe roentgenogramă 9 linii, în timp ce în setul B de probe 21 linii.

Datele roentgenografice pentru setul A de probe sînt sintetizate în tabelele 1—4, în care sînt prezentate intensitățile absolute ale liniilor de difracție,

Tabel 1

2% CeO_2

Nr	Int	d[A°]	(hkl) Al_2O_3	(hkl) (CeO_2)
1	i	2 4964	2 2 1	
2	i	2 4187	3 1 0	
3	s	2.1434	2 2 2	
4	m	1 8864	4 0 0	
5	m	1 8265	4 1 0	
6	s	1 6285		3 1 1
7	m	1 4780	5 1 0	
8	s	1 3238	4 4 0	
9	s	1 2251		4 2 0
a(Å)			7 52	5 44

Tabel 2

4%CeO_2

Nr	Int	96%Al_2O_3 d[A°]	(hkl) Al_2O_3	(hkl) (CeO_2)
1	s	2 4589	3 0 0	
2	s	2.0213		2 2 0
3	i	1.8613	4 0 0	
4	i	1 8264		3 1 0
5	m	1 6285	4 2 0	
6	s	1 4780	4 3 0	
7	s	1 3400		4 1 1
8	s	1 1732	6 2 0	
a(Å)			7401	5 702

Tabel 3

6% CeO_2

Nr.	Int	d_0[A°]	(hkl) Al_2O_3	(hkl) CeO_2
1	s	2 4619	3 0 0	
2	s	2 1484	2 2 2	
3	m	2 0600	3 2 0	
4	m	1 8471		3 0 0
5	i	1 8264	4 0 0	
6	i	1 8280		3 1 1
7	m	1 6180	4 2 1	
8	fs	1 5212		4 1 0
9	fs	1 4822	4 3 0	
10	fs	1 4662	4 3 1	
11	s	1 3111	4 4 4	
12	s	1 2749		4 2 2
13	m	1 1685	5 2 0	
14	s	1 1066		5 2 1
a(Å)			7 4028	6 0823

Tabel 4

8% CeO_2

Nr	Int.	d_0[A°]	(hkl) Al_2O_3	[hkl] CeO_2
1	fs	2 9228		2 0 0
2	fs	2 594		2 1 0
3	i	2 2777	2 2 2	
4	i	2 2240	3 2 1	
5	m	1.9914	4 0 0	
6	fs	1 8824	4 1 1	
7	fs	1.7996		3 1 0
8	m	1 3975	4 4 0	
9	m	1 2940		3 3 1
10	m	1 2186		4 2 2
11	s	1.0353	6 3 2	
a(Å)			7 943	5 74

marcate prin simbolurile de prescurtare i s foarte slab, s — slab, m — mediu, i — intens În tabele mai sînt date distanțele interplanare, indicii Miller și valorile parametrului reticular În aceeași manieră sînt redate și datele pentru setul B de probe în tabelele 5—8.

Tabel 5

2% CeO_2

Nr	Int.	d_0[A°]	hkl Al_2O_3	hkl CeO_2
1	s	3 5060	2 1 0	
2	s	3.1550	2 1 1	
3	s	2 8600		2 0 0
4	i	2 5684	3 0 0	2 1 0
5	s	2 4164	3 1 0	
6	m	2 1294	3 2 0	
7	m	1 9496	4 0 0	
8	m	1 7936		3 1 0
9	m	1 6500	3 3 2	3 1 1
10	m	1 6129		2 2 2
11	fs	1 4209	4 3 2	
12	m	1 3827	4 0 0	3 3 0
13	m	1 3351	4 4 1	
14	fs	1 2941	5 3 1	3 3 1
15	s	1.2700	6 1 0	
16	fs	1 2559	6 1 1	
17	fs	1 2027	6 2 1	3 3 2
18	fs	1.1454	6 3 0	4 2 2
19	s	1 1371	6 3 1	
20	s	1 0703	7 1 1	
21	s	1 0310	7 2 1	
a(Å)			7 76	5 69

Tabel 6

4% CeO_2

Nr	Int.	d_0[A°]	hkl Al_2O_3	hkl CeO_2
1	s	3 4502	2 1 0	
2	i	2.5862	3 0 0	2 1 0
3	i	2 4183	3 1 0	
4	m	2.1926	2 2 2	
5	m	2.1430	3 2 0	
6	fs	1.9087		2 2 0
7	fs	1.7083	4 0 0	
8	sd	1 4823	4 2 0	3 1 1
9	sd	1 4139	5 1 1	
10	ts	1 3916	5 2 0	
11	ts	1 3528	5 2 1	
12	sd	1 3528	4 4 0	
13	m	1 2353		4 2 1
a(Å			7 64	5 68

Tabel 7

6% CeO_2

Nr	Int.	d_0[A°]	hkl Al_2O_3	hkl CeO_2
1	s	3.5262		1 1 1
2	fs	2 9297		2 0 0
3	fs	2 8387	2 2 0	
4	i	2 7007	3 0 0	
5	i	2 6295		2 1 0
6	m	2 5623	3 1 0	
7	m	2 3064	2 2 2	
8	s	2 160	3 2 1	
9	s	2 0910		2 2 0
10	s	2 0660	4 0 0	
11	s	1 8050	4 2 0	3 1 1
12	s	1 7522	4 2 1	
13	m	1 5768	4 3 1	
14	s	1 4900	5 2 1	
15	s	1 4848	4 4 0	4 1 1
16	m	1 3238		4 2 0
a(Å)			8 03	5 89

Tabel 8

8% CeO_2

Nr	Int	d_0[A°]	hkl Al_2O_3	hkl CeO_2
1	s	2 7158	3 0 0	
2	ts	2 6534		2 0 0
3	i	2 4569	3 1 1	
4	i	2 4262		2 1 0
5	i	2 2452	3 2 0	2 1 1
6	fs	2 0870	3 2 1	
7	s	2 0423	4 0 0	
8	fs	1 9914	4 1 0	
9	s	1 7494	3 3 2	
10	s	1 7004		3 1 0
11	m	1 5124	4 3 2	3 2 0
12	ts	1 4992	4 4 0	3 2 1
13	fs	1 4143	4 3 3	
14	m	1 3711	5 3 1	
a(Å)			8 178	5 43

Din tabele se poate constata că în ambele seturi de probe s-a identificat existența unui amestec mecanic de două faze: faza ηAl_2O_3 și αCeO_2, ceea ce justifică denumirea catalizatorului de bioxid de ceriu pe suport de alumină. Se vede de asemenea că valorile parametrilor reticulari pentru cele două faze se modifică în funcție de conținutul de CeO_2. La concentrații mici influența adaosului de CeO_2 se reduce numai la variații ale parametrilor reticulari, în timp ce la concentrații mari, pe lîngă acest efect, mai apare alături de modificația ηAl_2O_3 și modificația $\gamma' Al_2O_3$ sub influența unor tratamente diferite, cum este cel cu glicol la cald.

Apariția fazelor ηAl_2O_3 și αCeO_2 se explică prin diferențe foarte mari între razele ionice, aluminiul avînd raza ionică de 0,57 Å iar ceriul de 1,08 Å Avînd raza mai mare, ionul de ceriu nu poate ocupa pozițiile tetraedrice vacante din rețeaua spinelului ηAl_2O_3, și nici nu poate substitui ionul de aluminiu din rețea pentru formarea unui compus sau a unei soluții solide.

Variațiile observate în valorile parametrilor reticulari pentru cele două faze, în funcție de conținutul de CeO_2, pot fi totuși corelate într-un anume mod.

Reprezentînd grafic dependența parametrului reticular pentru ηAl_2O_3 de concentrația CeO_2, așa cum este redat în figurile 1 și 2, se vede că aliura curbelor pentru cele două seturi de probe A și B este asemănătoare.

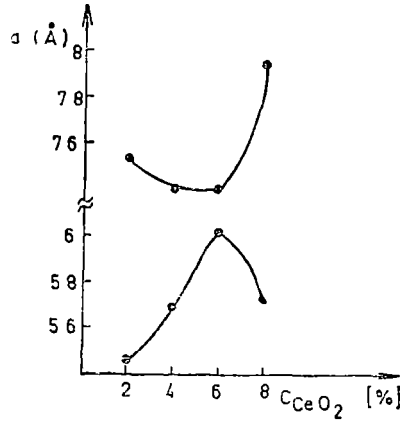

Fig. 1.

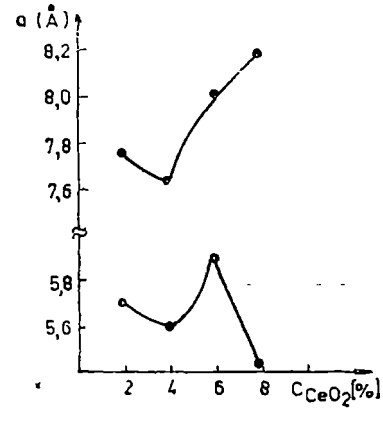

Fig. 2.

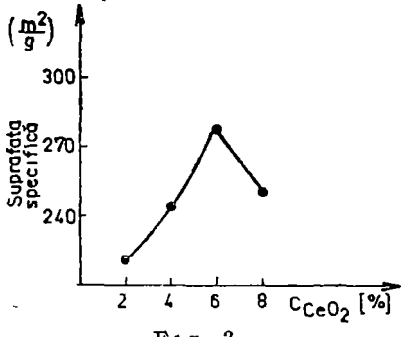

Fig. 3.

Dependența parametrului reticular pentru ηAl_2O_3 prezintă un minim la concentrația de 4% CeO_2, în timp ce pentru αCeO_2 are un maxim la concentrația de 6% CeO_2.

Dependența valorilor suprafeței specifice pentru setul A de probe, redată în figura 3, în funcție de concentrația de CeO_2, este în bună concordanță cu dependența parametrului reticular de concentrația de CeO_2 prezentată mai sus. Această concordanță duce la concluzia că suprafața specifică și parametrul reticular al modificației ηAl_2O_3 se pot corela prin con-

centrația oxidului elementului de tranziție. Contracția rețelei cristaline în domeniul concentrațiilor 2—6% CeO_2 concordă cu creșterea suprafeței specifice a catalizatorului. La 6% CeO_2 parametrul reticular al ηAl_2O_3 prezintă un minim, în timp ce suprafața specifică prezintă un maxim. Dilatarea rețelei cristaline pentru ηAl_2O_3 implică o micșorare a suprafeței specifice a catalizatorului.

Prin urmare, introducerea bioxidului de ceriu în alumină îi imprimă acesteia proprietăți catalitice remarcabile, fără a produce modificări structurale radicale, efectul concentrației repercutîndu-se asupra valorii suprafeței specifice a catalizatorului.

(Intrat în redacție la 4 februarie 1978)

BIBLIOGRAFIE

1 I. Pop, N. Dulămiță, V Crișan, R Goss, Studia, Univ Babeș—Bolyai, Phys 2, 62, (1977).
2 I. Pop, V Crișan, N Dulămiță, R Goss, Studia Univ Babeș — Bolyai, Phys, 2, 62 (1978)

STRUCTURAL PROPERTIES OF ALUMINA PROMOTED WITH CeO_2

(Summary)

The structure properties of aluminium oxides promoted with CeO_2 in low concentration, are sensitive to the preparation method and CeO_2 concentration

STUDIA UNIV. BABEŞ—BOLYAI, PHYSICA, 2, 1978

CONTRIBUŢII LA STUDIUL PROPRIETĂŢILOR MAGNETICE ŞI TERMICE ALE SISTEMULUI 50% Cr_2O_3—50% SnO_2 (ECHIMOLAR)

Á. NÉDA, M. MATHÉ şi O. POP

Introducere. Proprietăţile magnetice, electrice şi termice ale sistemului Cr_2O_3—SnO_2 au fost studiate detaliat în lucrările [1, 2, 3, 4] Din punct de vedere magnetic s-a precizat că, în cazul compusului Cr_2O_3, în afară de anomalia corespunzătoare temperaturii de tranziţie ordine-dezordine, situată în apropierea temperaturii de 314 K, susceptibilitatea magnetică mai depinde anomal de temperatură pînă la aproximativ 600 K La temperaturi mai înalte comportarea magnetică corespunde unei stări paramagnetice normale Măsurătorile privind dependenţa de temperatură a coeficientului de difuzivitate termică, în cazul fiecărui compus al sistemului $x(Cr_2O_3) + (1-x)(SnO_2)$ (pentru $x \neq 0$) au pus în evidenţă o comportare anomală în jurul temperaturii de tranziţie semnalate mai sus. La temperatura amintită panta curbei de variaţie a coeficientului de difuzivitate termică în funcţie de temperatură suferă o schimbare pronunţată [3, 4]. În cazul probei de Cr_2O_3, care este antiferomagnetic, peste temperatura Néel (314 K), dependenţa coeficientului de difuzivitate termică de temperatură este anomală, prezentînd minime şi maxime, fapt ce arată că nu s-a stabilit încă o fază paramagnetică normală Corelînd această constatare cu cea referitoare la dependenţa anomală a susceptibilităţii magnetice, s-a tras concluzia că ordinea la distanţă a fost distrusă la temperatura Néel, dar ordinea apropiată se mai menţine încă pînă la 600 K Acest rezultat este în bun acord cu datele relative la dependenţa de cîmp a susceptibilităţii magnetice [5].

Studiind proprietăţile termice (coeficient de difuzivitate termică şi căldură specifică) ale sistemului $x(Cr_2O_3) + (1-x)\ SnO_2$ $(0 \leqslant x \leqslant 1)$, pentru $x = 0{,}5$ s-a obţinut o dependenţă singulară în funcţie de temperatură

Coeficientul de difuzivitate termică a fost determinat prin metoda impulsului de căldură [6], iar căldura specifică cu un calorimetru adiabatic [7]

Rezultate experimentale şi discuţii. Pentru proba 50% Cr_2O_3 + 50% SnO_2 variaţia coeficientului de difuzivitate termică (curba a) şi a căldurii specifice (curba b) cu temperatura este prezentată în figura 1 Urmărind variaţia în funcţie de temperatură a coeficientului de difuzivitate termică, se poate constata că în intervalul de temperatură 180—205 K apare un minim şi un maxim local. Peste temperatura de 210 K variaţia coeficientului de difuzivitate termică este asemănătoare cu cea a oxidului Cr_2O_3 [4] Aproximativ pînă la 310 K, temperatură foarte apropiată de temperatura critică Néel, coeficientul de difuzivitate termică scade monoton, iar peste această temperatură prezintă o dependenţă anomală cu minime şi maxime

În lucrările [3, 4] s-a demonstrat că în sistemul Cr_2O_3—SnO_2 conducţia termică este pur fononică, iar schimbarea pantei de variaţie a coeficientului de difuzivitate termică este cauzată de modul diferit de împrăştiere al purtătorilor energiei termice pe magnoni, în starea magnetic ordonată faţă de cea

dezordonată. În felul acesta se poate trage concluzia că anomalia semnalată la temperatura de 310 K, apare datorită tranziției de fază magnetică

Comparînd variația cu temperatura a căldurii specifice și a coeficientului de difuzivitate termică, se constată că temperatura la care apare saltul (picul) în căldura specifică coincide cu temperatura (cca 180 K) la care apare minimul

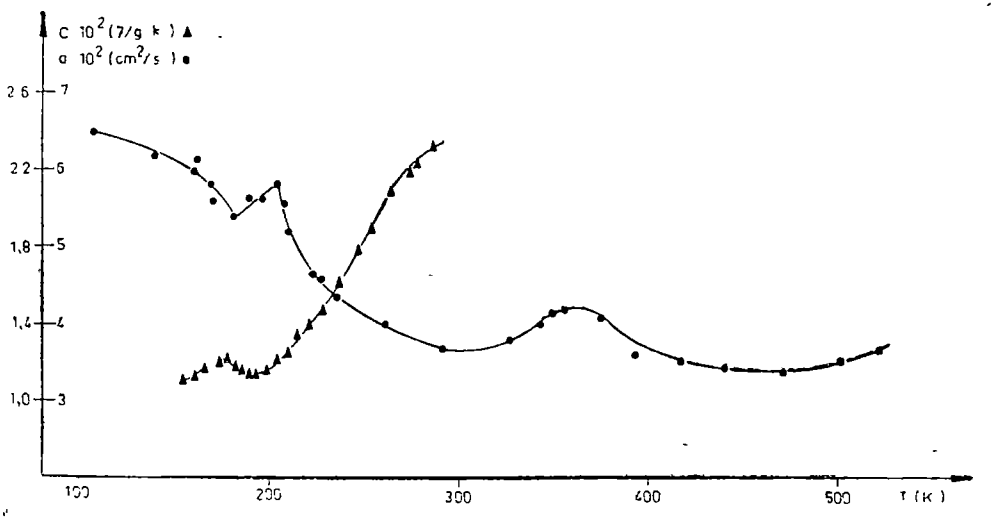

Fig 1

semnalat al coeficientului de difuzivitate termică Aceste comportări denotă o tranziție de fază la această temperatură, saltul căldurii specifice fiind caracteristic unei tranziții de fază de speța a II-a

În condițiile noastre de preparare a probelor și la raportul echimolar de amestecare există posibilitatea apariției combinației chimice $Cr_2Sn_2O_7$ [8] Dacă randamentul reacției ar fi ideal, proba ar conține un amestec mecanic de 50% mol. Cr_2O_3 și 50% mol. $Cr_2Sn_2O_7$ Într-adevăr, din măsurători electrice și termice [2, 3] rezultă că domeniul soluțiilor solide este foarte îngust, astfel soluția solidă pe bază de Cr_2O_3 se limitează la cca 1% molar de SnO_2, iar cea pe bază de SnO_2 la aproximativ 2% molar Cr_2O_3 În restul domeniului de concentrație există numai amestec mecanic de două faze.

Oxidul Cr_2O_3 este antiferomagnetic, avînd momentele magnetice compensate. Valoarea momentului magnetic pentru Cr^{3+}, determinat prin măsurători de susceptibilitate magnetică, este de 3,84 μ_B foarte apropiată de valoarea teoretică (3,872 μ_B).

În lucrarea [2] se afirmă că odată cu introducerea SnO_2 în Cr_2O_3 pe lîngă ionii de Cr^{3+} apar și ionii Cr^{4+}. Astfel, este posibil ca în compusul $Cr_2Sn_2O_7$ momentele magnetice să fie necompensate. În favoarea acestei afirmații se poate cita lucrarea [9], în care se arată că în proba avînd concentrația de 50% mol. valoarea momentului magnetic este intermediară, (3,66 μ_B), între valorile teoretice

obţinute pentru Cr^{3+} (3,8 μ_B) şi Cr^{4+} (2,88 μ_B). Această constatare atestă prezenţa ionilor Cr^{4+}.

Presupunînd că în timpul preparării probei are loc reacţia

$$2(Cr_2O_3) + 2(SnO_2) = Cr_2Sn_2O_7 + Cr_2O_3 \quad (1)$$

şi luînd în considerare că pentru momentul magnetic al probei s-a obţinut valoarea de 3,66 μ_B [9], se poate calcula valoarea momentului magnetic pentru $Cr_2Sn_2O_7$, cu relaţia

$$m_{exp} = \sqrt{f_1 \cdot m_1^2 + f_2 \cdot m_2^2}, \quad (2)$$

în care: f_1 şi f_2 reprezintă fracţiile molare pentru Cr_2O_3 şi $Cr_2Sn_2O_7$ ($f_1 = f_2 = 0{,}5$), în amestecul rezultat, m_1 şi m_2 valorile medii ale momentelor magnetice pentru un ion de Cr în Cr_2O_3, respectiv $Cr_2Sn_2O_7$ Utilizînd această formulă, se obţine $m_2 = 3{,}15$ μ_B. Pe baza acestei valori s-au determinat fracţiile molare ale ionilor Cr^{3+} (f_1') şi Cr^{4+} (f_2') în amestecul de concentraţie 50% folosind relaţia

$$m_2 = \sqrt{f_1' m_{Cr^{3+}}^2 + f_2' m_{Cr^{4+}}^2}, \quad (3)$$

unde: $m_{Cr^{3+}}$ şi $m_{Cr^{4+}}$ reprezintă momentul magnetic pentru un ion Cr^{3+} (3,8 μ_B), respectiv Cr^{4+} (2,88 μ_B). Calculate astfel, pentru fracţiile molare se obţin valorile $f_1' = 65{,}8\%$, respectiv 34,2%.

În această idee considerăm că tranziţia de fază semnalată în jurul temperaturii de 180 K este o tranziţie de faza din starea ferimagnetică în cea paramagnetică pentru $Cr_2Sn_2O_7$. Utilizînd datele experimentale referitoare la coeficientul de difuzivitate termică şi căldură specifică, respectiv densitate, s-a determinat valoarea coeficientului de conductibilitate termică cu relaţia

$$\lambda = C \cdot a \cdot \rho, \quad (4)$$

unde C — reprezintă căldura specifică, a — coeficientul de difuzivitate termică, iar ρ — densitatea Variaţia coeficientului de conductibilitate termică în funcţie de temperatură este dată în figura 2. Se constată că această mărime în vecinătatea temperaturii de 184 K are o valoare minimă. Comportări asemănătoare au mai fost observate în cazul oxizilor ferimagnetici, la temperatura ordonării magnetice, de către autorii lucrărilor [10, 11]. Această constatare vine în sprijinul ipotezei noastre.

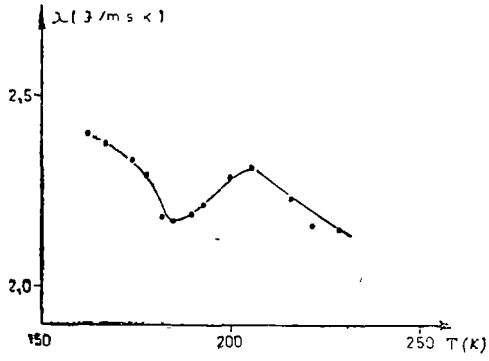

Fig. 2.

Urmărind figura 1 se poate constata că, peste temperatura de 200 K, variaţia coeficientului de difuzivitate termică este asemănătoare cu cea obţinută pentru Cr_2O_3 [4]. În felul acesta, presupunem că în cazul probei cu concentraţia 50% avem un amestec mecanic de compoziţie stabilită cu relaţia (1) şi deci apar două tranziţii magnetice La temperatura de 180 K apare tranziţia

de fază din starea ferimagnetică în cea paramagnetică pentru compusul $Cr_2Sn_2O_7$, iar în apropierea temperaturii de 314 K, din starea antiferomagnetică în cea paramagnetică pentru Cr_2O_3

Concluzii. Din studiul dependenței de temperatură a coeficientului de difuzivitate termică, a căldurii specifice și a coeficientului de conductibilitate termică pentru proba având concentrația 0,5 Cr_2O_3 + 0,5 SnO_2, rezultă două temperaturi de transformare magnetică (180 K, respectiv 310 K). Considerînd că acest compus este un amestec mecanic format din $Cr_2Sn_2O_7$ și Cr_2O_3, s-a arătat că temperatura de 180 K corespunde tranziției din starea ferimganetică în cea paramagnetică pentru $Cr_2Sn_2O_7$, iar temperatura de 310 K tranziției din starea antiferomagnetică în cea paramagnetică pentru Cr_2O_3

(Intrat în redacție la 2 februarie 1978)

BIBLIOGRAFIE

1 O Pop, Studia Univ Babeș—Bolyai, Phys, 1, 119 (1969)
2 O Pop, Bul Inst Politeh Cluj **11**, 41 (1969)
3 A Néda și O Pop, Ses Științ I P C, 22—23 II, 1974
4 O. Pop, A Néda, L Stănescu și L Homorodean, Studia Univ Babeș—Bolyai, Phys., 59 (1975)
5 V I Cecernikov, I S Liubitin, Vestnik Mosk. Univ, **1**, 20 (1963)
6 F Kelemen și A Néda, Studia Univ Babeș—Bolyai, Phys, 2, 107 (1967)
7 F Kelemen și A Néda, Studia Univ Babeș—Bolyai, Phys, 2, 39 (1970)
8 J Buisse and O Knap, Canad J Chem, **46**, 895 (1968)
9 H P. Walter, Z Chem, **8**, 473 (1968)
10. R G Moris, J Konantz, Intern Conf Magn Oxids, Bucharest, 10—14 sept 1968
11. R G Moris and J L Casan, Helv Phys. Acta, **41**, 1045 (1968)

ON MAGNETIC AND THERMAL PROPERTIES OF 50% Cr_2O_3—50%SnO_2 COMPOUNDS

(Summary)

The temperature dependence of thermal diffusivity, thermal conductivity, and specific heat for sample 50% Cr_2O_3 + 50% SnO_2 were investigated Two critical temperatures were obtained (180 K and 310 K). Supposing that the investigated compound represents a two-phasic mixture formed from $Cr_2Sn_2O_7$ and Cr_2O_3, it is pointed out that 180 K corresponds to ferrimagnetic-paramagnetic transition, for $Cr_2Sn_2O_7$, 310 K being the Néel temperature of Cr_2O_3

STUDIA UNIV. BABEŞ–BOLYAI, PHYSICA, 2, 1978

THE DOPING OF NaCl–TYPE SINGLE CRYSTALS WITH PARAMAGNETIC IONS

AL. DARABONT, P. FITORI and AL. NICULA

Introduction. The growth of NaCl-type single crystals with iron group paramagnetic ions presents a special interest in the studies of the paramagnetic ion-vacancy associations by the magnetic resonance absorption method, and in the problem of the elucidation of the mechanism and the parameters of the intrinsic conductivity.

There are many papers about the iron group paramagnetic ions doped in alkali halide single crystals Some of them are still intended to elucidate the growth mechanism of these crystals with paramagnetic ions

The present work deals with the growth of the NaCl single crystals with Mn^{2+} —, Fe^{3+}—, Cu^{2+} — and Ni^{2+} — ions, as paramagnetic impurities, using the following methods crystal growth from solution by evaporation procedure, from melt by the Czochralski-Kyropoulos technique, zone melting technique and impurification by diffusion These methods used by us are described in the special reference materials and to enumerate all of them would not be practically possible here. We are guided by the works [1,2,3,4,5,]. The existence and the valency of the paramagnetic ions in the samples were controlled by the EPR—method and chemical analysis The EPR measurements were carried out by means of an ESR—spectrometer of JES—3B type in X—band

Experimental results. 1 *NaCl · Mn^{2+} system* · To obtain this system we have used the same growth procedures which were described in the papers [6,7,8,9] and we have also observed that the EPR—spectrum of the Mn^{2+} ion was not resolved completely when the crystal was not annealed, a fact we have met in the papers [8,10,11,12]. Mn^{2+} ions agglomerate at the crystal defects and for this reason the spectrum remains unresolved The elimination of the agglomerates and the resolution of the resonance spectrum can be done by annealing the crystals, that is a heating up to 400—500 °C and a subsequently cooling to the room or liquid nitrogen temperature But the resolution of the spectrum disappears in time because of the reformed Mn^{2+} ion agglomerations at the lattice defects This reformation process takes place — at room temperature — in a couple of days

To increase the stability of the Mn^{2+} ions diffused in the lattice we have introduced these ions simultaneously with the Fe^{3+} ions The paramagnetic resonance spectrum of the Mn^{2+} and Fe^{3+} ions doped simultaneously in NaCl single crystal shows a broad line with a factor $g = 2{,}009 \pm 0{,}007$ due to the agglomeration which contains Fe^{3+} and the resolved spectrum of the Mn^{2+} ion superimposed on it [13], these ions are in substitutional positions of the cubic symmetry [13]. The Mn^{2+} and Fe^{3+} ions were doped in NaCl single crystals by diffusion at 360—400 °C

2. *NaCl Fe^{3+} system* In connection with the growth of the alkali halide single crystals with iron impurities there are indications in [6,9, 21] In these

papers it is also analysed the EPR absorption Andrews and Kim [14] give a resonance spectrum for Fe^{3+} in NaF obtained by X-ray irradiation of the crystal. They do not indicate the crystal growth and doping procedures

We have proposed to study the impurification procedure of NaCl with Fe^{3+} and then to identify by the paramagnetic resonance method The tests used to obtain single crystals of NaCl with Fe^{3+} by crystal growth from solution by evaporation procedure or from melt by the Czochralski-Kyropoulos technique in argon atmosphere were not successful We consider that in the first case the iron ion is absent from the samples but in the second case, if it is present, it is in the Fe^{2+} state due to the decomposition of the $FeCl_3$ (440 °C) To avoid the decomposition of the $FeCl_3$ we have resorted to the impurification by low temperature diffusion method (301—360 °C) for 3—4 months For this we have used little pure NaCl single crystals and $FeCl_3$ purified by repeated sublimations which were closed together in a quartz tube at a vacuum about 10^{-5} mmHg Besides the diffusion method we have tried the growth of the crystals in chlorine atmosphere by zone melting technique From these crystals we kept homogeneous crystals about $5 \times 5 \times 8$ mm^3 The crystals obtained by both methods had a light yellow-brown colour These crystals give a paramagnetic resonance spectrum at room temperature and at the liquid nitrogen temperature too, which consists of a broad line without the fine structure with factor $g = 2\,007 \pm \pm 0.006$ and 114 ± 6G linewidth due to the Fe^{3+} agglomeration at the lattice defects. The chemically determined iron concentration is about 0 017% in weight for crystals impurified by diffusion.

NaCl Cu^{2+} system To obtain this system we tried the Czochralski — Kyropoulos technique in argon atmosphere adding anhydrous $CuCl_2$ to the melt The crystals obtained in this way have not presented paramagnetic resonance spectrum we consider that the copper is present in the sample in Cu^+ state as $CuCl_2$ decomposes to CuCl and Cl_2 In order to avoid this we have resorted again to the zone melting growth in chlorine atmosphere The crystals obtained in this way present a light yellow colour The average copper concentration indicated by the chemical analysis was about 0 05% in weight These crystals give paramagnetic resonance spectrum at room temperature as well as at the liquid nitrogen temperature only after their annealing The annealed samples present a paramagnetic centre with tetragonal symmetry having its symmetry axis parallel to the cube edge ([100] direction) The g — values determined from the line positions are . $g_{\parallel} = 2.298 \pm 0.004$ (for the centres with symmetry axes parallel to the applied magnetic field) and $g_{\perp} = 2\,058 \pm 0\,004$ (for the centres with symmetry axes perpendicular to the applied magnetic field) The complete paramagnetic resonance study of this system constitutes the subject of papers [15,16] The isolated Cu^{2+} ions produced by X — rays or Co — γ-rays were studied in single crystals of NaCl by Borcherts et al [17], in single crystal of LiCl by Pilarow and Stevenson [18]. Abe et al [6] studied the EPR spectrum of copper in polycrystalline NaCl

NaCl Ni^{2+} system For this system we have used the same technique as for the NaCl·Cu^{2+} system The Czochralski-Kyropoulos technique was unsuccessful as the $NiCl_2$ has been separated from the crystal during the growth or the nickel was present in a monovalent state in the NaCl Positive results were obtained in this case also by the zone melting technique in chlorine atmosphere

working with NaCl and anhydrous $NiCl_2$ mixture The crystals obtained in this way were coloured in yellow-violet. The violet colour was accentuated by the annealing of the crystals at 550°C. The chemical analysis indicates an average concentration in nickel about 0 08 % in weight The paramagnetic resonance spectrum we have got at 77°K for this system gave a single line with 120 ± 6G width and has a factor $g = 2\,245 \pm 0\,006$ The crystals did not present a paramagnetic resonance spectrum at room temperature even if they were annealed All our measurements were carried out in 500—10 500 G range. In this range we have not observed other lines for Ni^{2+}, as it was indicated in [19] which studied the EPR of Ni^{2+} ions in AgBr. Other EPR studies are found for Ni^{2+} ion doped in alkali halides in papers [6,9,20]

Conclusions.

1. All the methods used by us in order to obtain impurified NaCl single crystals: crystal growth from the solution, form the melt, zone melting, impurification by diffusion give positive results for Mn^{2+} ions.

2. In the case of the Fe^{3+} only the slow diffusion for 3—4 months and the zone melting technique in chlorine atmosphere give positive results.

3 For the Cu^{2+} and Ni^{2+} only the zone melting technique in chlorine atmosphere was successful The diffusion method was not tried for Cu^{2+} and Ni^{2+} cases

Our second and third observation confirm that Fe^{3+}, Cu^{2+}, Ni^{2+} states of the added impurity ions are promoted by the presence of the chlorine atmosphere. The fact that the valency of the impurity ions depend critically on the chlorine pressure surrounding the crystal it is easy to understand if we apply the mass action principles for the chemical equation·

$$2MCl_2 \leftrightarrows 2MCl + Cl_2$$

where M stands for the metal in question. It follows that a high external chlorine pressure will favour the oxidation of the metal to the oxidized state from the reduced state This fact has been also observed in the case of silver halides and other metal oxides [3]

(Received February 4, 1978)

REFERENCES

1. K. Th Wilke, *Methoden der Kristallzuchtung*, VEB Deutscher Verlag der Wissenschaften, Berlin, 1963
2 K Th. Wilke, *Kristallzuchtung*, VEB Deutscher Verlag der Wissenschaften, Berlin, 1973.
3. F A. Kroger, *The Chemistry of Imperfect Crystals*, North-Holland Publishing Company-Amsterdam, 1964
4. S. Gîdea, M Protopopescu, D Drimer, *Metalurgia fizică a semiconductorilor*, Ed Academiei R.P R, 1963
5. I. Tarjan, M Mátrai, *Laboratory Manual on Crystal Growth*, Akadémiai Kiado, Budapest, 1972 (By arrangement with UNESCO)
6. H. Abe, H. Nagano, M Nagusa, Oshima Keichi, J Chem Phys., **25**, 378 (1956).
7. A. Mehra, Phys stat. sol., **29**, 847 (1968).

8. R Böttcher, W. Windsch, W. Ludke, Phys. stat sol. **20,** 121 (1967).
9 T P P Hall, W Hayes, R W. H Stevenson, J Wilkens, J Chem Phys, **38,** 1977 (1963), **39,** 35 (1963)
10 G D Watkins, Phys Rev **113,** 79 (1959)
11. P. Forrester, E E Schneider, Proc Phys. Soc., **B69,** 837 (1956)
12 M. Sumita, Japan J Appl Phys, **6,** 789, 903, 1009, 1021, 1472 (1967)
13 A. Darabont, S. V Nistor, Rev. Roum. Phys, **15,** 603 (1970).
14. A Andrews, Y. W Kim, Phys Rev, **154,** 220 (1967)
15. S I Fărcaş, A Darabont, A Nicula, Phys stat sol. (b) **50,** 755 (1972)
16 S I Fărcaş, A Darabont, A Nicula, *Al patrulea Simpozion Internaţional de Rrezonanţă Magnetică,* Rehovoth, 1971
17 R H Borcherts, H Kazaki, H. Abe, Phys Rev. **2B,** 23 (1970)
18. I R Pilbrow, R W H. Stevenson, Phys stat sol **34,** 293 (1969).
19 J Busse, Phys stat sol, **3,** 1892 (1963).
20 W Hayes, J Wilkens, Proc Roy. Soc. **A281,** 340 (1964)
21 I Ursu, S V Nistor, A Nicula and V Niculescu, Proc XIV-th Coll AMPERE, Ljubljana (1966)

DOPAREA MONOCRISTALELOR DE TIPUL NaCl CU IONI PARAMAGNETICI

(Rezumat)

Această lucrare prezintă condiţiile de dopare ale monocristalelor de tipul NaCl cu ioni paramagnetici ca Mn^{2+}, Fe^{3+}, Cu^{2+} şi Ni^{2+} A fost utilizată metoda RES pentru controlul prezenţei acestora în cristalul gazdă

STUDIA UNIV BABEŞ–BOLYAI, PHYSICA, 2, 1978

SUPERHYPERFINE INTERACTIONS IN KDP: Cu^{2+} SINGLE CRYSTALS

AL. NICULA, M. PETEANU and C. HĂGAN

1. **Introduction.** As it is known, KH_2PO_4 (KDP) belongs to the hydrogen-bonded ferroelectrics The structural studies performed on KDP single crystals and its isomorphs reveal a tetragonal lattice structure at room temperature (paraelectric phase), which changes in an orthorombic one below the Curie temperature (123°K) The basic units in this structure are the PO_4 tetrahedra disposed in a diamond type lattice, connected by hydrogen bonds of about 2 48 Å

Structural analyses by means of X rays (West [1], Frazer and Pepinsky [2]) or neutron diffraction (Bacon and Pease [3]) gave the KDP lattice unit cell constants in paraelectric phase, as being a=b=7 43 Å and c = 6.94 Å. The four molecules composing the unit cell are spatially disposed in such a manner that each potassium ion is surrounded by eight oxigen atoms, distributed in two almost regular tetrahedra (S_4 symmetry) having a common weight center, occupied by the potassium ion The dimensions of these two tetrahedra being different (K—O distances are 2.82 Å and 2 89 Å respectively) it results, from a crystallographic point of view, two unequivalent sites for the potassium atoms [4].

KDP crystals do not exhibit electronic paramagnetism Therefore, paramagnetic centers must be artificially induced by doping these crystals with transition elements ions, or by irradiating them with X or gamma rays. Consequently we used the ionic impurifying method, by controlled doping of Cu^{2+} paramagnetic ions into the KDP host crystals

2. **ESR spectra of Cu^{2+} impurities in KDP.** In order to study the peculiarities of the ESR spectra due to Cu^{2+} ions in the KDP crystal lattice chosen for magnetic dilution, we have grown single crystals from an aqueous KDP solution containing 5 mol % cupric nitrate, $Cu(NO_3)_2 \cdot 3H_20$ The growth was stimulated by using phosphoric acid, H_3PO_4 of 20 mol % against KDP The temperature of the solution was kept constant to be 25°C for prevent the crystals stressing and to assure a uniform growth of them. As result, we obtained platelike, colorless and transparent single crystals of about 2 × 1 × 5 mm

The ESR spectra recorded in paraelectric phase, at room temperature, for H//c show the existence of two unequivalent positions of the Cu^{2+} ions in the host lattice, for each one corresponding a four-lines-group in the spectrum. This is due to the hyperfine interaction between the 3d electrons and the cooper nuclear spin, I = 3/2 The spectra corresponding to these two positions are A and B in figure 1 Further, the A spectrum lines are splitted into equidistant components

By rotating the crystal in the ac (or bc) plane, we noticed that more we depart from the c axis the spectrum A becomes more complicated, each line being splitted in four groups of signals, these indicating the unequivalence of the A type positions too. This situation is clearly plotted in the angular dependence of figure 2. One can also observe a deviation of the z axis of the paramagnetic center

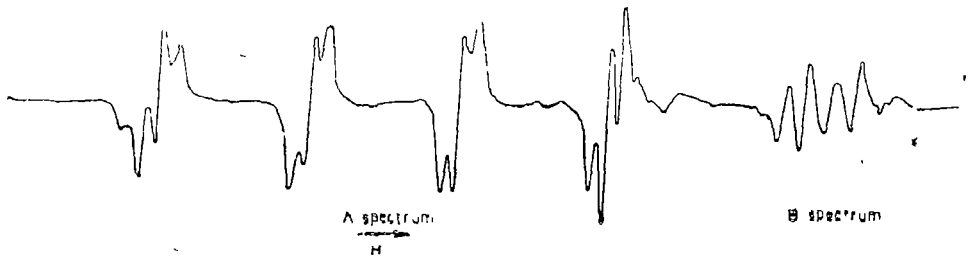

Fig 1 ESR spectrum of KDP Cu^{2+} crystals recorded for a H | | c direction

from the c axis of the single crystal, the resonance spectra having maximum of their extention in the angular dependence at a position at about 23° against the c axis Taking into account the lattice symmetry (tetragonal in paraelectric phase) one can explain the unequivalency of the A type sites by four possible directions of their bonds in the crystal lattice [5] The presence of groups of resonance signals, therefore an additional structure of the spectra, proves the existence of some interactions which must be taken into account for a complete understanding of the spectra Otani and Makishima [5] explained this additional splitting by means of the isotopic effect, both Cu^{63} and Cu^{65} having $I = 3/2$, and of slight misorientation of the crystal.

The isotopic effect appears clearly in our spectra too, but as presented in fig. 3 for the H//a (or b) direction, it is visible especially at the bordering lines of hyperfine structure, the hyperfine coupling constant values characteristic for the two isotopes not differing very much In fact, for the above-mentioned spectrum, we estimated for the B type centers the values $A^{63} = 135\,09 \times 10^{-4}$ cm^{-1} and $A^{65} = 147\,5 \times 10^{-1}$ cm^{-1} in good agreement with the magnetic moment values (in multiples of the nuclear magneton) $\mu^{63} = 2\,2206$ and $\mu^{65} = 2.3790$. We have chosen the B centers spectrum for estimating the hyperfine coupling constants of the two isotopes because of their simplicity compared to the A type spectra Of course, the isotopic effect is identical in the case of the A centers, but cannot explain the additional splitting of the central lines in the hyperfine transitions group

Having in view the additional splitting typical for all the hyperfine transitions of the four superposed spectra due to the four unequivalent A type sites (fig. 1) and the fact that these lines are split in groups of signals almost equidistant we are able to explain this structure by means of the superhyperfine interactions between the paramagnetic ion and the phosphorous nuclei ($I = 1/2$) from the neighbouring tetrahedra For a H//c position of the crystal, when the four directions of the possible partial directions for the A type centers bonds are equivalent, that is their spectra coincide, remain visible only the hyperfine structure, isotopic effect and the superhyperfine interaction in the spectrum. The bordering groups of transitions have more peaks than the central ones because of the isotopic effect.

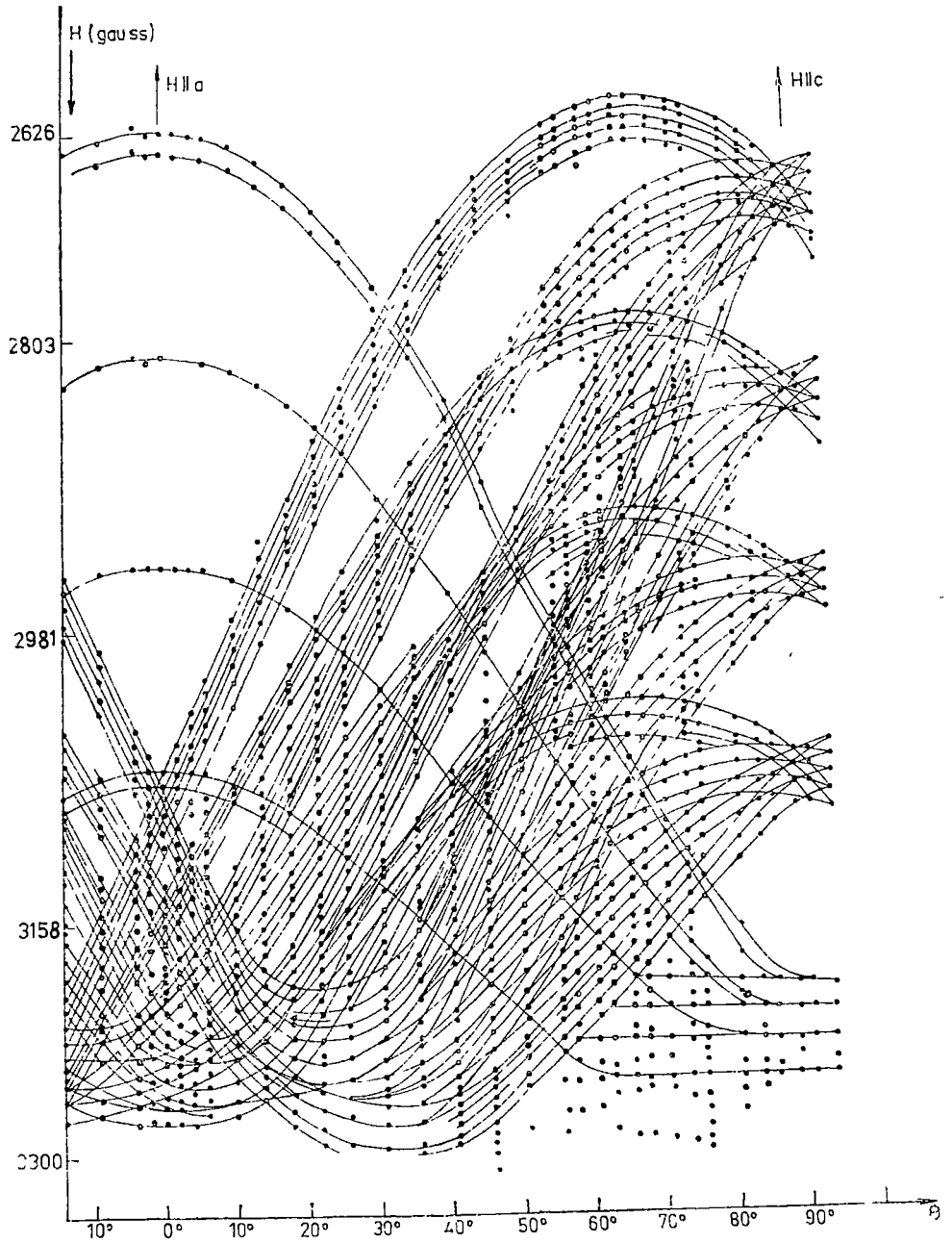

Fig. 2 Angular dependence of the ESR signals by rotating the KDP crystal in the resonant cavity, the magnetic static field lies in the (ab) plane.

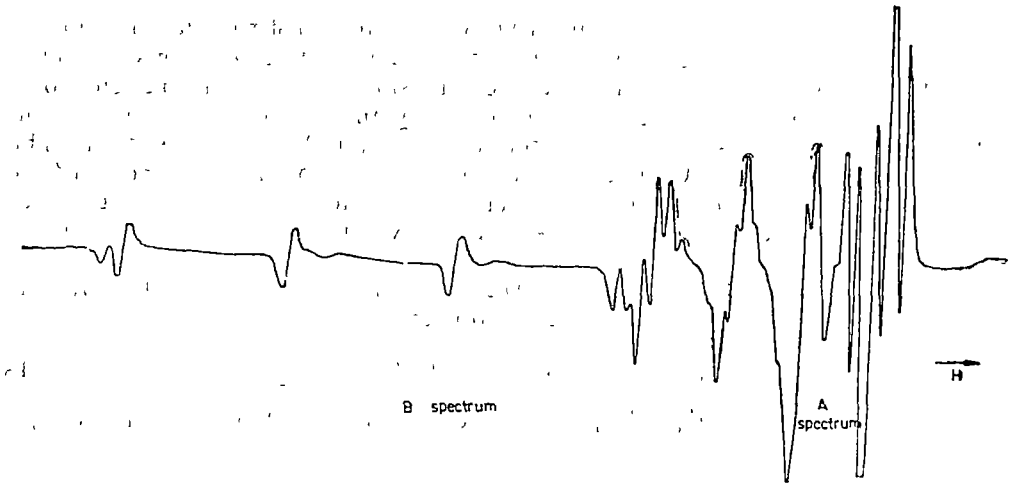

Fig. 3 ESR spectrum of KDP . Cu^{2+} recorded for a H | | a direction.

The B sites spectra, whose angular dependence is also indicated in fig 2, show the occupation of almost uniaxial field sites, the z axis of the paramagnetic center being nearly parallel to the a (or b) axis.

The resonance spectra gave us the possibility of evaluating the experimental values for the g factors and hyperfine coupling constants. These values are tabulated in Table 1, compared with other experimental values of already published papers.

Table 1

Substance		$g_{\parallel}$	$g_{\perp}$	$A_{\parallel}$ ($\times 10^{-4}$cm^{-1})	$A_{\parallel}$ ($\times 10^{-4}$cm^{-1})	$A_{\perp}$ ($\times 10^{-4}$cm^{-1})	Ref.
KDP : Cu	A	2 364	2 080	142	19	—	[5]
	B	2 340	2 072	145	20	—	
KDP : Cu		2 388	2 060	148 5	19·1	—	[6]
$Cu[S_2P(OC_2H_5)_2]_2$		2 085	2 025	149 6 (^{63}Cu) 160 8 (^{65}Cu)	32,5	9 6	[7]
$Cu[S_2P(OC_2H_5)_2]_2$		2 081	2 024	146 7	26 5	8 5	[8]
KDP Cu	A	2 3326	2 0655	129 36	23 04	8.8	our paper [9]
	B	2 3151	2 0648	135.09 (^{63}Cu) 147.5 (^{65}Cu)	18.11	—	

3. Theory. Taking into account that Cu^{2+} ions substitute for K^+ in the host lattice, we must consider its effect in rearranging the PO^{3-}_4 ions in such a manner that every Cu^{2+} ion to be octahedrally surounded by six oxigen atoms [6]: four of them almost tetragonally in the (ab) plane, and other two above and below the (ab) plane respectively, at the same distance from the K^+ ion. The ionic radius of Cu^{2+} being 0.54 times smaller than that of K^+, it tends to take an octahedral coordination with six oxigen atoms. This would explain the fact that ESR spectra show the effects of an axial crystal field of symmetry higher than C_s.

The features of the resonance spectra which have a strong axial character, may be described by using the spin hamiltonian

$$\mathcal{H} = g_{//}\beta H S_z + g_\perp \beta (S_x H_x + S_y H_y) + A_{//} I_z S_z + A_\perp (I_x S_x + I_y S_y) \qquad (1)$$

The angular dependence for the ESR transitions characteristic for the Cu^{2+} ions, may be described by

$$h\nu = g\beta H + Km + \frac{A_\perp^2}{4g\beta H_0}\left(\frac{A_{//}^2 + K^2}{K^2}\right)[I(I+1) - m^2] + \frac{1}{2g\beta H_0}\left(\frac{A_{//}^2 - A_\perp^2}{K^2}\right)^2\left(\frac{g_{//}^2 g_\perp^2}{g^2}\right) \cdot$$

$$\cdot\, m^2 \sin^2\theta\cos^2\theta + \frac{2}{K} Q^2 \sin^2\theta\cos^2\theta \left(\frac{A_{//}A_\perp g_{//}g_\perp}{K^2 g^2}\right)^2 m\,[8m^2 + 1 - 4I(I+1)] +$$

$$+ \frac{Q^2}{2K}\sin^4\theta\left(\frac{A_\perp g_\perp}{Kg}\right)^4 m\,[2I(I+1) - 2m^2 - 1] \qquad (2)$$

where

$$g^2 = g_{//}^2 \cos^2\theta + g_\perp^2 \sin^2\theta$$

$$K^2 g^2 = A_{//}^2 g_{//}^2 \cos^2\theta + A_\perp^2 g_\perp^2 \sin^2\theta$$

Using the ESR spectra recorded for H // a and H // c, that is the transition field values into equation (2) written for $\theta = 0°$ and $\theta = 90°$ respectively, we obtained theoretically the spin hamiltonian constants. These values are:

$$Q = 1.735 \times 10^{-4}\ \text{cm}^{-1}$$

$$A// = 101.56 \times 10^{-4}\ \text{cm}^{-1} \qquad (3)$$

$$A_\perp = 17.54 \times 10^{-4}\ \text{cm}^{-1}$$

The discrepancy between them and those already given in Table 1 is caused by the fact that the experimental values are the field separations between the ESR central lines of the hyperfine group and would correspond in first approximation to the hyperfine coupling constant only if the transitions equidistancy would be rigorously respected. Because the line separations are gradually increasing we had to use theoretically a higher order of approximation.

The additional splitting observed in the A type spectra we attribute to the superhyperfine interactions of the electron spin with the neighbouring ions

nuclei. The equidistancy between the signals of such a group (fig. 4) supports this statement. Consequently the spin hamiltonian will contain the term

$$\mathcal{H}_{shf} = \sum_{n} SA_p^n I_p^n \qquad (4)$$

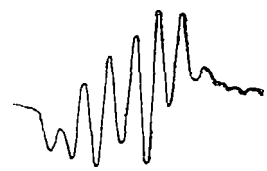

Fig. 4 Superhyperfine group of lines, showing typical characteristics for shf interactions.

corresponding to these interactions In (4) S is the electronic spin 1/2 of Cu^{2+} ions, A_P^n is the superhiperfine interaction tensor with the n-th phosphorous nucleus, and I = 1/2 the nuclear spin of this.

It is easy to observe from the angular dependence (fig. 2) that the superhyperfine interaction is isotrope, having the coupling constant $A = 8.8 \times 10^{-4}cm^{-1}$.

Our statement regarding these interactions is supported by the similarity of our spectra recorded for H//c, when site unequivalents are eliminated, and that characteristic for copper diethylditiophosphate [7], [8], where Cu-P interractions are not doubted. The spin hamiltonian parameters reported in [7] and [8] are in good agreement with those obtained by us (Table 1) These arguments seem sufficient to us to consider superhyperfine interraction as explaining quite well the structure of our spectra.

(Received February 4, 1978)

REFERENCES

1 I West, Z Krist 74, 306 (1930)
2. B. C Frazer, R. Pepinsky, Acta Cryst, 6, 273 (1953)
3 G. E Bacon, R E Pease, Proc. Roy Soc. (London), A220, 397 (1953), A230, 359 (1955)
4. P. R Sartene, O Parodis, J Phys, 28, 301 (1967)
5. A. Otani, S. Makishima, J. Phys Soc of Japan, 26, 85 (1969).
6. H Koga, K. Hukuda, J Phys Soc Japan, 25, 630 (1968)
7. R K Corosik, R Srinivason, J Chem Phys., 59, 5517 (1973)
8. N. Vezentan, O Cozar, I Milea, Studia Univ Babeș—Bolyai, Phys, 10 (1975)

INTERACȚIUNI SUPERHIPERFINE ÎN MONOCRISTALE KDP . Cu^{2+}

(Rezumat)

Lucrarea prezintă concluziile obținute prin RES în identificarea diverselor tipuri de poziții neechivalente ocupate de ionii Cu^{2+} în rețeaua monocristalelor de KH_2PO_4. Se explică structura spectrelor de rezonanță pe baza interacțiunilor de tip hiperfin, a efectului izotopic și a interacțiunilor superhiperfine cu nucleele ^{31}P.

STUDIA UNIV. BABEŞ–BOLYAI, PHYSICA, 2, 1978

THE FERROELECTRIC PHASE TRANSITION IN THE $\varphi^3+\varphi^4$—MODEL (I)

M. CRIŞAN, D. URSCHITZ, AL. ANGHEL

I. **Introduction.** The theory of the second order phase transitions was recently developed by Wilson using the φ^4—model. The presence of the φ^3—term plays a crucial role in the Landau theory of phase transitions and up to now it is not clear what the role of the cubic term is.

Alexander [1] pointed out that the second order phase transition is possible in the $\varphi^3+\varphi^4$ model, using the Ginsburg-Landau theory. A more sofisticated theory was developed by Alexander and Amit [2] for this model the main result of this paper being the existence of the critical point in the first order phase transition. This critical point „seems to be" the isolated Landau point which may exist in the first order phase transition. Such a problem was treated by Lubensky and Priest [3] in connection with the phase transitions in the liquid crystals, but the model is also a good one for ferroelectrics as $SrTiO_3$ [4]. In these papers as well as in [5] the RNG method which was used, pointed out the possibility of the phase transition in $4-\in$—dimensions. However there is a point in which all the calculations performed in [3—4] fail, namely if the bare interactions V_3 respectively U_4 are taken zero the recursion relation and the dimensions are not identical with those of the φ^3 or φ^4 pure models.

We believe, that in $4-\in$ dimensions which are considered by Alexander and Amit [3] the model is correct for a small value of U_3. In the language of the perturbation theory Crişan and Anghel [5] used only a class of dyagrams (divergent in $4-\in$) to analyse the $V_3\varphi^3+U_4\varphi^4$ model.

The purpose of this paper is to use the Wilson [7] recursion relation method in order to analyse the $\varphi^3+\varphi^4$—model.

Alexander and Amit [3] started this problem using the field theoretical method given by Biezin et al. [6] However it is our intention to get correct recurrence relation. More exactly, we look for such recursion relations that if we consider $U_4=0$ we get the recursion relations for φ^3—model and if $U_3=0$ we should obtain the recursion relations for φ^4—model

Before we apply the Wilson recursion relation we are going to analyse the model in the Ginsburg-Landau theory in section II.

II. **The Ginsburg—Landau Theory.** The free energy of the $V_3\varphi^3+U_4\varphi^4$ model is

$$F(\varphi)=r\varphi^2+V_3\varphi^3+U_4\varphi^4 \tag{1}$$

and in this relation we write down φ as

$$\varphi=\Phi+\psi \tag{2}$$

Using (1) and (2) we get for ψ the value

$$\psi = -\frac{V_3}{4U_4} \tag{3}$$

if the cubic term is eliminated from the free energy. The free energy (1) becomes

$$F(\Phi) = C(V_3, U_4) - \frac{V_3}{4U_4}\left(2r - \frac{V_3^2}{2U_4}\right)\Phi + \left(r - \frac{V_3^2}{2U_4}\right)\Phi^2 + U_4\Phi^4 \tag{4}$$

and the phase transition appears if the "effective external field"

$$H_{eff} = \frac{V_3}{4U_4}\left(2r - \frac{V_3^2}{2U_4}\right) \tag{5}$$

is zero, then

$$V_3 = 0 \tag{6.a}$$

$$r = \frac{V_3^2}{4U_4} \tag{6.b}$$

The relation (6.a) will give the usual Φ^4-theory and (6 b) describes an ordered phase
if

$$r = r_c < 0 \tag{7}$$

The next case is much more interesting; indeed if (6 b) is used in (4) we get

$$F(\Phi) = C(V_3, V_4) - \frac{V_3^2}{4U_4}\Phi^2 + U_4\Phi^4 \tag{8}$$

and this Hamiltonian describes a Φ^4—model with the ordered phase if

$$\frac{V_3^2}{4U_4} < |r_c| \tag{9}$$

In this case there is a new critical point defined as

$$\frac{V_3^2}{4U_4} = |r_c| \tag{10}$$

for $V_3 \neq 0$ and $V_4 \neq 0$.

These results present a real interest because in the next chapter we have to analyse, by RNG method, the real gaussian point obtained for $U_3 = 0$, $U_4 = 0$ and the other critical points obtained for $U_3 \neq 0$ and $U_4 \neq 0$.

III. **The Recursion Relations.** The Hamiltonian associated with the free energy (1) is

$$H = \int_x \left[\frac{1}{2}|\nabla\varphi_l(x)|^2 + Q_f(\varphi_l)\right] \tag{11}$$

where

$$Q_l(\varphi) = r_f\varphi^2 + v_l\varphi^3 + u_l\varphi^4 \tag{12}$$

The general form of the Wilson [7] recursion relation is

$$Q_{l+1}(y) = -2^D \ln\left[\frac{I_l(2 \cdot 2^{-D/2}y)}{I_l(0)}\right] \tag{13}$$

where the integral I_l is expressed as

$$I_l(z) = \int_{-\infty}^{+\infty} exp\left[-y^2 - \frac{1}{2}\, Q_l(z+y) - \frac{1}{2}\, Q_l(z-y)\right]$$

Using (11—13) we get the following recursion relations:

$$r_{l+1} = 4r_l + 12q_l u_l - 36q_l^3 u_l^2 - 9q_l^2 v_l^2 - \frac{351}{8}\, q_l^4 u_l v_l^2 - \frac{585}{8}\, q_l^5 u_l^3 \tag{14}$$

$$u_{l+1} = 2^{4-D}\left(u_l - 9q_l u_l^2 - \frac{243}{8}\, q_l^3 u_l v_l^2 - \frac{351}{8}\, q_l^4 u_l^3 + \ldots\right) \tag{15}$$

$$v_{l+1} = 2^{3-\frac{D}{2}}\left(v_l - 9q_l^2 u_l v_l - \frac{135}{4}\, q_l^4 u_l^2 v_l - \frac{81}{16}\, q_l^5 v_l^3\right) \tag{16}$$

where $q_l = \dfrac{1}{1+r}$.

These relations are quite general and selfconsistent Indeed if $V_l = 0$ we get the usual recursion relations for the φ^4—theory, and if $U_l = 0$ we get the recursion relations

$$r_{l+1} = 4r_l - 9q_l v_l^2 \tag{17}$$

$$v_{l+1} = 2^{\frac{6-D}{2}}\left(v_l - \frac{81}{16}\, q_l^3 v_l^3\right) \tag{18}$$

which are in fact the recursion relations for φ_3—theory The fixed point obtained from (18) is

$$v^* = \frac{4}{9}\sqrt{\frac{\ln 2}{2}}\, \varepsilon^{1/2} \tag{19}$$

in $D = 6 - \varepsilon$.

IV. **The Phase Transition.** Now we analyse the problem of the existence of phase transition in the model described by the Hamiltonian (1). From (14) results that in this phase transition we have the condition

$$\frac{3v_l^2}{4u} = 1 \tag{20}$$

in order to have $r_l = r_{l+1} = 0$

The fixed points of the recurrence relations (15—16) are:

$$\begin{cases} u^* = 0 \\ v^* = 0 \end{cases} \quad \text{the gaussian fixed point} \tag{21}$$

$$\begin{cases} u^* = 0 \\ v^* = 0{,}314 + 0{,}078 \in \ln 2 \end{cases} \tag{22}$$

$$\begin{cases} u^* = 0 \\ v^* = -0{,}314 - 0{,}078 \in \ln 2 \end{cases} \tag{23}$$

$$\begin{cases} u^* = -0{,}276 - 0{,}007 \in \ln 2 \\ v^* = 0{,}286 + 0{,}061 \in \ln 2 \end{cases} \tag{24}$$

$$\begin{cases} u^* = -0{,}276 - 0{,}007 \in \ln 2 \\ v^* = -0{,}286 - 0{,}061 \ \omega \in \ln 2 \end{cases} \tag{25}$$

These fixed points show the existence of the second order phase transition in $4 - \varepsilon$ dimensions for the $\varphi^3 + \varphi^4$—model.

In the next paper we are going to point out the eigenvalues of RNG and the critical exponents. However, we can conclude that for some ferroelectrics with a special symmetry where the φ_3—term is present, the phase transition can be strongly affected by this interaction. Our self—consistent treatment is a good starting point in the problem of the phase transitions in ferroelectrics with $\varphi^3 + \varphi^4$ interaction

(Received February 6, 1978)

REFERENCES

1 S Alexander, Solid St Commun, **14**, 1069 (1974)
2. S Alexander, D J Amit, J Phys **A8**, 1988 (1973)
3 R G. Priest, T C. Lubenski (preprint), 1974
4 E V Bursian, *Neliniinîi cristal*, (Nauka), Moskca, 1974
5 M. Crişan, Al Anghel, Phys Lett **54A**, 357 (1975)
6 E Brezin, D Walace, K G Wilson, Phys Rev **B7**, 232 (1973)
7 K. G Wilson, Phys, Rev, **B4**, 3174, 3184 (1971)

TRANZIŢIA DE FAZĂ FEROELECTRICĂ ÎN MODELUL $\varphi^3 + \varphi^4$ (I)

(Rezumat)

Se studiază existenţa tranziţiei de fază în modelul $\varphi^3 + \varphi^4$ folosind metoda grupului de renormare. Termenul de interacţiune $\varphi_3 + \varphi^4$ este folosit în descrierea tranziţiilor de fază în feroelectrici

STUDIA UNIV . BABEŞ–BOLYAI, PHYSICA, 2, 1978

EINE NICHTSTATIONÄRE METHODE FÜR MESSUNG DER WÄRMELEITFÄHIGKEIT DER KLEINEN PROBEKÖRPER

FRIEDRICH KELEMEN

Einleitung. Die Autoren [1] beschreiben eine nichtstationare Methode, deren Vorteil es ist, die Moglichkeit direkter Bestimmung der Warmeleitfahigkeit bei Probekörpern mit kleiner Dimension und mit Warmeleitfähigkeit der Grössenordnung von 10^{-1} bis 10^{-3} Watt/cm∘grad zu bieten. Die Funktion, die die zeitliche Anderung der Temperatur und die systematischen Fehler dieser Methode beschreibt, wurde theoretisch von [2] gepruft

Die vorerwahnte Methode wird in der physikalischen Literatur oft zitiert [3, 4]. Aber sie wurde experimentell nur durch Messungen bei Zimmertemperatur geprüft. Im allgemein aber ist die Messung der Warmeleitfahigkeit in einem grosseren Temperaturintervall notig. Unsere Studien uber Verwendungsmöglichkeiten der vorerwähnten Methode zwischen 100 und 450 K fuhrten zum Ergebnis, dass das experimentelle Verfahren praktischer wird, wenn die Variationsgeschwindigkeit der Temperatur ungefähr linear proportinal mit der Zeit ist, und nicht so schnell wie bei der [1] bezeichneten Methode. In diesem Fall ist die Registrierung der Temperaturvariationen genauer Unser experimentelles Verfahren ist neu, und deshalb beschreiben wir dessen Prinzip.

Prinzip der Methode. Der Probekorper wird zwischen zwei Kupferblocke gefasst (Abb. 1.a.), und der untere Block B_2 wird langsam mit einer konstanten Geschwindigkeit gekühlt, z.B. mit Stickstoffdampfen Kurze Zeit nach dem Beginn der Kühlung, bildet sich im Probekorper P ein Temperaturgefalle dT/dx, das sich in der Zeit langsam verandert, und die Temperaturveräderung des Blockes B_1 wird gerade proportional mit dem Temperaturabfall des Blockes B_2. Indem man den Warmewiderstand der Kontakte zwischen der Probe P und den Blocken B_1 und B_2 vernachlässigt, kan man $\frac{dT}{dx} = \frac{T_1 - T_2}{L}$ beschreiben, wo T_1 und T_2 die Temperaturen an den Enden der Blocke B_1 und B_2 darstellen, und L die Länge der Probe P bedeutet.

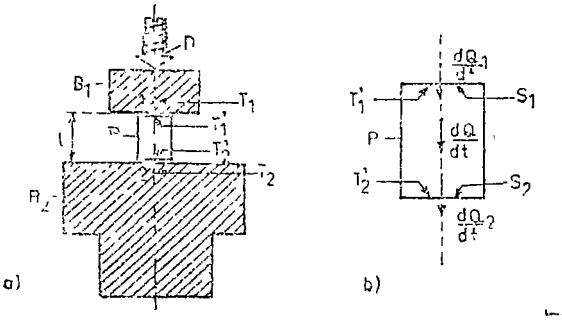

Abb. 1.a, und 1 b. Zur Erlauterung des Prinzips der Methode.

Wenn man vom Warmeubergang zwischen B_1 und der Umgebung absieht und die Wärmekapazitat C der Probe P gegenuber C_1 des Blockes B_1 nicht in Betracht gezogen wird, (also $C \ll C_1$), so kann der Warmestrom, der durch den Querschnitt S der Probe P geht, als gleich mit der von B_1 in der Zeiteinheit

verlorenen Wärmemenge betrachtet werden. In diesem Fall kann man beschreiben ·

$$C_1 \cdot \frac{dT_1}{dt} = \frac{T_1 - T_2}{W_m}, \tag{1}$$

wo

$$W_m = \frac{L}{K_m \cdot S} \tag{2}$$

und reprasentiert de Warmewiderstand zwischen den Punkten 1 und 2, aufgenommen in B_1 und B_2 (Abb.1 a), K_m ist der Koeffizient fur die erwähnten Verhältnisse bestimmten Warmeleitfahigkeit der Probe P.

In algemeinen aber wachst die Warmeleitfahigkeit der Kristalle schnell mit der Temperaturabfall Im Falle der Proben mit 1—2 cm Länge kann man den Wärmewiderstand der Kontakte nicht unbeachtet lassen im Vergleich zum Warmewiderstand der Probe, das bedeutet, dass die Temperaturen T_1 und T_2 von den Temperaturen T_1' und T_2' der Enden des Probekörpers verschieden sind (Abb. 1. a, b) Wenn durch die Kontaktoberflachen S_1 und S_2 und durch den Querschnitt S der Probe derselbe Warmestrom ubergeht (Abb 1.b), kann man schreiben

$$C_1 \quad \frac{dT_1}{dt} = \frac{T_1 - T_2}{W_{c,2} + W + W_{c,1}}, \tag{3}$$

wo

$$W_{c,1} = \frac{L_{c,1}}{K_{c,2} \cdot S_1}, \quad W_{c,2} = \frac{L_{c,2}}{K_{c,1} \cdot S_2}, \quad W = \frac{L}{K \cdot S}. \tag{4 a, b,c}$$

Die letzteren drei Formeln reprasentieren die Wärmewiderstande der Kontakte und der Probe Aus den Gleichungen (1) und (3) folgt

$$W_m = 2W_c + W, \tag{5}$$

wenn man voraussetzt, dass $W_{c,1} + W_{c,2} = 2W_c$. Weil die Blocke B_1 und B_2 aus demselben Metall (Kupfer) bereitet sind, kann man schreiben $W_{c,1} = W_{c,2} = W$, wenn die Temperatur T_1 sich nicht sehr von T_2 unterscheidet.

Aus den Gleichungen (2), (4c) und (5) folgt:

$$K = K_m \left(1 + \frac{2W_c}{W}\right). \tag{6}$$

Von hier ist ersichtlich, dass der systematische Fehler, der aus dem Wärmewiderstand W_c der Kontakten stammt, nicht unebbeachtet beliben kann, ausser Falle, wenn $2W_c$ nicht hloher ist als ungerfahr 3% der W_c.

Den Wärmewiderstand W_c bei einer gegebenen Temperatur kann man mit einem Probekörper bestimmen, dessen Warmeleitfahigkeit bekannt ist. Nach [1] kann man eine aus Blei verfertigte Probe benutzen. Aber der Wert von W_c, bezogen auf die Oberflächeneinheit, hängt von der Qualität (Glattheit) der Kontaktoberfläche ab, und, eventuell, auch von der Eigenschaft der Körper, die in Kontakt sind. Den Wärmewiderstand W_c kann man auch so bestimmen,

dass man die Messungen an zwei Probekörpern aus demselben Stoffe aber verschiedener Länge macht. Wenn die Querschnitte der Proben sich nicht auch in der Länge verändern, dann kann man nach den Gleichungen (4 a, b, c) und (5) für alle Proben schreiben:

$$\frac{L}{K} = \frac{L}{K_m} - \frac{2L_c}{K_c} \tag{7}$$

Wenn die Messungen an zwei Proben, mit Längen L_1 und L_2 (eventuell mit gleichen Querschnitten, $S_1 = S_2$) vorgenommen werden, ist die Wärmeleitfähigkeit

$$K = \frac{L_2 - L_1}{\frac{L_2}{K_{m,2}} - \frac{L_1}{K_{m,1}}}, \tag{8}$$

wo $K_{m,1}$ und $K_{m,2}$ die Werte der Wärmeleitfähigkeit an den zwei Proben nach der Gleichung (1) erhalten sind. Ebenfalls aus den Gleichungen (4 a, b, c) und (5) folgt, dass der Wärmewiderstand der Kontakte von der Gleichung gegeben ist:

$$2W_c = \frac{L_1}{S_1} \cdot \left(\frac{1}{K_{m,1}} - \frac{1}{K}\right), \text{ oder } 2W_c = \frac{L_2}{S_2} \cdot \left(\frac{1}{K_{m,2}} - \frac{1}{K}\right) \tag{9a, b}$$

Wenn die Beidngung $C \ll C_1$ nicht erfüllt ist, so ist der Temperaturunterschied $(T_1 - T_2)$ messbar beeinflusst auch von der bei der Probe verlorenen Wärmemenge. Der Wärmestrom, der von der Kühlung der Probe stammt, ist $\frac{dQ_p}{dt} = \frac{C}{2} \cdot \frac{d(T_1 + T_2)}{dt}$. Dieses Glied muss man zu der linken Seite der Gleichung (1) oder (3) hinzufügen, damit man den realen Wert des K_m erhällt, also

$$K_m = \frac{LC_1}{S\ (T_1 - T_2)} \cdot \frac{dT_1}{dt}\left(1 + \frac{C}{2C_1} \cdot \frac{dT_1 + dT_2}{dT_1}\right). \tag{10}$$

Wenn die Messungen durch Erwarmung des Blockes B_2 gemacht wurden, ist das zweite Glied in der Klammer der Gleichung (10) negativ, weil man den Warmestrom $^{dQ}p/dt$ zur Erwarmung der Probe benutzt.

Wenn die Messungen sowohl durch Kuhlung als auch durch Erwärmung gemacht werden, kann man den Quotienten C/C_1 annaherend bestimmen aus der Gleichung

$$\frac{C}{2C_1} = \left(\frac{K_{m,w}}{K_{m,k}} - 1\right) \cdot \left[1 - \frac{1}{2} \cdot \left(\frac{dT_{2,k}}{dT_{1,k}} + \frac{dT_{2,w}}{dT_{1,w}}\right)\right], \tag{11}$$

wo $K_{m,w}$, resp $K_{m,k}$ der Wert von K_m ist, bestimmt aus Gleichung (1), aus den Messungen durch Erwärmung, resp Kuhlung, und $dT_{1,w}$ und $dT_{2,w}$ resp. $dT_{1,k}$ und $dT_{2,k}$ sind die Variationen der Temperaturen T_1 und T_2 in Zeit dt bei Erwärnung, resp Kuhlung.

Beschreibung der Versuchsapparatur. Der vertikale Schnitt dessen Teiles der Versuchsapparatur, in welche die Probe montiert ist, wird in Abb. 2. dargestellt. Um das System Block B_1-Probe P-Block B_2 wird ein parallelepipedförmiger

Messigschutzmantel A verwendet Der niedrigere Teil dieses Mantels ist an der Block B_2 befestigt, und seine vordere Seite ist abmontierbar Das System Mantel A- Block B_2 wird im Block B_3 in eniem zylinderförmiger Hohlraum montiert Durch den Hohlraum C, der sich im niedrigen Teil des Blockes B_3 befindet, strömen Stickstoffdampfe, die denselben akbuhlen. Ausserdem kann den Block B_3 mit Hilfe eines Heizdrahtes, der auf seine seitliche Oberflache gewickelt wurde, erwärmt werden Auf diese Art kann die Temperatur des B_3 sowohl durch Kühlung als auch durch Erwarmung geandeit werden. Das gesamte beschriebene System ist in einem Vakuumgefass montiert

Bei der Kuhlung, resp. bei Erwärmung des Blockes B_2 bildet sich in den Wanden des Gefasses A, sowie in seinem inneren Teil ein Temperaturgefälle in dieselbe Richtung wie in dem System Probe P — Block B_1-Stab D. Durch die Benutzung des Mantels A sinkt gleichzeitig die Warmeströmung, die dem Betrieb der Vakuumpumpe entstammt In dieser Art fallt der Warmeubergang zwischen dem System Probe P — Block B_1 und der Umgebung wesentlich ab.

Block B_1 wird an die Probe P mit Hilfe eines zugespitzene Glasstabes D gepresst, um die Kontaktoberfläche zwischen ihnen zu verkleinern Der Glasstab D wird durch die Springfeder R gedruckt Dieses Befestigungssystem bietet eine genügende Elastizität für die Warmeausdehnung des Probekörpers.

Die Eisen-Konstatan Thermoelemente Te_1, Te_2 und Te_3 sind aus Drahten von 0.2 mm Durchmesser hergestellt. Te_1 misst die Temperatur des Körpers B_1, Te_2 die des Blockes B_2 und Te_3 die Temperatur in dem Gefäss A an der Höhe des Blockes B_1. Die thermoelektrische Spannung wurde mit Hilfe einer Kompensationsbrucke, von Präzision 10^{-7} V, gemessen. Der zu dieser Brucke benutzte Galvanometer hat eine Empfindlichkeit von 10^{-6} V/div. Auf diese Art haben die Temperaturmessungen eine Präzision von umgefähr 0,02 K Das bedeutet einen experimentellen Fehler von 0,2 bis 0,4% bei Messungen de Temperaturunterschiedes $(T_1 - T_2)$, und von 0,3 bis 0,6% bei Messung der Temperaturänderung ΔT_1. Um die Präzision zu vergrössen, wurden die Temperaturen T_1, T_2 und T_3 nacheinander gemessen

Mit kleinen Ergänzungen kann man die Versuchsapparatur auch fur stationare Messungen gebrauchen.

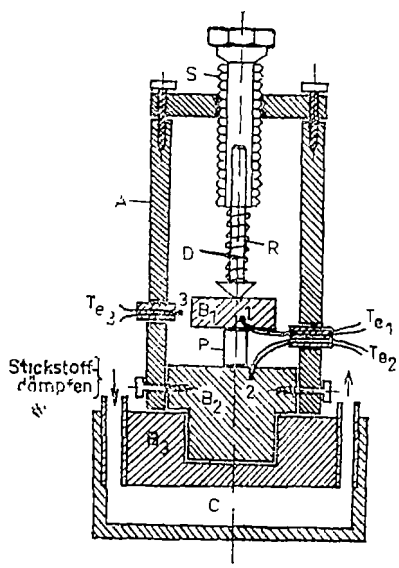

Abb 2 Versuchsapparatur

Versuchsergebnisse. Um die vorliegende Methode und die Versuchsapparatur experimentell zu prufen, wurden Messungen mit NaCl-Proben durchgefuhrt. Es wurde NaCl gewählt, weil die experimentellen Ergebnisse der verschiedenen Autoren fur die Wärmeleitfähigkeit dieser Substanz ubereinstimmen Deshalb können die NaCl— (oder KCl—) Proben als Wärmeleitfahigkeitsetalon verwendet werden [5]. Die NaCl Monokristalle wurden mit der Kiropoulos-Methode aus

chemisch reinen Stoffen verfegtigt. (Auch bei dieser Gelegenheit danke ich dem Kollegen A. Darabont fur die NaCl Monokristalle, die er mir zur Verfügung gestellt hat.).

Die ersten Messungen wurden mit drei Proben verschiedener Lange $L_1 = 0{,}385$ cm, $L_2 = 0{,}692$ cm, $L_3 = 1{,}478$ cm), ohne Verbesserung der Kontakte zwischen den Blocken B_1, B_2 und den Proben P, duchgeführt. Sie haben bewiesen, dass die Wärmewiderstände der Luftkontakte beachtlich grosse sind. Um die Warmewiderstande der Kontakte zu vermindern, sind bestimmte Flüssigkeiten, Vacuumsöle, oder Amalgame (z B. In-Ga) benutzt. Ich habe fur diesen Zweck Zapfenschmiere benützt. Vor den Messungen wurde der Probekorper in der Versuchsapparatur bis zu ungefahr 500 K ervarmt, und nach der Temperaturstabilisierung wurden die Messungen durch Kuhlung durchgefuhrt. Ohne vorhergegangene Erwarmung der Probe war der Warmewiderstand der Kontakte, bei der Benützung der Zapfelschmiere, grosser.

Abb. 3. zeigt die Änderung der Werte des Koeffizienten K, nach der Gleichung (10)berechnet, als Funktion der Temperatur T. Die Werte der Kurwe $K_{m,1}$ beziehen sich auf die Probe mit Lange $L_1 = 0{,}7237$ cm, die Kurve $K_{m,2}$ zu $L_2 = 1{,}1555$ cm, und $K_{m,3}$ zu $L_3 = 1{,}7282$ cm. Die ununterbrochene Kurve K stellt die Warmeleitfahigkeit des NaCl nach den Messungen [5] dar Die, mit kleinen Kreisen dargestellten Werten wurden aus der Gleichung (8).

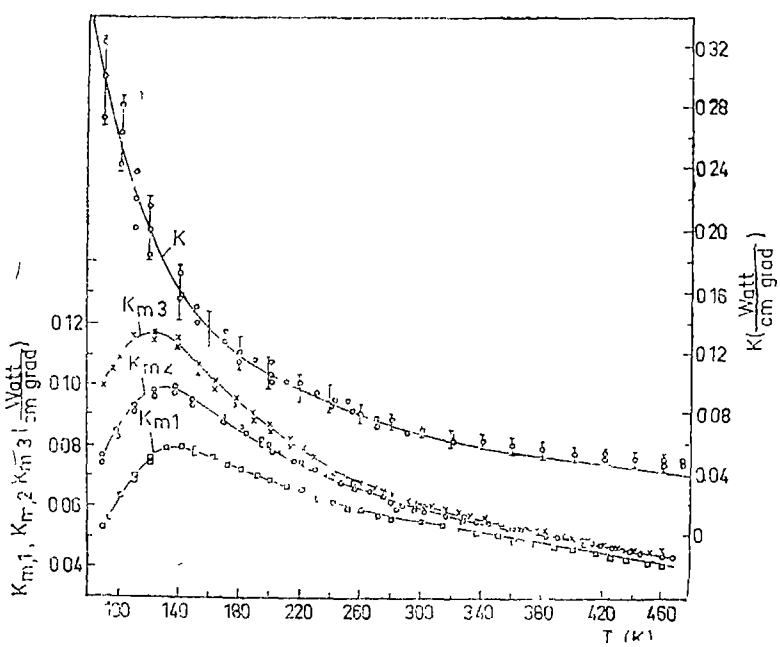

Abb 3 Die Änderung der Koeffizientem $K_{m,1}$, $K_{m,2}$, $K_{m,3}$ und K als Funktion der TemperaturaT. $K_{m,1}$, $K_{m,2}$, $K_{m,3}$ sind bei Proben mit Lange $L_1 = 0{,}7237$ cm, $L_2 = 1{,}15555$ cm und $L_3 = 1{,}7282$ cm gemessen.

auf Grund der Kurven $K_{m,1}$, $K_{m,2}$ und $K_{m,3}$ berechnet. Die ubereinstimmung zwischen unseren und den von [5] erhaltenen Werten ist entsprechend.

Abb. 4. stellt den Wärmewiderstand $W_{c,0} = W_d \cdot S$ dar. Die Kurve 1 bezieht sich auf Kontakte mit Zapfenschmiere, und die Kurve 2 auf jene mit Luftschichten. Aus den Werten der Kurve 2 ergibt sich, dass die Dicke der Luftschicht zwischen der Probe und den Blocken B_1 und B_2 ungefahr $1{,}3 \cdot 10^{-3}$ cm ist und sich mit der Temperatur erhoht. Deshalb kann die Vorliegende Methode auch fur die Bestimmung der Warmeleitfahigkeit der Gase und Flussigkeiten angewendet werden

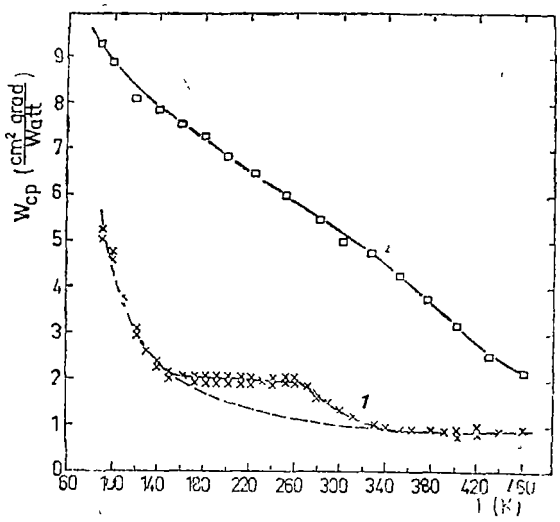

Abb 4 Die Anderung des Warmewiderstandes $W_{c,0}$ als Funktion der Temperatur Die Kurve 1 bezieht sich zum Kontakte mit Zapfenschmiere und die Kurve 2 zum Kontakte mit Luftschichte

Messfehler und Fehlerquellen. Die Präzision, mit der man den Koeffizienten K_m bestimmen kann, hangt von den Messfehlern der Temperaturen T_1 und T_2 ab. Wie sich erwahnt habe, bleiben diese Fehler unter 1%, wenn die Messungen sorgfaltig durchgefuhrt waren Deshalb kann man die Bestimmung des K_m, entsprechend der Gleichung (1) oder (10), mit einer Präzision von 2—3% erzielen.

Der relative Fehler bei der Bestimmung de Koeffizienten K nach der Gleichung (8) ist ungefahr·

$$\frac{\Delta K}{K} = \pm \left[\frac{\Delta K_{m\,1}}{K_{m,1}} + \frac{\Delta K_{m,2}}{K_{m,2}} + \frac{\Delta K_{m,1} + \Delta K_{m,2}}{K_{m,2} - K_{m,1}} \right], \qquad (12)$$

dementsprechend kann man den Wert des K mit einer Präzision von ungefähr 10% bestimmen Die Fehler, die aus den experimentellen Daten bei veschiedenen Temperaturen stammen, sind auf der Kurve K in Abb. 3 angezeigt Die Prazision ist grosser, wenn die Messungen mit zwei Proben sehr verschiedener Länge L_1 und L_2 durchgefuhrt wurden.

Wenn der Warmewiderstand W_c der Kontakte bekannt ist oder unbeachtet bleiben kann ($W_c \ll W$), unterschiedet sich ΔK nicht von ΔK_m.

Es gibt Fehlerquellen auch aus folgenden Grunden· (a) Warmeleitung der Luft in der Umgebung der Probe; (b) Warmeubergang zwischen B_1 und seiner Umgebung; (c) Wärmeleitung durch die Kontaktoberflache zwischen B_1 und D. Die ersten zwei erwähten Fehlerquellen sind nicht beachtbar, wenn das in der Versuchsapparatur erzeugte Vakuum besser als 10^{-3} Torr ist. Weil die Temperatur der Stabes D sich von der T_1 unterscheidet, kann der Wärmes-

trom durch die Kontaktoberfläche der B_1 und D nur in dem Falle vernachlässigt werden, wenn der Wärmewiderstand des Kontaktes viel grösser ist als der der Probe P.

Die erwähnten Fehlerquellen erklaren es, dass bei Temperaturen uber 350 K die aus der Gleichung (8) berechneten Werte des K grösser werden als die aus der Arbeit [5] entnommenen Werte

(Eingegangen am 9 Februar, 1978)

LITERATUR

1 A. V. Joffei A F. Joffe, Zh TF, **22** (12), 2005 (1952) **ZhTF**, **28** (11), 2357 (1958)
2 M A Kaganow, Zh.T.F, **28** (11), 2364 (1958)
3 J R Drabble and H J Goldsmid, *Thermal Conduction in Semiconductors*, Pergamon Press, Oxford—London—New York—Paris, 1961, russisch Izd innostrannoi Lit., Moskva, 1963, S 33
4 P Nath and K L Chopra, Thin Solid Films, **18**, 29 (1973).
5 E D Dewjatkowai I A Smirnow FTT, **4** (7), **1972** (1962), F.T T, **4** (9), 2507 (1962)

O METODĂ NESTAŢIONARĂ PENTRU MĂSURAREA CONDUCTIBILITĂŢII TERMICE A PROBELOR MICI

(Rezumat)

Se descrie o metodă nestaţionară pentru măsurarea coductibilităţii termice a probelor mici Ea se bazează pe măsurarea rezistenţei termice între cele două capete ale probei Proba este montată între două blocuri de cupru şi blocul inferior este răcit sau încălzit în mod continuu. Pentru determinarea precisă a coeficientului de conductibilitate termică a probei este necesar să se cunoască, sau să se determine, şi rezistenţa termică a contactelor între probă şi blocurile de cupru Măsurătorile de verificare s-au făcut cu proba de NaCl de lungimi diferite

STUDIA UNIV. BABEŞ–BOLYAI, PHYSICA, 2, 1978

MOLECULAR g VALUE CALCULATIONS FOR AXIALLY DISTORTED d^7 LOW SPIN CONFIGURATION IN STRONG CRYSTAL FIELD

LIVIU V. GIURGIU*, AL. NICULA

I. Introduction. Metal complexes, based on platinum atoms, which possess a columnar structure and contain an infinite number of directly interacting metal atoms arranged in a linear chain throughout the crystal, have attracted considerable attention [1] as a result of the highly anisotropic character of their electrical properties The ESR measurements were reported for some of these complexes [2, 3, 4, 5] showing that the observed magnetic centers are holes in d_{z^2} like states. In the case of $Pt(NH_3)PtCl_4$, such states are formally equivalent to the localized Pt^{3+} like states [2]. As ESR provides a tool for determining the relative ordering of the d-orbital energy levels, one has to compare the experimental g values with the calculated ones, in order to determine the character of the ground state. Being involved in a systematic study of one-dimensional complexes containing platinum species, we undertook a theoretical calculation for the case of a Pt^{3+} complex, with axially symmetric g value, in a $5d^7$ low spin configuration, $S = 1/2$

II. The first-order g tensor calculation in strong crystal field The d-orbital energy level schemes in tetragonally distorted octahedral complexes and in planar complexes, can be predicted by considering symmetry arguments [6] For Pt species in a $5d^7$ configuration, $S = 1/2$, with an axially tetragonal distorsion, the d_{z^2}, d_{xy} or $d_{x^2-y^2}$ orbitals are the possible ground states.

The metal ground state is subject to admixture of various excited states by spin-orbit coupling It is possible to calculate the g tensor elements directly from a well-known general formula [6]. In the case of strong crystal field problem, it is better to perform the sequential perturbations of spin-orbit coupling over the ground state wave function $|0>$, followed by the Zeeman interaction [7]. The principal g tensor elements are:

$$g_{xx} = 2\sum_i < \alpha |l_{ix} + 2s_{ix}| \beta >$$

$$g_{yy} = 2i\sum_i < \alpha |l_{iy} + 2s_{iy}| \beta > \qquad (1)$$

$$g_{zz} = 2\sum_i < \alpha |l_{iz} + 2s_{iz}| \beta >$$

where $|\alpha>$ and $|\beta>$ are the doublet ground state improved wave functions.

* Institute of Isotopic and Molecular Technology, Cluj-Napoca

As an example, the case of a complex with an axially symmetric g value ($g_{zz} = g_{\parallel}$, $g_{xx} = g_{yy} = g_{\perp}$) and the unpaired electron in d_{z^2} and d_{xy} orbitals will be examined. In the hole formalism, the zero order Kramer's doublet, for a d_{z^2} ground state is:

$$\begin{aligned} |0^+> &= |(x^2-y^2)^2(z^2)^+> \\ |0^-> &= |(x^2-y^2)^2(z^2)^-> \end{aligned} \tag{2}$$

and for a d_{xy} ground state.

$$\begin{aligned} |0^+> &= |(x^2-y^2)^2(xy)^+> \\ |0^-> &= |(x^2-y^2)^2(xy)^-> \end{aligned} \tag{3}$$

where $|0>$ refers to the ground state wave function. The calculation is facilitated by the use of two tables: the first, the effect of the operator $\bar{l}\cdot\bar{s}$ on the d-orbital set is represented in Ballhausen's book [8], the second, giving the matrix elements of the orbital angular momentum within the d-orbital set, is compiled in Mc. Garvey's review [9] The first-order improved configurational wave function $|\alpha>$ for d_{z^2} ground state, is obtained by applying the spin-orbit interaction Hamiltonian, as a peturbation, and using standard first-order perturbation theory:

$$\begin{aligned} |\alpha> = N\{&|(x^2-y^2)^2(z^2)^+> + ia_1|(x^2-y^2)^-(xy)^+(z^2)^+> - \\ &- ia_1|(x^2-y^2)^+(xy)^-(z^2)^+> - ia_2/2\,|(x^2-y^2)^-(yz)^-(z^2)^+> - \\ &- ia_4/2\,|(x^2-y^2)^+(yz)^+(z^2)^+> + a_2/2\,|(x^2-y^2)^-(xz)^-(z^2)^+> - \\ &- a_4/2\,|(x^2-y^2)^+(xz)^-(z^2)^+> - a_3\sqrt{3}/2\,|(x^2-y^2)^2(xz)^-> - \\ &- ia_3\sqrt{3}/2\,|(x^2-y^2)^2(yz)^->\} \end{aligned} \tag{4}$$

where N is a normalization constant and a_i are the mixing parameters, $a_i = \zeta/\Delta E_i$, ζ being one-electron metal spin-orbit coupling constant (ζ is always positive), and ΔE_i a configurational excitation energy. The first order $|\beta>$ function is found from $(x^2-y^2)^2(z^2)^->$ in a similar manner

For d_{xy} ground state, the wave function $|\alpha>$ is·

$$\begin{aligned} |\alpha> = N\{&|(x^2-y^2)^2(xy)^+> - ia_1|(x^2-y^2)^+(xy)^-(xy)^+> - \\ &-ia_2/2\,|(x^2-y^2)^-(yz)^-(xy)^+> - ia_4/2\,|(x^2-y^2)^+(yz)^+(xy)^+> + \\ &+a_2/2\,|(x^2-y^2)^-(xz)^-(xy)^+> - a_4/2\,|(x^2-y^2)^+(xz)^+(xy)^+> + \\ &+a_3/2\,|(x^2-y^2)^2(yz)^->+ ia_3/2\,|(x^2-y^2)^2(xz)^->\} \end{aligned} \tag{5}$$

and similarly we can obtain the first order $|\beta>$function.

With doublet ground state wave functions $|\alpha>$ and $|\beta>$, by using the Zeeman spin-Hamiltonian expressions of Equation (1), the following principal g tensor elements were found:

— for d_{z^2} ground state:

$$\begin{aligned} g_{\parallel} &= 2N^2 + N^2(4a_1^2 - 2a_2^2 + 4a_4^2) \\ g_{\perp} &= 2N^2 + 6Na_3 + N^2(4a_1^2 + a_2^2 + a_4^2) \end{aligned} \tag{6}$$

— for d_{xy} ground state:

$$\begin{aligned} g_{\parallel} &= 2N^2 - 8Na_1 + N^2(2a_1^2 - 2a_2^2 - 2a_3a_2 - a_3^2 - 3a_4^2 - 2a_3a_4) \\ g_{\perp} &= 2N^2 + 2Na_3 + N^2(a_2^2 + a_4^2 - 2a_1^2 - a_1a_4) \end{aligned} \tag{7}$$

The perturbation coefficients, a_i, being usually small enough, any product of two coefficients can be ignored, and equations (6) and (7) become:

$$\begin{aligned} g_{\parallel} &= 2N^2 \\ g_{\perp} &= 2N^2 + 6N\zeta/\Delta E_3 \end{aligned} \tag{6'}$$

and

$$\begin{aligned} g_{\parallel} &= 2N^2 - 8N\zeta/\Delta E_1 \\ g_{\perp} &= 2N^2 + 2N\zeta/\Delta E_2 \end{aligned} \tag{7'}$$

where $\Delta E_1 = |E(x^2 - y^2) - E(xy)|$; $\Delta E_2 = |E(xz, yz) - E(xy)|$; $\Delta E_3 = |E(xz, yz) - E(z^2)|$

In the case of a complex with $d_{x^2-y^2}$ ground state, by using the same method, the principal g tensor elements are:

$$\begin{aligned} g_{\parallel} &= 2N^2 + 8N\zeta/\Delta E_4 \\ g_{\perp} &= 2N^2 + 2N\zeta/\Delta E_4 \end{aligned} \tag{8}$$

where $\Delta E_4 = |E(xz, yz) - E(x^2 - y^2)|$

III. The second-order g tensor calculation in strong crystal field.

Due to the large spin-orbit coupling constant of Pt^{3+} ion, an improved set of crystal field g values was calculated by carrying the treatment to second order. The second-order correction terms can be computed by the method of Tippins [10], or one has to derive a ground state wave function correct to second order in ζ and then apply the magnetic perturbation. By calculating

the third-order correction to the energy of the ground state, Tippins obtained the following general formulae for the second-order g shifts ($\Delta g_{ik} = g_{ik} - 2$):

$$\Delta g_{||}^{(2)} = \zeta^2[\sum_{j,k}'(i/\Delta E_j \Delta E_k)(z_{0j}x_{jk}y_{k0} + x_{0j}y_{jk}z_{k0} + x_{0j}z_{jk}y_{k0}) - \\ - \sum_j'(1/\Delta E_j^2)(|x_{0j}|^2 + |y_{0j}|^2)] \tag{9}$$

$$\Delta g_{\perp}^{(2)} = \zeta^2[\sum_{j,k}'(i/\Delta E_j \Delta E_k)(y_{0j}x_{jk}z_{k0} + x_{0j}y_{jk}z_{k0} + y_{0j}z_{jk}x_{k0}) - \\ - \sum_j'(1/\Delta E_j^2)(|y_{0j}|^2 + |z_{0j}|^2)] \tag{10}$$

where $x_{jk} = \langle j|l_x|k\rangle$ and similarly for the other components of the angular momentum $\bar{l}$, ΔE_j being as before.

For the d_{x^2} ground state, the nonzero matrix elements of the angular momentum are:

$$\langle d_{x^2}|l_x|d_{yz}\rangle = i\sqrt{3}$$
$$\langle d_{x^2}|l_y|d_{xz}\rangle = -i\sqrt{3} \tag{11}$$
$$\langle d_{xz}|l_z|d_{yz}\rangle = -i$$

and from the expressions (9) (10), also considering the normalization constant N of the zero-order configuration in the wave function that arises from the spin-orbit interaction, we obtained:

$$\Delta g_{||}^{(2)} = -3N^2\zeta^2/\Delta E_3^2$$
$$\Delta g_{\perp}^{(2)} = -6N^2\zeta^2/\Delta E_3^2 \tag{12}$$

For the d_{xy} ground state, similarly were found:

$$\Delta g_{||}^{(2)} = -4N^2\zeta^2/\Delta E_1 \Delta E_2 - 3N^2\zeta^2/\Delta E_2^2$$
$$\Delta g_{\perp}^{(2)} = -4N^2\zeta^2/\Delta E_1^2 \tag{13}$$

For the $d_{x^2-y^2}$ ground state the results are:

$$\Delta g_{||}^{(2)} = -4N^2\zeta^2/\Delta E_1 \Delta E_4 - 3N^2\zeta^2/\Delta E_4^2$$
$$\Delta g_{\perp}^{(2)} = -4N^2\zeta^2/\Delta E_1^2 \tag{14}$$

The calculated g values for d^7 low spin state are summarized in table 1.

Table 1

5d orbital	$g_{\|\|}$	$g_\perp$	order
d_{z^2}	$2N^2 - 3N^2\zeta^2/\Delta E_3^2$	$2N^2 + 6N\zeta/\Delta E_3 - 6N^2\zeta^2/\Delta E_3^2$	$g_\perp > g_{\|\|} \simeq 2$
d_{xy}	$2N^2 - 8N\zeta/\Delta E_1 - 4N^2\zeta^2/\Delta E_1\Delta E_2 - 3N^2\zeta^2/\Delta E_2^2$	$2N^2 + 2N\zeta/\Delta E_2 - 4N^2\zeta^2/\Delta E_1^2$	$g_\perp > 2 > g_{\|\|}$
$d_{x^2-y^2}$	$2N^2 + 8N\zeta/\Delta E_1 - 4N^2\zeta^2/\Delta E_1\Delta E_4 - 3N^2\zeta^2/\Delta E_4^2$	$2N^2 + 2N\zeta/\Delta E_4 - 4N^2\zeta^2/\Delta E_1^2$	$g_{\|\|} > g_\perp > 2$

$\Delta E_1 = |E(x^2 - y^2) - E(xy)|$, $\Delta E_2 = |E(xz, yz) - E(xy)|$, $\Delta E_3 = |E(xz, yz) - E(z^2)|$; $\Delta E_4 = |E(xz, yz) - E(x^2 - y^2)|$,

IV. Conclusions. The comparison between the magnitudes of the experimental g values with the calculated ones (table 1), allows a correct determination of the ground state for d^7 low spin complexes [2].

(Received February 20, 1978)

REFERENCES

1 *Proc. NATO Summer Institute on Low Dimensional Conductors*, Plenum Press, New York, 1975
2. Liviu V. Giurgiu, I. Ursu, *Proc XIX Congres AMPERE*, 1976, p 622
3 F Mehran, B A Scott, Phys Rev Lett., **31**, 99 (1973)
4 F Mehran, B A Scott, Phys Rev Lett., **31**, 1347(1973)
5 M Gaerttner, T Cole, R Jaklevic, R. Saillant, J. Phys Chem Solids, **37**, 495 (1976)
6. I Ursu, *La Résonance Paramagnétique Électronique*, Ed Dunod, Paris, 1968
7 T Krigas, M. T. Rogers, J Chem Phys, **55**, 3035 (1971).
8 C J. Ballhausen, *Introduction to Ligand Field Theory*, New York, 1962
9 B R. Mc Garvey, *Transition Metal Chemistry*, New York, 1966
10 H H. Tippins, Phys Rev., **160**, 343 (1967)

CALCULAREA VALORILOR g MOLECULARE PENTRU CONFIGURAȚIA DE SPIN MIC d^7, DISTORSIONATĂ AXIAL ÎN CÎMP CRISTALIN PUTERNIC

(Rezumat)

Pentru configurația electronică d^7, de spin mic $S = 1/2$, au fost calculate expresiile teoretice ale tensorului g axial în aproximația cîmpului cristalin puternic Funcțiile de undă caracteristice stărilor fundamentale de tipul d_{z^2}, d_{xy} și $d_{x^2-y^2}$-au obținut în urma aplicării interacțiunii de cuplaj spin orbită asupra funcțiilor de undă ale dubleților Kramers respectivi S-au determinat corecțiile de ordinul doi ale tensorilor g axiali pentru fiecare stare fundamentală

STUDIA UNIV. BABEŞ–BOLYAI, PHYSICA, 2, 1978

SUR UN MODÈLE DE PLASMA COSMIQUE AVEC UNE DENSITÉ VARIABLE

MIRCEA VASIU

1. **Introduction.** Dans le présent mémoire nous voulons déduire l'équation de dispersion d'un modèle de plasma infini, compressible, visqueux, doué d'une pression anisotrope et d'une conductivité électrique finie, avec une densité variable, en mouvement de rotation, en présence du courant Hall, sous l'action de son propre champ gravifique et aussi sous l'action d'un champ magnétique uniforme-axial.

Nous utilisons les résultats obtenus par Sharma, Prakash [1] et par Bhatia, Gupta [2]. À la difference des travaux cités, nous prenons en considération, simultanément, l'action des grandeurs physiques qui définissent le modèle de plasma analysé : la *compressibilité*, la viscosité, l'*anisotropie de la pression*, la conductivité électrique finie, la *densite variable*, le mouvement de rotation, la présence du courant Hall, l'action de son propre champ gravifique et d'un champ magnétique uniforme-axial.

Nous choisirons comme système de référence le système de coordonnées cartésiennes Oxyz. On suppose que, dans l'état d'équilibre, le plasma possède une vitesse nule ($\vec{v}_0 = 0$), une composante Ω du vecteur vitesse angulaire $\vec{\Omega}$, dirigée d'après l'axe Oz ($\vec{\Omega}(0, 0, \Omega)$)et aussi une composante $\vec{H}_0$ du vecteur champ magnétique $\vec{H}_0$, dirigée d'après l'axe Oz ($\vec{H}_0(0, 0, H_0)$). La densité ρ_0 et aussi le potentiel gravifique V_0 sont fonctions de variable z [2] :

$$\rho_0(z) = \rho_1 \exp(\beta z) \tag{1}$$

et

$$V_0(z) = \frac{4\pi G\rho_1}{\beta^2}[-\exp(\beta z) + \beta z + 1] \tag{2}$$

où ρ_1 est la densité ρ_0 pour $z = 0$, β est une constante et G est la constante gravitationnelle.

Nous admettons des variations de type adiabatique pour la pression du plasma

2. **L'état perturbé du plasma.** Admettons maintenant que de petites perturbations de la densité, de la vitesse, de la pression, du potentiel gravifique et du champ magnétique se superposent à l'état d'équilibre du plasma, de manière qu'on peut écrire

$$\begin{gathered} v = v_0 + v'(x, y, z, t) = v'(x, y, z, t), \\ \rho = \rho_0(z) + \rho'(x, y, z, t),\ p = p_0 + p'(x, y, z, t) \\ V = V_0(z) + V'(x, y, z, t),\ \vec{H} = \vec{H}_0 + \vec{H}'(x, y, z, t) \end{gathered} \tag{3}$$

Les perturbations peuvent être considérées comme petites, de sorte que leurs carrés et leurs produits peuvent être négligés. En remplaçant les perturbations (3) dans les équations magnétohydrodynamiques pour le modèle de plasma étudié, on obtient le système d'équations

$$\rho_0 \frac{\partial \vec{v}'}{\partial t} = -\nabla(p' + \overleftarrow{p}') + \frac{1}{4\pi}(\nabla \times \vec{H}') \times \vec{H} + \rho_0 \nabla V' + \rho' \nabla V_0 + \\ + 2\rho_0(\vec{v}' \times \vec{\Omega}) + \tilde{\mu}\Delta\vec{v}' + \frac{\vec{\mu}}{3}\nabla(\nabla \cdot \vec{v}') \tag{4}$$

$$\frac{\partial \rho'}{\partial t} + \rho_0 \nabla \cdot \vec{v}' = -(\vec{v}' \cdot \nabla)\rho_0 \tag{5}$$

$$\frac{\partial \vec{H}'}{\partial t} = \nabla \times (\vec{v}' \times \vec{H}_0) + \nu_m \Delta \vec{H}' - K\nabla \times [(\nabla \times \vec{H}') \times \vec{H}_0] \tag{6}$$

$$\nabla \cdot \vec{H}' = 0 \tag{7}$$

$$\Delta V' = -4\pi G\rho' \tag{8}$$

où ∇ est l'opérateur *nabla*, Δ est l'opérateur de Laplace, $\overleftarrow{p}'$ est la perturbation du tenseur de la pression, p' est la perturbation de la pression du plasma, ρ' est la perturbation de la densité, V' est la perturbation du potentiel gravifique, $\vec{v}'$ est la perturbation de la vitesse du plasma, $\vec{H}'$ est la perturbation du champ magnétique appliqué, $\tilde{\mu}$ est le coefficient de viscosité du plasma, ν_m est le coefficient de viscosité magnétique du plasma, $K = \frac{c}{4\pi Ne}$, où c est la vitesse de la lumière en espace libre, N est le nombre de densité des particules chargées du plasma, e est la charge électrique. On suppose que les perturbations se propagent dans le plasma sous la forme

$$\varphi = \varphi_0 \exp\, i(k_x x + k_z z + \omega t) \tag{9}$$

où φ' est la perturbation considérée, k_x, k_z sont les composantes du vecteur d'onde $\vec{k}$, ω est la pulsation d'onde.

Les composantes p'_{jk} $(j, k = 1, 2, 3)$ du tenseur p' s'écrivent sous la forme [1]

$$p'_{xx} = -\rho_0\nu\left(\frac{\partial v'_x}{\partial y} + \frac{\partial v'_y}{\partial x}\right);\ p'_{yy} = \rho_0\nu\left(\frac{\partial v'_x}{\partial y} + \frac{\partial v'_y}{\partial x}\right);\ p'_{zz} = 0$$

$$p'_{xy} = p'_{yx} = \rho_0\nu\left(\frac{\partial v'_x}{\partial x} - \frac{\partial v'_y}{\partial y}\right),\ p'_{xz} = p_{zx} = -2\rho_0\nu\left(\frac{\partial v'_y}{\partial z} + \frac{\partial v'_z}{\partial y}\right) \tag{10}$$

$$p'_{yz} = p'_{zy} = 2\rho_0\nu\left(\frac{\partial v'_z}{\partial x} + \frac{\partial v'_x}{\partial z}\right)$$

où $\rho_0\nu = \frac{NT}{4\omega_L}$ (T est la température du plasma, $\omega_L = \frac{eH_0}{M}$ est la pulsation cyclotronique pour le plasma, M est la masse des particules (ions) du plasma).

On peut écrire les vecteurs $(\nabla \times \vec{H}') \times \vec{H}_0$, $\nabla \times [(\nabla \times \vec{H}') \times \vec{H}_0]$, $\nabla \times (\vec{v}' \times \vec{H}_0)$, $\vec{v}' \times \vec{\Omega}$ sous la forme

$$(\nabla \times \vec{H}') \times \vec{H}_0 = \vec{\varepsilon}_x H_0 \left(\frac{\partial H'_x}{\partial z} - \frac{\partial H'_z}{\partial x}\right) - \vec{\varepsilon}_y H_0 \left(\frac{\partial H'_z}{\partial y} - \frac{\partial H'_y}{\partial z}\right) \tag{11}$$

$$\nabla \times [(\nabla \times \vec{H}') \times \vec{H}_0] = \vec{\varepsilon}_x H_0 \left(\frac{\partial^2 H'_z}{\partial y \partial z} - \frac{\partial^2 H'_y}{\partial z^2}\right) + \vec{\varepsilon}_y H_0 \left(\frac{\partial^2 H'_x}{\partial z^2} - \frac{\partial^2 H'_z}{\partial x \partial z}\right) -$$

$$- \vec{\varepsilon}_z H_0 \left[\left(\frac{\partial^2 H'_z}{\partial x \partial y} - \frac{\partial^2 H'_y}{\partial x \partial z}\right) + \left(\frac{\partial^2 H'_x}{\partial y \partial z} - \frac{\partial^2 H'_z}{\partial x \partial y}\right)\right] \tag{12}$$

$$\nabla \times (\vec{v}' \times \vec{H}_0) = H_0 \frac{\partial \vec{v}'}{\partial z} - \vec{\varepsilon}_z H_0 \nabla \cdot \vec{v}' \tag{13}$$

$$\vec{v}' \times \vec{\Omega} = \vec{\varepsilon}_x v'_y \Omega - \vec{\varepsilon}_y v'_x \Omega \tag{14}$$

où $\vec{\varepsilon}_x$, $\vec{\varepsilon}_y$, $\vec{\varepsilon}_z$ sont les verseurs du système de référence $Oxyz$.

La substitution des perturbations (9) dans les équations (4)—(8) nous conduit, en négligeant les carrés et les produits des perturbations et tenant compte de (11)—(14), au système d'équations, qui, en projections sur les axes Ox, Oy, Oz, prend la forme

$$\left[\omega - \frac{i\tilde{\mu}}{3}(3k^2 + k_x^2)\right] v_x = -\left(\frac{k_x}{k^2}\Omega_y^2\right)\frac{\rho'}{\rho_0} - [2i\Omega - i\nu(k^2 + k_z^2)]v'_y +$$

$$+ \frac{i\vec{\mu}}{3} k_x k_z v'_z + \frac{H_0}{4\pi\rho_0}(k_z H'_x - k_x H'_z) \tag{15}$$

$$(\omega - i\tilde{\mu}k^2)v'_y = [-i\nu(k^2 + k_z^2) + 2i\Omega]v'_x - 2i\nu k_x k_y v'_z + \frac{H_0}{4\pi\rho_0} k_z H'_y \tag{16}$$

$$\left[\omega - i\tilde{\mu}\left(k^2 + \frac{k_x^2}{3}\right)\right] v'_z = 2i\nu k_x k_z v'_y + \frac{i\vec{\mu}}{3} k_x k_z v'_x - \left[\frac{k_z}{k^2}\Omega_z^2 + iDV_0\right]\frac{\rho'}{\rho_0} \tag{17}$$

$$\rho' = -\frac{(\rho_0 k_z - iD\rho_0)v'_z - \rho_0 k_z v'_x}{\omega} \tag{18}$$

$$(i\omega + \nu_m k^2)H'_x = ik_z H_0 v'_x - KH_0 k_z^2 H'_y \tag{19}$$

$$(i\omega + \nu_m k^2)H'_y = ik_z H_0 v'_y - KH_0(k_x k_z H'_z - k_z^2 H'_x) \tag{20}$$

$$(i\omega + \nu_m k^2)H'_z = -\imath k_x H_0 v'_x + KH_0 k_x k_z H'_y \tag{21}$$

$$\imath k_x H'_x + i k_z H'_z = 0 \tag{22}$$

$$k^2 V' = 4\pi G\rho' \tag{23}$$

où $k^2 = k_x^2 + k_z^2$, $p' = V_s^2\rho'$, V_s est la vitesse du son dans le plasma et $D = \frac{\mathrm{d}}{\mathrm{d}z}$.

Si l'on applique l'opérateur *divergence* ($\nabla\cdot$) dans l'équation (4) et tenant compte des égalités suivantes

$$\rho_0 \frac{\partial}{\partial t}(\nabla \cdot v') = \rho_0 \frac{\partial}{\partial t}\left\{-\frac{1}{\rho_0}\left[\frac{\partial \rho'}{\partial t} + (D\rho_0)\, v'_z\right]\right\} = -\frac{\partial^2 \rho'}{\partial t^2} -$$

$$-(D\rho_0)\frac{\partial v'_z}{\partial t} = \omega^2\rho' - i\omega(D\rho_0)v'_z,$$

$$\nabla \cdot (\nabla p') = \Delta p' = -k^2 p' = -k^2 V_s^2 \rho',$$

$$\nabla \cdot (\overleftrightarrow{\nabla p'}) = \nabla \cdot \left[\vec{\varepsilon}\left(\frac{\partial p'_{xx}}{\partial x} + \frac{\partial p'_{xz}}{\partial z}\right) + \vec{\varepsilon}_y\left(\frac{\partial p'_{yx}}{\partial x} + \frac{\partial p'_{yz}}{\partial z}\right) +\right.$$

$$\left. + \vec{\varepsilon}_z\left(\frac{\partial p'_{zx}}{\partial x} + \frac{\partial p'_{zz}}{\partial z}\right)\right] = ik_x\rho_0\nu(k_x^2 + 4k_z^2)v'_y, \tag{24}$$

$$\nabla \cdot [\nabla \times \vec{H}') \times \vec{H}_0] = -k_x k_z H_0 H'_x + k_x^2 H_0 H'_z,$$

$$\nabla \cdot (\Delta \vec{v}') = \nabla^2 \cdot [\nabla \cdot \vec{v}')] = -\imath k^2(k_x v'_x + k_z v'_z)$$

$$\nabla \cdot (\rho_0 \nabla V') = \nabla\rho_0 \cdot \nabla V' + \rho_0 \Delta V' = ik_z(D\rho_0)V' - 4\pi G\rho_0\rho',$$

$$\nabla \cdot (\rho' \nabla V_0) = \nabla\rho' \nabla V_0 + \rho' \Delta V_0 = \imath k_z (DV_0)\rho' - 4\pi G\rho_0\rho'$$

où $\nabla = \frac{\partial}{\partial x}\vec{\varepsilon}_x + \frac{\partial}{\partial z}\varepsilon_z$; $\Delta = \nabla^2 = \frac{\partial^2}{\partial x^2} + \frac{\partial^2}{\partial z^2}$; $D^2 = \frac{\mathrm{d}^2}{\mathrm{d}z^2}$, on obtient l'égalité

$$i\left(\frac{k_x^2 V_A^2}{\Omega_m} + \frac{4k_x k^2 \tilde{\mu}}{3}\right)V'_x + i[\nu(k_x^2 + 4k_u k_z^2) - 2k_x\Omega]v'_y -$$

$$-\mathrm{i}\left[\omega\,(D\rho_0) - \frac{4k^2 k_z \tilde{\mu}}{3}\right]v'_z + \frac{k_x k_z H_0}{4\pi\rho_0}H'_x - \frac{Kk_x^2 k_z V_A^2}{\Omega_m}H'_y + \tag{25}$$

$$+ [\omega^2 - \Omega^2_{J(z)(S)} - D^2(V_0)]\zeta' = 0,$$

où $\Omega_m = i\omega + \nu_m k^2$, $\Omega^2_{J(z)(S)} = V_s^2 k^2 + \frac{4\pi G}{k^2}[ik_z(D\rho_0) - k^2\rho_0] + ik_z(DV_0)$

Remplaçons maintenant dans l'équation (15) et aussi dans l'équation (20) la composante H'_x donnée par l'équation (21). On obtient

$$\left(\omega - \frac{i\tilde{\mu}(3k^2 + k_x^2)}{3} - \frac{ik_x^2V_A^2}{\Omega_m}\right)v'_x + i[2\Omega - \nu(k^2, + k_x^2)]v'_y - \\ - \frac{i\tilde{\mu}k_xk_z}{3}v'_z - \frac{H_0k_z}{4\pi\rho_0}H'_x + \frac{Kk_x^2k_zV_A^2}{\Omega_m}H'_y + \left(\frac{k_x}{k^2}\Omega_J^2\right)\zeta' = 0 \tag{26}$$

et

$$[\Omega_m^2 + (KH_0)^2k_x^2k_z^2]H'_y = \Omega_m(ik_zH_0v'_y) + KH_0k_x^2H'_z) + iK\,H_0^2k_x^2k_zv'_x. \tag{27}$$

Introduisons les notations suivantes

$$\Omega_{\tilde{\mu}} = i\tilde{\mu}k^2\,,\ \Omega^{(1)}_{\tilde{\mu}(x)} = \frac{i\tilde{\mu}}{3}(3k^2 + k_x^2)\,,\ \Omega^{(1)}_{\tilde{\mu}(z)} = \frac{i\tilde{\mu}}{3}(3k^2 + k_z^2)$$

$$\Omega_{\tilde{\mu}(z)} = \frac{4i\tilde{\mu}k^2k_z}{3};\ \Omega_{\tilde{\mu}(x)(z)} = \frac{i\tilde{\mu}k_xk_z}{3}\,,\ \Omega_{A\tilde{\mu}(x)} = \frac{ik_x^2V_A^2}{\Omega_m} +$$

$$+ \frac{4i\tilde{\mu}k_xk^2}{3};\ \Omega_{\nu(z)} = 2i\Omega - i\nu(k^2 + k_z^2)\,,\ \Omega_{\nu(x)(z)} = 2i\nu k_xk_z$$

$$\Omega^{(1)}_{\nu(x)(z)} = ik_x[\nu(k^2 + 3k_z^2) - 2\Omega]\,,\ \Omega_{A(x)} = \frac{ik_x^2V_A^2}{\Omega_m}$$

$$\Omega_{A(x)(z)} = \frac{K\,k_x^2k_zV_A^2}{\Omega_m};\ \Omega^{(1)}_{A(x)(z)} = \frac{Kk_x^2k_zV_A^2}{\Omega_m}\,, \tag{28}$$

$$\Omega^2_{0J(z)} = \Omega^2_{J(z)(S)} + D^2(V_0);\ \Omega_{J(z)} = \frac{k_z}{k^2}\Omega_J^2\,,\ \Omega_{J(z)} = \frac{k_x}{k^2}\Omega_J^2;\ \Omega^{(1)}_{J(z)} = iD(V_0) +$$

$$+ \frac{k_z}{k^2}\Omega_J^2;\ A_{(z)} = \frac{k_zH_0}{4\pi\rho_0}\,,\ A_{(x)(z)} = \frac{k_xk_zH_0}{4\pi\rho_0};\ C = iD\rho_0\,,$$

$$D_{(z)} = ik_zH_0\,,\ D^{(1)}_{(z)} = KH_0k_z^2;\ D_{(x)(z)} = iKH_0^2k_x^2k_z;\ D_{m(z)} = i\Omega_mk_zH_0$$

$$D^{(1)}_{m(z)} = KH_0\Omega_mk_z^2;\ D^{(2)}_{m(z)(z)} = \Omega_m^2 + (KH_0)^2k_x^2k_z^2.$$

Le système d'équations (16), (17), (19), (25), (26) et (27), tenant compte de notations (28), prend la forme

$$\Omega_{\nu(x)}v'_x + (\Omega_{\tilde{\mu}} - \omega)v'_y - \Omega_{\nu(x)(z)}v'_z + A_{(z)}H'_y = 0, \tag{29}$$

$$\Omega_{\tilde{\mu}(x)(z)}v'_x + \Omega_{\nu(x)(z)}v'_y - (\omega - \Omega^{(1)}_{\tilde{\mu}(z)})v'_z - \Omega^{(1)}_{J(z)}\zeta' = 0. \tag{30}$$

$$D_{(z)}v'_x - \Omega_m H'_x - D^{(1)}_{(z)}H'_y = 0 \tag{31}$$

$$\begin{aligned}\Omega_{A\tilde{\mu}(x)}v'_x + \Omega^{(1)}_{\nu(x)(z)}v'_y - (C\omega - \Omega_{\tilde{\mu}(z)})v'_z + \\ + A_{(x)(z)}H'_x - \Omega_{A(z)}H'_y + (\omega^2 - \Omega^2_{0J(z)})\zeta' = 0\end{aligned} \tag{32}$$

$$\begin{aligned}(\omega - \Omega^{(1)}_{\tilde{\mu}(x)} - \Omega_{A(x)})v'_x + \Omega_{\nu(z)}v'_y - \\ - \Omega_{\tilde{\mu}(x)(z)}v'_z - A_{(z)}H'_x + \Omega_{A(x)(z)}H'_y + \Omega_{J(x)}\zeta' = 0\end{aligned} \tag{33}$$

$$D_{(x)(z)}v'_x + D_{m(z)}v'_y + D^{(1)}_{m(z)}H'_x - D^2_{m(x)(z)}H'_y = 0. \tag{34}$$

3. **L'équation de dispersion.** L'équation de dispersion pour le modèle de plasma étudié s'obtient par l'annulation du déterminant D formé par les coefficients des grandeurs v'_x, v'_y, v'_z, H'_x, H'_y et ζ'.

$$\begin{vmatrix}
\Omega_{\nu(z)} & \Omega_{\tilde{\mu}} - \omega & -\Omega_{\nu(x)(z)} & 0 & A_{(z)} & 0 \\
\Omega_{\tilde{\mu}(x)(z)} & \Omega_{\nu(x)(z)} & \Omega^{(1)}_{\mu(z)} - \omega & 0 & 0 & -\Omega^{(1)}_{J(z)} \\
D_{(z)} & 0 & 0 & -\Omega_m & -D^{(1)}_{(z)} & 0 \\
\Omega_{A\tilde{\mu}(x)} & \Omega^{(1)}_{\nu(x)(z)} & \Omega_{\tilde{\mu}(z)} - C\omega & A_{(x)(z)} & -\Omega_{A(z)} & \omega^2 - \Omega^2_{0J(z)} \\
\omega - \Omega^{(1)}_{\tilde{\mu}(x)} - & & & & & \\
-\Omega_{A(x)} & \Omega_{\nu(z)} & -\Omega_{\tilde{\mu}(x)(z)} & -A_{(z)} & \Omega_{A(x)(z)} & \Omega_{J(x)} \\
D_{(x)(z)} & D_{m(z)} & 0 & D^{(1)}_{m(z)} & -D^2_{m(x)(z)} & 0
\end{vmatrix} = 0 \tag{35}$$

On obtient alors l'égalité

$$\begin{aligned}[\Omega_m D^2_{m(z)(z)} + D^{(1)}_{(z)} D^{(1)}_{m(z)}]\{(\omega^2 - \Omega^2_{0J(z)})[(\Omega_{\tilde{\mu}} - \omega)\Omega^2_{\tilde{\mu}(x)(z)} + \\ - \Omega_{\nu(x)}\Omega_{\nu(z)(z)}\Omega_{\tilde{\mu}(x)(z)} - \Omega^2_{\nu(z)}(\Omega^{(1)}_{\tilde{\mu}(x)} - \omega) + \\ + (\Omega_{\tilde{\mu}} - \omega)(\Omega^{(1)}_{\tilde{\mu}(x)} - \omega)(\omega - \Omega_{\tilde{\mu}(x)} - \Omega_{A(x)}) - \\ - \Omega_{\mu(x)(z)}\Omega_{\nu(x)(z)}\Omega_{\nu(z)} + (\omega - \Omega_{\tilde{\mu}(x)} - \Omega_{\tilde{A}(v)})\Omega^2_{\nu(v)(z)}] +\end{aligned}$$

$$
\begin{aligned}
&+ (\Omega_{\tilde{\mu}(z)} - C\omega)\,[(\Omega_{\tilde{\mu}} - \omega)\Omega_{J(z)}\,\Omega_{\tilde{\mu}(x)(z)} + (\omega - \\
&- \Omega_{\tilde{\mu}(\lambda)} - \Omega_{A(\lambda)})(\Omega_{\tilde{\mu}} - \omega)\Omega^{(1)}_{J(z)} - \Omega_{\nu(z)}\,(\Omega_{\nu(x)(z)}\,\Omega_{J(\lambda)} + \\
&+ \Omega_{\nu(z)}\,\Omega^{(1)}_{J(z)})\,] + (\Omega_{\tilde{\mu}} - \omega)\,[\Omega_{A\tilde{\mu}(\lambda)}\,\Omega_{\tilde{\mu}(\lambda)(z)}\,\Omega^{(1)}_{J(z} - \\
&- (\Omega^{(1)}_{\tilde{\mu}(z)} - \omega)\,\Omega_{A\tilde{\mu}(x)}\,\Omega_{J(x)}\,] + \Omega^{(1)}_{\nu(\lambda)(z)}\,(\Omega_{\nu(x)(z)}\,[(\omega - \\
&- \Omega_{\tilde{\mu}(x)} - \Omega_{A(\lambda)})\,\Omega^{(1)}_{J(z)} + \Omega_{\tilde{\mu}(x)(z)}\,\Omega_{J(x)}\,] + \\
&+ \Omega_{\nu(z)}\,[\Omega_{J(\lambda)}\,(\Omega^{(1)}_{\tilde{\mu}(z)} - \omega) - \Omega^{(1)}_{J(z)}\,\Omega_{\tilde{\mu}(x)(z)}\,])\,] - \\
&- \Omega_{A\tilde{\mu}(x)}\,(\Omega_{\nu(z)}\,\Omega_{\nu(x)(z)}\,\Omega^{(1)}_{J(z)} + \Omega^{2}_{\nu(x)(z)}\,\Omega_{J(\lambda)})\}\,- \\
&- [\Omega_{m}\Omega_{A(x)(z)} + A_{(z)}\,D^{(1)}_{(z)}]\,\{[(\Omega^{(1)}_{\tilde{\mu}(z)} - \omega)\Omega_{\nu(z)} + \Omega_{\nu(x)(z)}\,\Omega_{\tilde{\mu}(x)(z)}]\,[(\omega^2 - \\
&- \Omega^2_{0J(z)})\,D_{m(z)}\,] + (\Omega_{\tilde{\nu}\mu(z)} - C\omega)\,\Omega_{\nu(z)}\,\Omega_{J(z)}\,D_{m(z)} - \\
&- (\Omega^{(1)}_{\tilde{\mu}(z)} - \omega)(\Omega_{\tilde{\mu}} - \omega)(\omega^2 - \Omega^2_{0J(z)})\,D_{(x)(z)}\}\,- \\
&- [\Omega_{m}\Omega_{A(z)} + A_{(\lambda)(z)}\,D^{(1)}_{(z)}]\,\{[(\Omega^{(1)}_{\tilde{\mu}(z)} - \omega)\,\Omega_{\nu(z)} + \\
&+ \Omega_{\nu(x)(z)}\,\Omega_{\tilde{\mu}(x)(z)}]\,\Omega_{J(x)}\,D_{m(z)}\,(\Omega^{(1)}_{\tilde{\mu}(z)} - \omega)(\Omega_{\tilde{\mu}} - \\
&- \omega\,)D_{(x)(z)}\Omega_{J(x)} - \Omega_{\nu(x)}\,\Omega_{\tilde{\mu}(x)(z)}\,D_{m(z)}\,\Omega^{(1)}_{J(z)}\}\,+ \\
&+ [\Omega_{m}\,D_{(x)(z)} + D_{(z)}D^{(1)}_{m(z)}]\,\{[(\Omega_{\tilde{\mu}(z)} - C\omega)\Omega_{A(x)(z)} - \qquad (36)\\
&- \Omega_{\tilde{\mu}(x)(z)}\,\Omega_{A(z)}](\Omega_{\tilde{\mu}} - \omega)\Omega_{J(z)} + (\omega^2 - \Omega^2_{0J(z)})(\Omega_{A(x)(z)}\Omega_{\nu(x)(z)} - \\
&- \Omega_{\tilde{\mu}(\lambda)(z)}A_{(z)}) - (\Omega^{(1)}_{\tilde{\mu}(z} - \omega)\Omega_{\nu(z)}\,A_{(z)}] + [(\Omega^{(1)}_{\tilde{\mu}(z)} - \omega)\Omega^{(1)}_{\nu(x)(z)} - \\
&- (\Omega_{\tilde{\nu}(z)} - C\omega)\Omega_{\nu(x)(z)}\,]\Omega_{J(x)}A_{(z)} + [(\Omega^{(1)}_{\nu(x)(z)}\,\Omega_{A(\nu)(z)} + \\
&+ \Omega_{\nu(z)}\Omega_{A(z)})\Omega^{(1)}_{J(z)} + \Omega_{A(z)}\Omega_{\nu(\lambda)(z)}\Omega_{J(\lambda)}\,]\Omega_{\nu(\lambda)(z)}\}\,+ \\
&+ [D^{(1)}_{(z)}D_{(x)(z)} - D_{(z)}D^{2}_{m(x)(z)}]\,\{(\Omega_{\tilde{\mu}} - \omega)\,[(\Omega_{\tilde{\mu}(z)} - C\omega)\Omega^{(1)}_{J(z)}A_{(z)} - \\
&- \Omega_{\tilde{\mu}(x)(z)}\Omega^{(1)}_{J(z)}A_{(x)(z)}\,] + [(\omega^2 - \Omega^2_{0J(x)})\Omega_{\nu(x)(z)}A_{(z)} + \\
&+ \Omega_{\nu(\lambda)(z)}\Omega_{J(\lambda)}\,A_{(x)(z)} + \Omega_{\nu(z)}\,\Omega^{(1)}_{J(z)}\,A_{(\lambda)(z)} + \\
&+ \Omega^{(1)}_{\nu(x)(z)}\Omega^{(1)}_{J(z)}A_{(z)}\,]\Omega_{\nu(x)(z)}\}\,+ \Omega_{\tilde{\mu}(x)(z)}\Omega^{(1)}_{J(z)}A_{(z)}\,[\Omega_{m}(\Omega_{A\tilde{\mu}(x)}\,D_{m(z)} - \\
&- \Omega^{(1)}_{\nu(x)(z)}D_{(x)(z)})\,] + (\Omega^{(1)}_{\tilde{\mu}(z)} - \omega)\,(\omega^2 - \Omega^2_{0J(z)})\,[A_{(z)}\Omega_{m}D_{m(z)}(\omega - \\
&- \Omega_{\tilde{\mu}(x)} - \Omega_{A(x)}) - A^2_{(z)}D_{(z)}\,D_{m(z)} - D_{(z)}(\Omega^{\sim} - \omega)(A_{(z)}D^2_{m(x)(z)} - \\
&- \Omega_{A(x)(z)}D^{(1)}_{m(z)})\,] + (\Omega^{(1)}_{\tilde{\mu}(z)} - \omega)\Omega_{J(\lambda)}\,[(\Omega_{\tilde{\mu}} - \omega)D_{(z)}(\Omega_{A(z)}D^{(1)}_{m(z)} -
\end{aligned}
$$

$$- A_{(x)(z)} D^2_{m(x)(z)}) - A_{(z)} D_{m(z)} (A_{(\lambda)(z)} D_{(z)} + \Omega_m \Omega_{A\tilde{\mu}(x)})] -$$
$$- A_{(z)} \Omega^{(1)}_{J(z)} (\Omega_{\tilde{\mu}(z)} - C\omega) \{D_{(z)} (A_{(z)} D_{m(z)} + D^{(1)}_{m(z)} \Omega_{\nu(z)}) +$$
$$+ \Omega_m [D_{m(z)} (\Omega_{A(\lambda)} + \Omega_{\tilde{\mu}(x)} - \omega) + D_{(\lambda)(z)} \Omega_{\nu(z)} - D_{m(z)} \Omega_{\tilde{\mu}(x)(z)}]\} +$$
$$+ A_{(z)} \Omega_m D_{m(z)} (\omega^2 - \Omega^2_{0J(z)}) \Omega^2_{\tilde{\mu}(x)(z)} = 0$$

Cas particulier. Pour le cas d'un modèle de plasma infini, non visqueux, compressible, en mouvement de rotation, doué d'une conductivité électrique finie et d'une *densite constante*, avec une pression anisotrope, en présence du courant Hall, sous l'action de son propre champ gravifique et aussi sous l'action d'un champ magnétique uniforme-axial, nous avons satisfait aux conditions suivantes. $\tilde{\mu} = 0$, $\rho_0 = \text{const.}$, $V_0 = \text{const}$, $D(\rho_0) = 0, D^2(\rho_0) = 0$, $D(V_0) = 0$, $D^2(V_0) = 0$ et les grandeurs $\Omega_{\tilde{\mu}}$, $\Omega_{\tilde{\nu}(x)}$, $\Omega_{\tilde{\mu}(\lambda)(z)}$, $\Omega_{4\tilde{\mu}(\lambda)}$, $\Omega_{\tilde{\mu}(z)}$, $\Omega^{(1)}_{\tilde{\mu}(z)}$, $\Omega^2_{0J(z)}$, $\Omega^{(1)}_{J(z)}$, C deviennent $\Omega_{\tilde{\mu}} = 0$, $\Omega_{\tilde{\mu}(\lambda)} = 0$, $\Omega_{\tilde{\mu}(x)(z)} = 0$, $\Omega_{4\tilde{\mu}(\lambda)} = \frac{\iota k_x^2 V_A^2}{\Omega_m}$,

$\Omega_{\tilde{\mu}(z)} = 0$, $\Omega^{(1)}_{\tilde{\mu}(z)} = 0$, $\Omega^2_{0J(z)} = \Omega^2_J$, $\Omega^{(1)}_{J(z)} = \Omega_{J(z)} = \frac{k}{k^2} \Omega^2_J$, $C = 0$.

Dans ce cas particulier, l'équation de dispersion (36) se réduit à l'équation de dispersion obtenue par Sharma et Prakash [1]

L'équation de dispersion (36) a une grande importance pour l'établissement du critère de l'instabilité magnétohydrodynamique du modèle de plasma étudié, problème qui sera analysé dans un autre mémoire

(Manuscrit reçu le 10 juin 1978)

BIBLIOGRAPHIE

1 R C Sharma, K. Prakash, Ind J Phys, **48** (9), 836–840 (1974)
2 P. K Bhatia, P N Gupta, Beitr Plasmaphysik, **16** (1), 55–64 (1976)

ASUPRA UNUI MODEL DE PLASMĂ COSMICĂ CU DENSITATE VARIABILĂ

(Rezumat)

În lucrare se stabilește ecuația de dispersie pentru un model de plasmă **cosmică**. Autorul ia în considerare acțiunea simultană a compresibilității, a viscozității plasmei, **anizotropia** presiunii, conductivitatea electrică finită, prezența curentului Hall, mișcarea de rotație, densitatea variabilă a plasmei și acțiunea propriului său cîmp gravitațional și a unui cîmp magnetic uniform-axial

Ecuația de dispersie obținută generalizează ecuațiile de dispersie stabilite de autorii citați în lucrare.

STUDIA UNIV BABEŞ–BOLYAI, PHYSICA, 2, 1978

LE SPECTRE D'AMPLITUDE DU CHAMP ÉLECTRIQUE PRODUIT PAR LES ÉCLAIRS

STELA GÎJU

1. **Introduction.** Pour déterminer le nombre des décharges électriques atmosphériques dans une région quelconque, on avait créé de nombreux types d'appareils Parmi ceux-ci, les compteurs d'éclairs jouent un rôle important, grâce à leur multiples possibilités d'utilisation [1, 2, 3] Les compteurs d'éclairs sont des appareils à l'aide desquels on peut compter les impulsions à basse fréquence, provenues des éclairs dont le champ électrique induit dans l'antenne dépasse un certain niveau indiqué · le seuil de sensibilité de l'appareil.

2. **La description de l'appareil.** En partant du schéma du compteur de type Pierce à tubes de décharge [4], nous avons construit un compteur d'éclairs formé par trois étages, mais ayant en commun l'antenne, le circuit d'alimentation et le circuit d'étalonnage (fig. 1). Les trois étages ont les seuils de sensibilité $1{,}25\ \frac{V}{m}$; $2{,}5\ \frac{V}{m}$ et $3{,}75\ \frac{V}{m}$ à correspondre aux tensions 5 V; 10 V, respectivement 15 V. Le comptage des éclairs est accompli par voie électromagnétique. A l'approche d'un orage, celui-ci est signalé d'abord par les compteurs à sensibilité majeure, puis en ordre de succession par les autres, selon la sensibilité décroissante

L'appareil permet l'étude du spectre d'amplitude du champ électrique produit par les éclairs à l'endroit du récepteur, en enregistrant le nombre d'éclairs qui produisent au récepteur un champ électrique au-dessus de la valeur de seuil E_0 bien définie

3. **Les résultats expérimentaux.** L'amplitude du champ électrique E, causé par une décharge électrique atmosphérique, est soumise à l'endroit de la source à une loi logarithmique normale de distribution D'après Horner [5], la probabilité de la formation d'une décharge électrique à l'amplitude du champ électrique E, est définie par la relation :

$$P(u) = \frac{1}{\sigma\sqrt{2\pi}} e^{\frac{-u^2}{2\sigma^2}} \qquad (1)$$

où $\mu = ln\ E$, et π représente l'écart normal de la distribution.

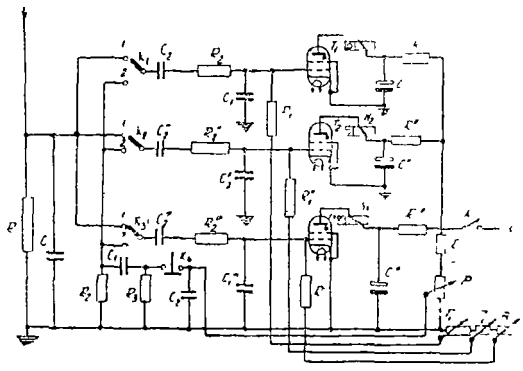

Fig 1 Le compteur d'éclairs à 3 étages

* Institut pédagogique de Tîrgu-Mureş

Pour distances suffisamment importantes et pour de plus longues périodes d'observation, on peut admettre, à bonne approximation, que les éclairs sont uniformément distribués, c'est-à-dire le nombre moyen des décharges électriques dans l'unité de surface ne dépend pas de la distance. En ce cas, le nombre des décharges électriques, qui produisent dans l'endroit du récepteur un champ électrique à l'amplitude $\mu \geqslant \mu_0$, c'est-à-dire comptable par un appareil à sensibilité de seuil $\mu_0 = ln\ E_0$, résulte [5] de la relation

$$g(E_0) = \frac{e^{2\sigma^2}\pi G}{E_0^2} \tag{2}$$

où G représente le nombre moyen des décharges électriques produites dans une unité de surface. La relation (2) peut être vérifiée expérimentalement

L'appareil construit fonctionne à partir de l'été de l'année 1974, chaque jour, entre 8 heures du matin jusqu'à 20 heures du soir, sauf l'hiver, la lecture ayant lieu de trois en trois heures

Le spectre d'amplitude du champ électrique produit par les éclairs à l'endroit du récepteur (fig. 2), en considérant le nombre des éclairs enregistrés pendant les mois de juin, juillet et août des années 1974, 1975 et 1976, montre que le nombre des éclairs, qui produisent au récepteur un champ électrique à amplitude mineure est beaucoup plus grand par rapport aux autres, parce qu'à cette valeur de la sensibilité de l'appareil, son rayon de réception est plus grand et peut détecter plus d'éclairs. En comparant les enrégistrements de 1974, 1975 et 1976, on peut constater qu'indifférémment de la période de temps considérée, le nombre des éclairs enregistré en 1975 est plus grand. Ce fait pourrait être en corrélation avec les

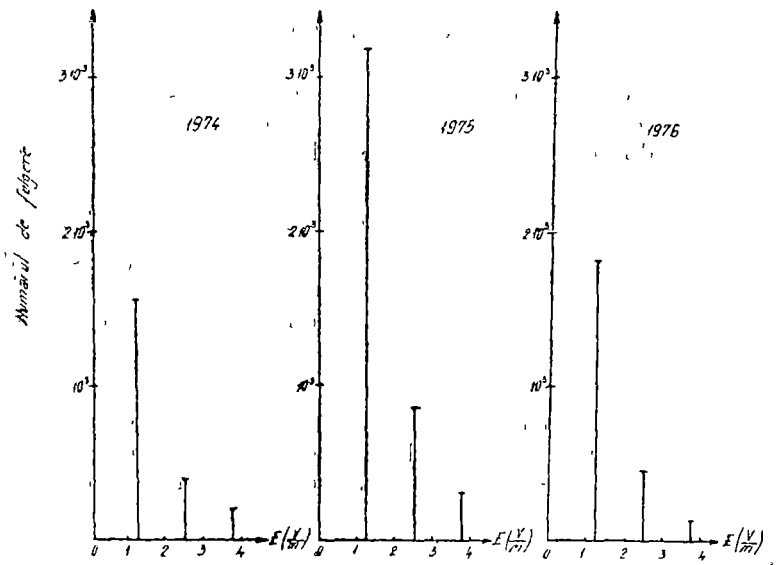

Fig 2 Le spectre d'amplitude du champ électrique produit par les éclairs au récepteur.

phénomenes météorologiques déterminant les inondations de juillet 1975 dans notre pays.

En vérifiant la relation (2), on avait obtenu les résultats suivants:

Tableau 1

$E_0 \left(\frac{V}{m}\right)$	Nombre d'éclairs			$g(E_0) \cdot E_0^2$			R(km)
	1974	1975	1976	1974	1975	1976	
1,25	1551	3217	1906	2423,43	5026,56	2978,12	60
2,5	391	859	418	2443,75	5368,75	2612,50	30
3,75	197	319	145	2770,31	4485,93	2039,06	10

Il est a remarquer que $g(E_0)\ E_0^2 = e^{2\sigma^2}\pi G$, représente en bonne approximation une constante pour les premiers deux étages, qui ont le rayon majeur de réception. Pour le troisième étage on peut constater des écarts plus importants, parce que le rayon de réception est trop réduit et le nombre d'éclairs, ne peut pas être considéré uniformément distribué, selon l'hypothèse admise.

L'appareil peut fournir des données évaluables en ce qui concerne la distance jusqu'à l'endroit de production des éclairs.

Chaque étage à seuil de sensibilité E_0 a un rayon moyen de réception R. Pour les distances suffisamment importantes, on peut admettre que l'amplitude du champ électrique, produit par les éclairs à l'endroit de réception, soit soumise à une loi de proportionnalité inverse à la distance R En ce cas

$$E_0 \cdot R = \text{constante} \tag{3}$$

Cette constante doit être la même pour tous les étages inclus dans l'appareil respectif [5, 6]. Si l'on peut déterminer le rayon de réception à l'un des étages conformément aux données expérimentales, alors le rayon de réception des autres étages sera donné par la relation (3).

En nos cas, selon la pratique, le rayon de réception de l'étage à seuil de sensibilité $E_0 = 2{,}5\ \frac{V}{m}$ monte à $R = 30$ km. Alors, pour l'étage à seuil de sensibilité $E_0 = 1{,}25\ \frac{V}{m}$, on obtient un rayon de réception de 60 km. Le rayon de réception de l'étage à $E_0 = 3{,}75\ \frac{V}{m}$ ne peut plus être déterminé de cette manière, parce qu'il ne s'encadre pas dans l'hypothèse admise. Le rayon de réception de cet étage s'étend à 10 km, et cela grâce à la sensibilité réglée de la sorte qu'il ne détecte que les éclairs produits par un centre rapproché d'orage, dont les tonnerres sont même audibles.

4. **Conclusions.** L'appareil peut être utilisé pour la détection des éclairs produits à distances jusqu'à environ 60 km. Le compteur d'éclairs à trois étages peut fournir des données évaluables en ce qui concerne la distance jusqu'à l'en-

droit de production des éclairs. On pourrait obtenir des résultats plus complets à l'aide des appareils avec un nombre plus important d'étages et à une sensibilité plus élevée. Mais, en augmentant la sensibilité, ces types de compteurs risquent d'être autoexcités ou bien de réceptionner de faux éclairs.

(Manuscrit reçu le 29 janvier 1977)

BIBLIOGRAPHIE

1. H. S. Chandrasekharaiah, R S N Rau, A A. Natarajan, Indian J Meteor. Geophys, **22**, 1, 103—107 (1971).
2 E. Kilinski, Electrie, **7**, 220—221 (1963).
3. M. Mezòsi, O.M.I, 1960, XXIV, 284—286 (1961)
4 S. Gîju, Studia Univ Babeş—Bolyai, ser Phys, 2, 87—92 (1973)
5 F. Horner, Proc I E E., **107** B, 321—323 (1960)
6 V Creţeanu, M Frimescu, *Culegere de lucrări ale Institutului Meteorologic*, Bucureşti, 1964

SPECTRUL DE AMPLITUDINE AL CÎMPULUI ELECTRIC PRODUS DE FULGERE

(Rezumat)

Lucrarea prezintă un contor de fulgere de tip Pierce cu tuburi de descărcare, cu trei etaje (fig 1), avînd în comun antena, circuitul de alimentare şi circuitul de etalonare. Cele trei etaje ale contorului au pragurile de sensibilitate $1{,}25\ \frac{V}{m}$, $2{,}5\ \frac{V}{m}$ şi $3{,}75\ \frac{V}{m}$

Aparatul permite studiul spectrului de amplitudine al cîmpului electric produs de fulgere la locul receptorului, prin înregistrarea numărului de fulgere care produc la receptor un cîmp electric mai mare decît o valoare de prag E_0 bine definită (fig 2) Contorul triplu de tip Pierce poate furniza date estimative cu privire la distanţa pînă la locul de producere a fulgerelor

RECENZII

Lucrările Simpozionului național de fizica solidului (Proceedings of the National Symposium on Solid State Physics), redactori coord Al Nicula și O Cozar, Cluj-Napoca, 1978 339 pag.

This volume contains 123 papers presented at the National Symposium on the Solid State Physics, which took place in Cluj-Napoca on 13–14 May 1978 The Symposium covered the new aspects of solid state physics, problems refering to some crystalline and noncrystalline materials

The volume is divided into three sections (A) – New materials and preparation technologies, (B) – Modern conceptions in the physics of crystalline and amorphous state, (C) – Up-to-date experimental methods in solid state physics

Section A contains 38 papers dealing with superconductive materials with high critical temperatures, alloys with special magnetic properties, semiconductors and photoelectric materials and preparation technologies of some one-dimensional molecular complexes

Section B contains 44 papers about electric transport phenomena, radiative processes in p–n junctions and heterojunctions, contributions on amorphous semiconductor modelling, some problems refering to the critical temperature and susceptibility in excitonic transitions, Hall and Seebeck effects in hopping conduction

Section C contains 41 papers presenting some F P R. results on the ferroelectric phase transitions, localized vibrations in solid and magnetic properties of iron ions in oxidic glasses The other papers are dealing with Mössbauer spectroscopy on some intermetallic compounds, solide state-ligand interface phenomena, fluorescence, X-ray diffraction and N M R studies of magnetic dipolar relaxation in uranium hexafluorine

R CÂMPEANU

M Crișan, **Teoria cuantică a magnetismului** (Quantum Theory of Magnetism), Ed Dacia Cluj-Napoca, 1977.

The book starts with a chapter treating the exchange interaction in the insulators, metals and alloys The second chapter contains a short review of the Green function method, with the perturbative dyagramatic expansion, the motion equation method, and the Bethe-Salpeter equation for the vertex function The third chapter deals with the Heisenberg ferromagnet treated by the motion equation method of the Green function in the Tyablikov and Callen approximations The antiferromagnetic ordered phase as well as the spin waves approximation are also discussed in this chapter The forth chapter contains the theory of the itinerant electron ferromagnetism. The fifth surveys the extensive theoretical results (Soviet school Swiss School) on the coexistence between superconductivity and magnetic order of impurities in the superconducting alloys.

The sixth chapter contains the problem the itinerant-electron antiferromagnetism in metals and alloys A part of these results have been obtained by the author in his Ph-D-thesis and published in prestigious journals The seventh chapter treats the Anderson theory of diluted alloys and the Kondo effect The last chapter describes the theory of critical phenomena The Ginsburg-Landau theory is presented and the perturbative calculation (on the basis of Sudakov equation) of the critical index is given The method presented by the author given by the Soviet School from Landau Institute of Theoretical Physics is quite general and equivalent with the RNG-Wilson theory

IULIU P...

Întreprinderea Poligrafică Cluj, Municipul Cluj-Napoca 396/1978

În cel de al XXIII-lea an (1978) *Studia Universitatis Babeş—Bolyai* apare semestrial în specialităţile:

matematică

fizică

chimie

geologie—geografie

biologie

filozofie

ştiinţe economice

ştiinţe juridice

istorie

filologie

На XXIII году издания (1978) *Studia Universitatis Babeş—Bolyai* выходит, два раза в год со следующими специальностями:

математика

физика

химия

геология—география

биология

философия

экономические науки

юридические науки

история

филология

Dans sa XXIII-e année (1978) *Studia Universitatis Babeş—Bolyai* paraît semestriellement les spécialités:

mathématiques

physique

chimie

géologie—géographie

biologie

philosophie

sciences économiques

sciences juridiques

histoire

philologie

Abonamentele se fac prin oficiile poștale, prin factorii poștali și prin difuzorii de presă, iar pentru străinătate prin ILEXIM, Departamentul export-import presă, P.O. Box 136—137, telex 11226, București, str. 13 Decembrie nr. 3.

Lei 10